ISSN 1349-1148
JAXA-RR-03-016E

JAXA Research and Development Report

Optimum Propeller or Windmill Design in a Wind Gradient

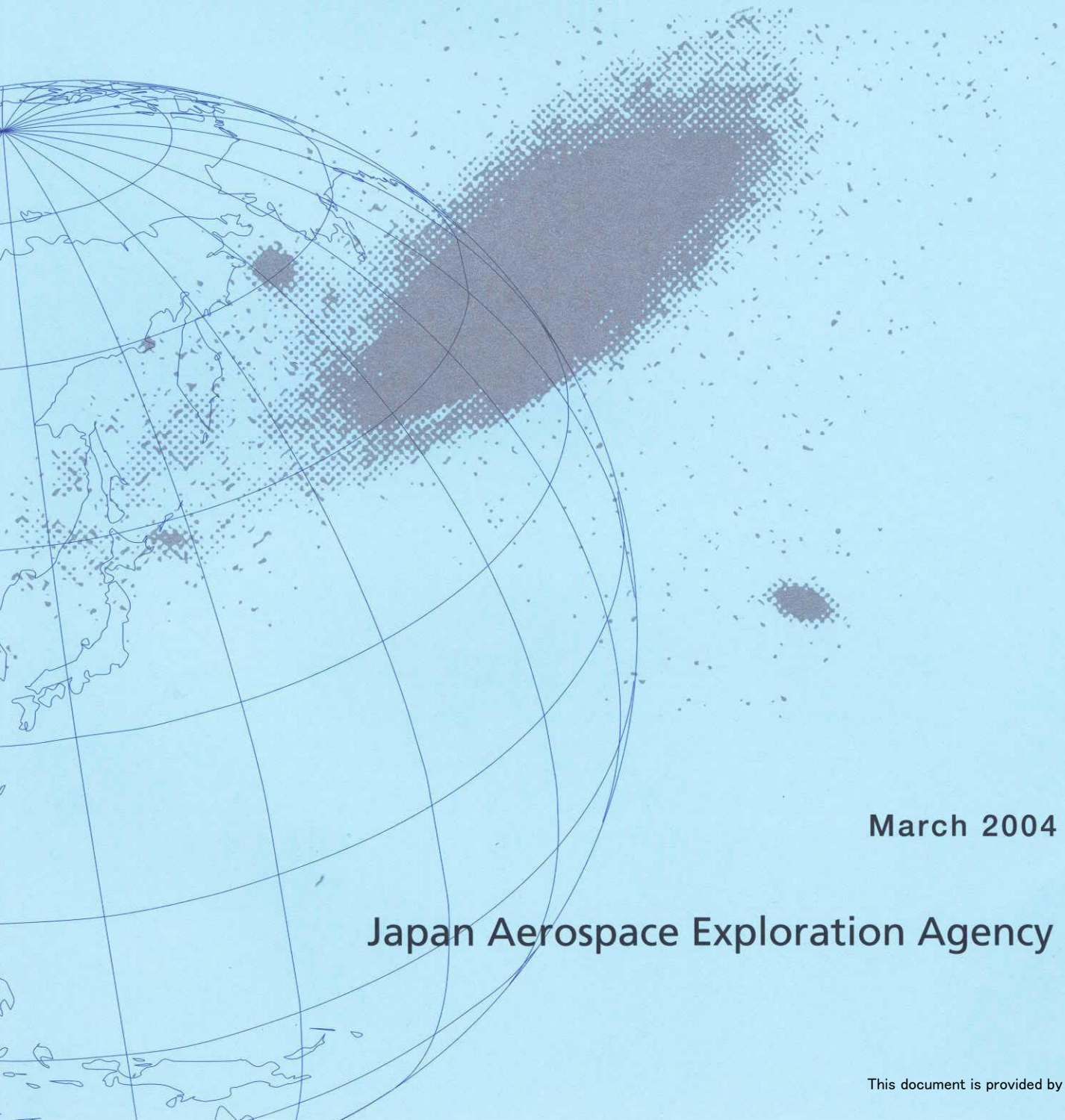

March 2004

Japan Aerospace Exploration Agency

JAXA-RR-03-016E

JAXA Research and Development Report
宇宙航空研究開発機構研究開発報告

Optimum Propeller or Windmill Design in a Wind Gradient
速度勾配中の最適なプロペラ及び風車の設計法

Masashi HARADA
原田　正志

Aeronautical Application Technology Center
Institute of Space Technology and Aeronautics
総合技術研究本部 航空利用技術開発センター

March 2004
2004年3月

Japan Aerospace Exploration Agency
宇宙航空研究開発機構

Table of Contents

Optimum Propeller or Windmill Design in a Wind Gradient*

Masashi HARADA[*1]

Abstract

A method for optimizing a propeller or windmill in a wind gradient has been developed, based on the lifting-line theory. This method takes the effect of trailing vortices and shed vortices into consideration, and consists of two fundamental major concepts. The first is the description of the problem by quadratic functions. The second concept is the reduction of the number of unknown variables using the periodical characteristics of the solution. In the first concept, optimum propeller design is converted into an optimization problem solved by a simple procedure. Using the latter concept, the number of design operations is reduced to a number exe-cuted within practical computation time. The validity and accuracy of the solution obtained by this method are carefully evaluated and proven using Prandtl's propeller theory. The solution shows that the propulsive efficiency of the optimum propeller with a wind gradient is larger than that without a wind gradient. The so-lution also shows that the optimum propeller in a wind gradient generates thrust even without an internal power supply. The windmill for a windmill ship is also designed, and the advantage of a windmill in a wind gradient shown.

Nomenclature

A	=	matrix of objective function	i	=	variable for time step from start of last cycle
b	=	variable for number of blades	I	=	variable for time step from initial time
B	=	number of blades	j	=	variable for blade segment
$\boldsymbol{B}$	=	vector of objective function	k	=	variable for time step from start of last cycle
c	=	variable for number of blades	K	=	variable for time step from initial time
c	=	blade section chord	l	=	variable for blade segment
$\boldsymbol{C}$	=	matrix of constraint function	L	=	lift
C_D	=	drag coefficient	L	=	number of cycles
C_{DH}	=	drag coefficient of hull	L/D	=	fineness ratio
C_L	=	lift coefficient	L_V	=	length of the vortex sheet
$C.P.$	=	control point	m	=	mass of air
d	=	propeller pitch	M	=	number of time steps
dR	=	width of blade segment	M_C	=	number of time steps in one cycle
dt	=	length of time step	n	=	natural number
D	=	drag	N	=	number of blade segments
$\boldsymbol{D}$	=	vector of constraint function	p	=	power per unit area
D_{AV}	=	average drag of windmill in one cycle	P	=	number of cycles; actual value
D_H	=	drag of hull	P	=	power consumed by propeller without effect of profile drag
$D.P.$	=	dividing point	P_{AV}	=	average power in one cycle
f	=	function of subscripts			
F	=	momentum loss function			
F_P	=	perpendicular component of force			
F_T	=	tangential component of force			

* received 16 February, 2004 (平成16年2月10日受付)

*1 Aeronautical Application Technology Center, Institute of Space Technology and Aeronautics
(総合技術研究本部 航空利用技術開発センター)

P_D = power consumed by propeller with effect of profile drag
Q = number of cycles; imaginary vast value
Q = volume of hull
r = distance between rotational center and control point
R = radius of blade
S = area of propeller disk
t = thrust per unit area
t' = thrust per unit area derived from $\bar{v}_X$
T = thrust generated by propeller without effect of profile drag
T_{AV} = average thrust in one cycle
T_D = thrust generated by propeller with effect of profile drag
T_E = effective thrust of windmill ship
T_S = thrust of screw
v = induced velocity at propeller disk
v_X = x component of v
$\bar{v}_X$ = average axial induced velocity at propeller disk
v_Y = y component of v
v_Z = z component of v
v_θ = tangential component of v
v' = vortex displacement velocity far behind propeller disk
v'_D = vortex displacement velocity at propeller disk
V = relative velocity between blade segment and air
V_{AV} = velocity of air ahead of propeller center
V_{INF} = velocity of air ahead of propeller
V_{GRAD} = wind gradient function
V_P = perpendicular component of V
V_S = velocity of windmill ship
V_T = tangential component of V
w = induced velocity of air far behind propeller disk
w_X = x component of w
w_θ = tangential component of w
x_W = wind coordinates system
x_{Bb} = blade coordinates system fixed on Blade #b
$\mathbb{X}$ = x component of influence coefficient
y_W = wind coordinates system
y_{Bb} = bladecoordinates system fixed on
$\mathbb{Y}$ = y component of influence coefficient
z_W = wind coordinates system
z_{Bb} = blade coordinates system fixed on Blade #b
$\mathbb{Z}$ = z component of influence coefficient
α = angle of attack
ε = index of error
ε_0 = constant for iteration
Γ = circulation around bound vortex, circulation around vortex ring
η = propulsive efficiency
η' = propulsive efficiency given by v'_D
θ = geometrical angle of blade
Θ = tangential component of influence coefficient
λ = Lagrange's parameter
ν = kinetic viscosity of air
ρ = density of air
ϕ = angle of flow to rotating disk
ϕ_v = helical angle
Ψ = azimuth angle
Ω = angular velocity

Superscripts

^ (hat) = range of suffix is converted
' (prime)
= summed value

Subscripts

$( )_{bij}$ = value at j-th blade segment of Blade #b at i-th time step
$( )_{bijckl}$ = value at j-th blade segment of Blade #b at i-th time step induced by vortex ring released by k-th blade segment of Blade #c at l-th time step
$( )_{ij}$ = value at j-th blade segment of Blade #1 at i-th time step
$( )_{ijkl}$ = value at j-th blade segment at of Blade #1 at i-th time step induced by vortex ring released by k-th blade Blade #b

segment of every blade at l-th time step

_(under score)

= time step from initial

1. INTRODUCTION

The earliest among the important studies of the propeller has been done by Betz[1]. He has shown the condition that the minimum induced loss propeller must satisfy, which is known as Betz condition. Prandtl obtained the approximate solution of the minimum induced loss propeller that satisfies the Betz condition. Further, Goldstein[2] obtained the exact solution of the minimum induced loss propeller that satisfies the Betz condition. The most important and fundamental studies of propellers were done by these researchers and are based on the lifting-line theory. Though it is known that these theories are valid even in the middle disk-loading condition in practice, these theories are only rigorous in the light disk-loading condition. Sometimes, however, a windmill, which is usually designed in the high disk loading condition, is designed by using a method based on Prandtl's approximate solution.

As described in Appendix A, vortex sheets are deformed by the velocity induced by themselves. On the other hand, performance of propellers heavily depends on the shape of vortex sheet which requires a vast number of calculations to be determined. The development of computers allows us to calculate the shape of the vortex sheet precisely. Consequently, use of the precise shape of the vortex sheet yields an accurate calculation of the performance of propellers or windmills. The use of vortex sheet is particularly important when we design a windmill and calculate its performance, since the windmills are designed to absorb the energy of air as much as possible, in other words, it is designed for the high disk-loading condition. Although the use of precise shape makes the calculation accurate, an increase of the accuracy is very small when the disk loading is light. Therefore, when the light disk loading condition is assumed, the rigid wake model, that is the vortex sheets from Archimedean screw-like surfaces with constant pitch and constant diameter, makes the calculation sufficiently accurate. Indeed, an ordinary propeller is usually designed in the light disk-loading condition.

Since 1998, the National Aerospace Laboratory of Japan (NAL), Telecommunications Advancement Organization of Japan (TAO) and Communi cations Research Laboratory (CRL) have developed a stratospheric platform that serves for the high-speed telecommunication, traffic observation and earth observation. This stratospheric platform is a blimp that absorbs energy by using the solar cells attached on the upper surface of the hull and stays 20km above a city for a few years. One of the difficulties of this stratospheric platform is the design of the propeller. The propeller and the propulsive system must be highly efficient and light, since the energy stored for night operation is limited and it is difficult to obtain buoyancy at high altitudes. From the standpoint of the aerodynamics, the single large-diameter propeller installed at the stern is ideal[3]. This concept can be seen in the early stage of the studies of the stratospheric platform[4), 5] and is very common in the field of submarines. The propeller at the stern is covered by the boundary layer whose velocity is lower than the outer flow, as shown in Fig 1.1.

Consequently, the propulsive efficiency of the propeller increases by 40% as shown by momentum theory. However, the propeller increases the drag of the hull, since the propeller sucks the hull backwards. As a result, the total increase of the propulsive efficiency is approximately 20%. Though this efficiency increase caused by the stern propeller is quite attractive, it is difficult to install one single large propulsive system at the stern, since the rigidity of the hull at the stern is not strong enough to support the system. Therefore, one must reinforce the stern structure by a hard material, which causes a weight increase of the blimp. Furthermore, the stern propeller causes a concentration of mass on the stern, which makes it difficult to place the center of gravity beneath the center of buoyancy. As a result, though the stern propeller is ideal aerodynamically, it is not ideal structurally.

The conventional blimp uses two propellers installed on a gondola that is supported by catenary curtains, and the internal combustion engines drive

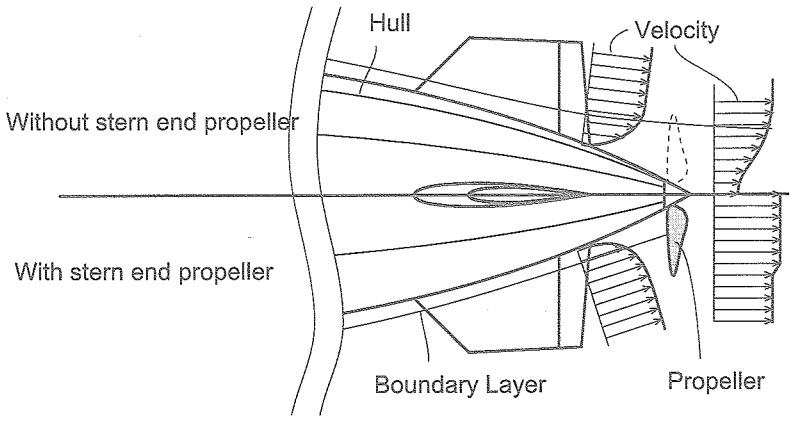

Fig. 1.1 Side view of stern propeller

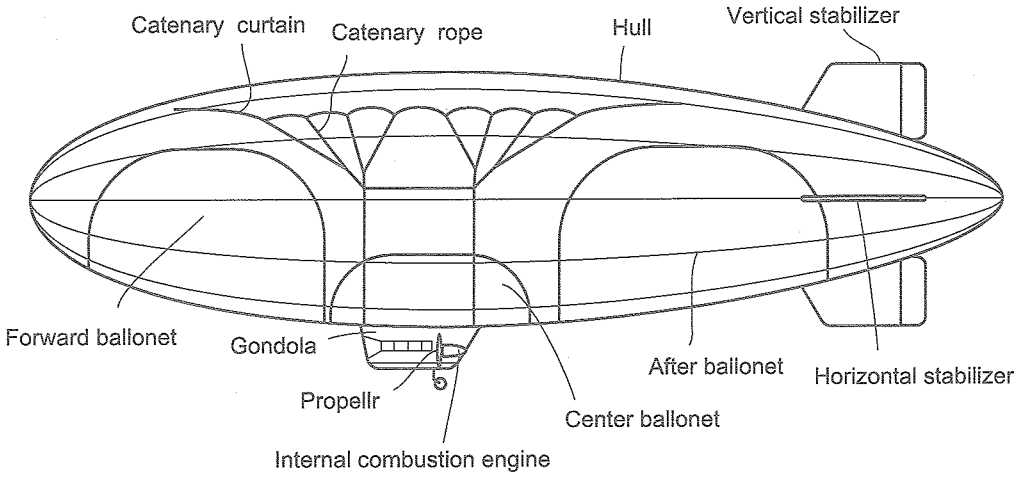

Fig. 1.2 Side view of a conventional blimp

the propellers as shown in Fig 1.2. This configuration is structurally quite rational, which enables the designer to concentrate heavy equipment such as the landing gear, the engines, the propellers and the payload into the gondola. The load caused by the concentrated mass is distributed by catenary curtains over the upper membrane of the hull. Though this configuration is structurally efficient, the diameter of the propeller is smaller than that required aerodynamically. This is partly because the large propeller requires heavy structures such as long struts and a tall gondola. Thus the efficiency of the propeller of the conventional blimp is as small as 60% because of its small diameter.

On the other hand, the concept that multiple small propulsive units be distributed on the surface of the hull, as shown in Fig. 1.3 and Fig. 1.4, is proposed by the authors. This concept makes it possible to remove the catenary curtain and gondola, since the propulsive unit is directly attached to the membrane of the hull. The validity of this concept was proved by the experiment shown in Fig. 1.5. Though the maximum thrust was as much as 50 N, the unit was attached to the inflated membrane firmly without any vibration. Further, by uniting the propeller, the motor and the batteries into one small unit as shown in Fig 1.4, the following merits are expected.

First, the length of the power line that causes the power loss and the increase of the weight is minimized. Second, the total weight of the propeller blades becomes light because of the scale effect. Third, the development of the stratospheric platform becomes easy, since the increase of the required thrust during the development of the stratospheric platform can be adjusted by the increase of the number of propulsive units. Fourth, the hull stress caused by the mass concentration is alleviated by distributing the propulsive unit, which is the heaviest among the equipment. Fifth, the disk-loading of propeller becomes light, which is the most important factor for increasing the propulsive efficiency since the total area of the propeller disks can be increased by increasing the number of the propulsive units. Sixth, and this is the issue treated in this paper, the increase of the propulsive efficiency is expected to increase in the same way as the propulsive efficiency of the stern propeller, since the small diameter propeller can be designed to work in the boundary layer.

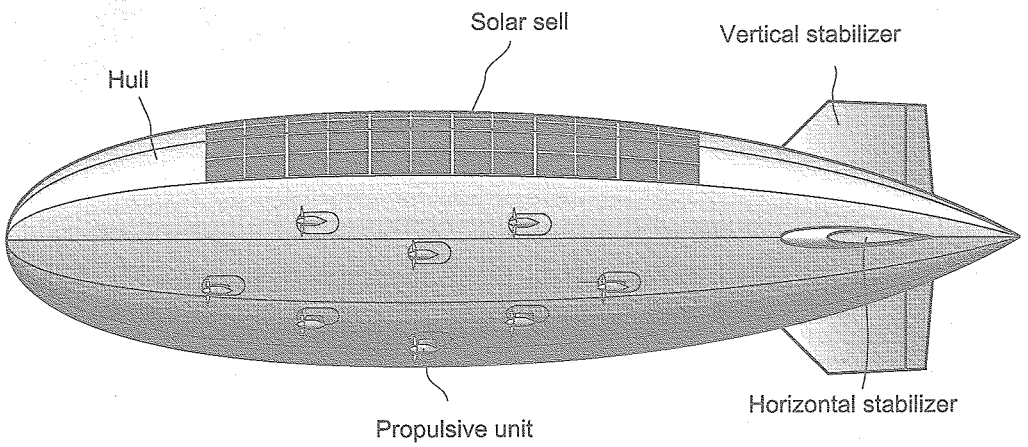

Fig.1.3 Concept of the multi small distributed propulsive unit. Side view of a 25m class blimp

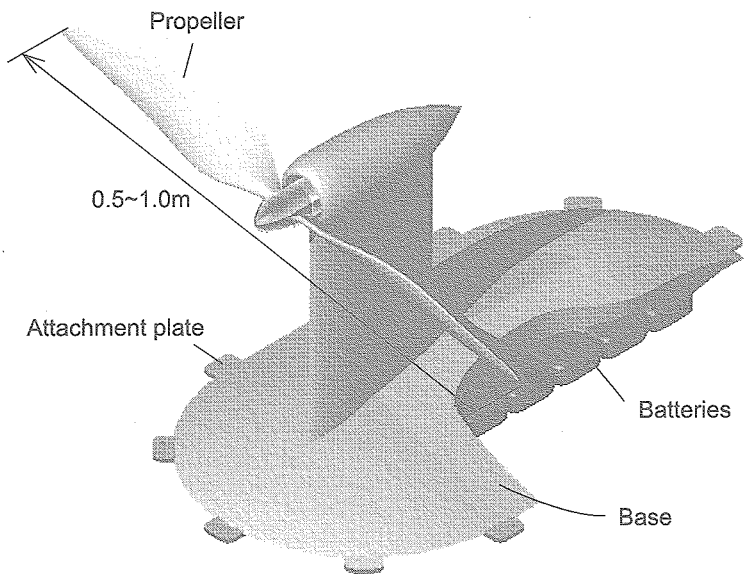

Fig. 1.4 Bird's eye view of the propulsive unit.

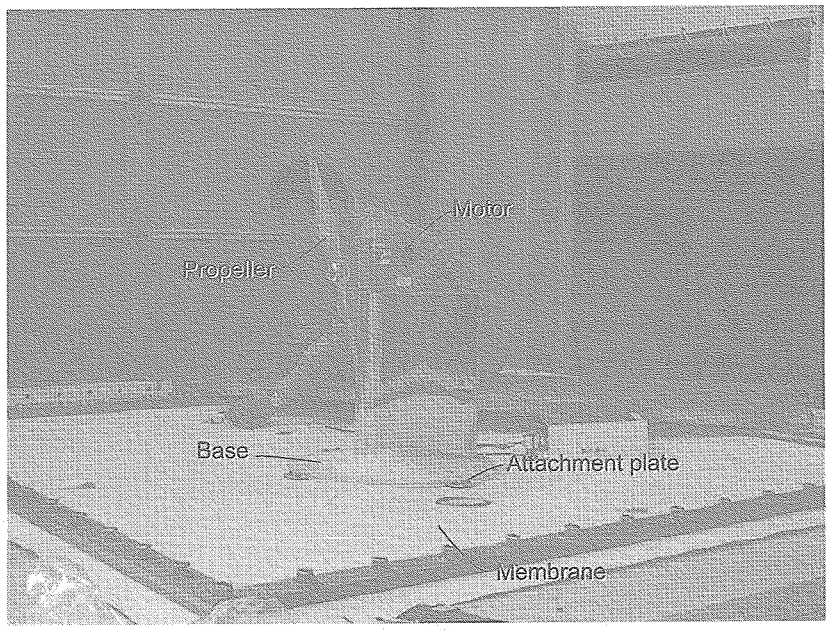

Fig. 1.5 Experiment of the propulsive unit. The power of the motor is 1kW. The weight of the unit is 1.5kg. The maximum thrust is 50N. The deferential pressure in the inflated membrane is 100~400Pa.

Of course, the efficiency of the small propeller may also be decreased by the effect of the lower Reynolds number.

It is estimated that the length of the stratospheric platform for commercial use is nearly 200m, the maximum velocity, U_{max}, is 30m/s and the flight altitude is 20km. If it is assumed that the hull is a flat plate and the boundary layer is the turbulent boundary layer, the thickness of the boundary layer, δ is given by[6];

$$\delta(x) = 0.37x(U_{max}x/\nu)^{-1/5} \qquad (1.1)$$

where x is the distance from the bow and ν is the kinetic viscosity of air. δ at x=100m is approximately 1.3m. Thus, a propeller with 1.0m diameter can work in the boundary layer whose velocity is lower than the outer flow. The propulsive efficiency of the propeller in the boundary layer is higher than that in the outer flow, as described in the explanation of the stern propeller. Unlike the stern propeller, however, the inflow velocity is not symmetrical about the rotating axis. Thus, the action of the propeller in the boundary layer is unsteady. The development of the optimum design of this unsteady propeller in the wind gradient is the purpose of this paper. The velocity of the air in the turbulent boundary layer, u, is approximately given by:

$$u/U_{max} = (y/\delta)^{1/7} \qquad (1.2)$$

where y is the vertical distance from the surface. Fig. 1.6 shows the profile of u/U_{max}. This also shows one of the propellers for the stratospheric platform. The diameter of this propeller, D, is 0.8δ and the clearance between the surface and the propeller is 0.2δ. In this case, the gradient of the velocity of the air that passes the propeller disk, w_G, is approximately given by:

$$w_G = 0.2U_{AV}/D \qquad (1.3)$$

This equation is only one of the equations that for w_G, whose value depends on the relative size of the propeller based on the value of δ.

Windmills have close relation to propellers and can be regarded as a special case of propellers that generate power instead of consuming power. It is

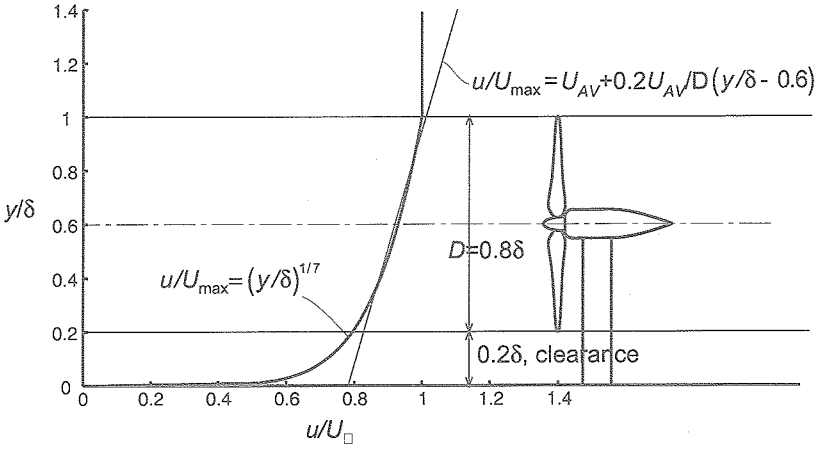

Fig. 1.6 Velocity of air in the turbulent boundary layer.

not, however, adequate to apply Prandtl's approximate solution to the design of the windmill, since the windmill is designed in the high disk-loading condition. This condition is inevitable, since the purpose of the windmill is absorb the energy of wind as much as possible. However, the rotor for a windmill ship is designed to minimize (drag)/(power). The concept of the windmill ship is old.

The windmill ship absorbs power from the wind by using roter, and rotates the screw by the power as shown in Fig 1.7. Though it is possible to travel against the wind by the power from the windmill, the practical windmill ship may use the combined system consisting the rotor and a conventional power source such as a diesel engine. When the windmill ship travels against the wind, it is required that the drag of the windmill be small. Thus, the light disk-loading assumption can be applied to thedesign of this windmill. It is known that there is a wind gradient over the sea and ground. The windmill on the ground can work in the uniform wind high above the ground by using a high pole. However, the use of a high mast in the windmill ship is dangerous, since the rolling moment caused by the windmill increases. Thus, the windmill ship must use low masts and the windmill works in the wind gradient.

The main purpose of this paper is to introduce a method for obtaining the optimum propeller (windmill) in the wind gradient, and to show examples of the calculation.

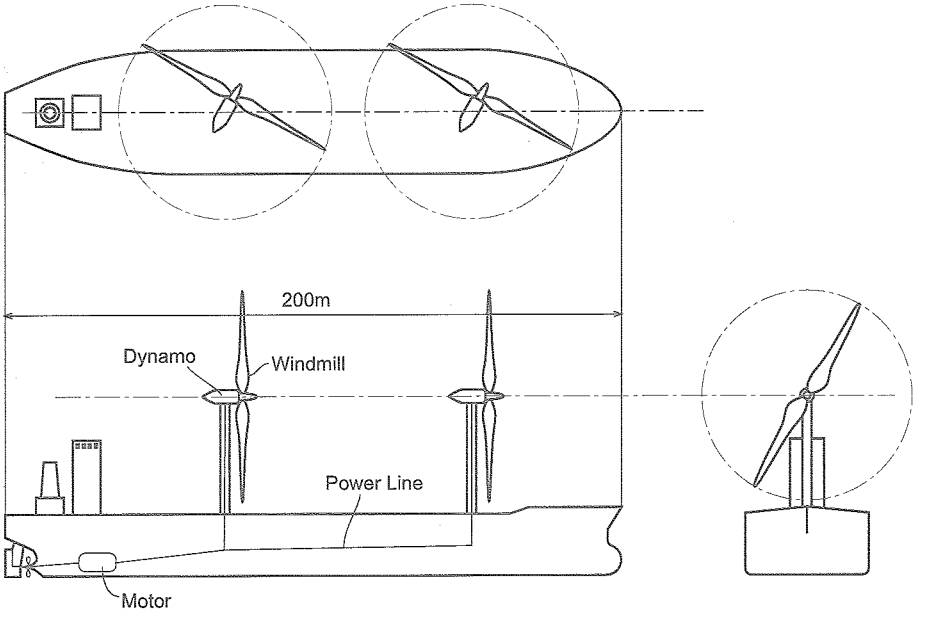

Fig 1.7 200m class windmill ship.

2. Optimum design by Momentum Theory

2.1. Problem

In this chapter, the thrust distribution of a propeller rotating in a wind gradient is optimized by using an expanded momentum theory. The radius of the propeller is R(m) and the angular velocity of the propeller is Ω(rad/s) as shown in Fig. 2.1. The velocity of the wind at z=0 is V_{AV}(m/s), and the wind gradient is a function of z, V_{GRAD}(z)(m/s); where z is the height from the axis of the propeller. Thus, the wind velocity far ahead of the propeller disk, V_{INF} (m/s), is given by :

$$V_{INF} = V_{AV} + V_{GRAD}(z) \qquad (2.1)$$

It is assumed that the flow behind the propeller is non-rotating and steady. By this assumption, a simple momentum theory can be used.

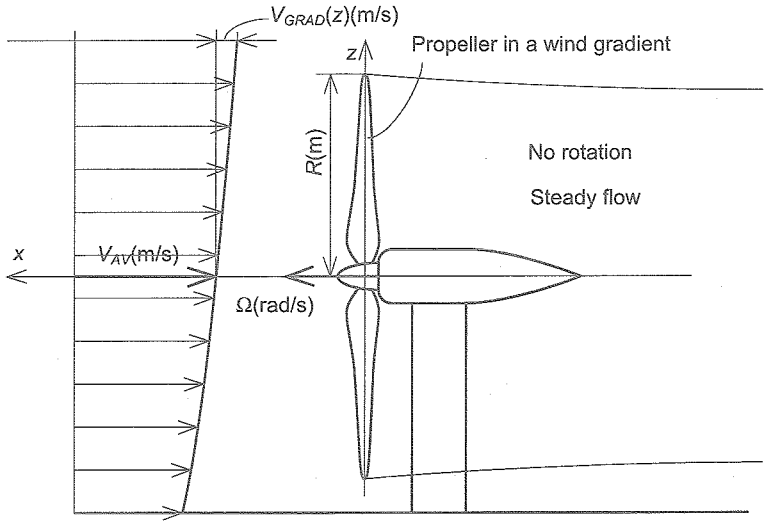

Fig. 2.1 Side view of a propeller in a wind gradient

2.2. Simple Momentum Theory

In this section, a conventional propeller in a uniform flow and the simple momentum theory are briefly discussed. It is assumed that the velocity behind the propeller is uniform. Fig. 2.2 shows the flow around the propeller. The velocity of the flow far ahead of the propeller is V_{INF}. The propeller accelerates the flow at the propeller disk, and the velocity becomes:

$$V_{DISK}=V_{INF}+v \qquad (2.2)$$

where v is the induced velocity. Far behind the propeller, the velocity becomes[7]:

$$V_{DOWN}=V_{INF}+2v \qquad (2.3)$$

The mass of the air that passes through the propeller disk per unit time, m(kg/s), is:

$$\dot{m} = \rho S(V_{INF} + v) \qquad (2.4)$$

where S(m^2) is the area of the propeller disk (also referred as the "actuator area") and ρ(kg/m^3) is the density of air. The thrust is the reaction of the increase of the momentum of the air. Thus, the thrust of the propeller is given by:

$$T = \dot{m}V_{DOWN} - \dot{m}V_{INF} = 2\rho Sv(V_{INF} + v) \qquad (2.5)$$

Furthermore, the power consumed by the propeller, P, equals the difference of energy between the upstream and downstream flow.

$$P = \frac{1}{2}\dot{m}V_{DOWN}^{\ 2} - \frac{1}{2}\dot{m}V_{INF}^{\ 2} \qquad (2.6)$$

From Eqs.(2.2), (2.3) and (2.6), P is given by:

$$P = 2\rho Sv(V_{INF} + v)^2 \qquad (2.7)$$

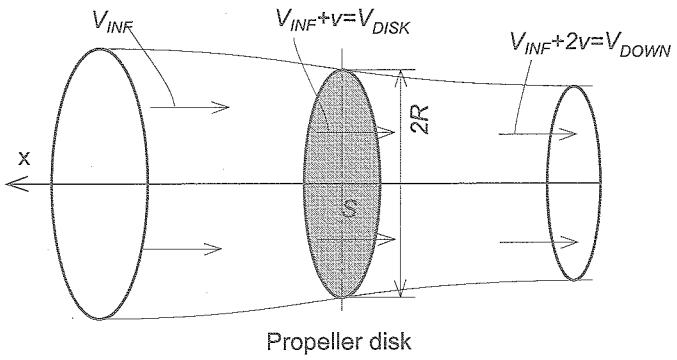

Fig. 2.2 Flow around the Propeller

2.3. Expanded Momentum Theory

In this section, the thrust distribution of a propeller rotating in a wind gradient is optimized. It is assumed that small segments of the propeller disk, *dydz*, do not interfere each other. Thus the simple momentum theory can be applied to each small segment as if the small segments were isolated small actuator areas. Fig. 2.3 shows this concept briefly. The velocity of the flow far ahead of propeller, V_{INF}, is given by Eq. (2.1). By expanding the concept of Eq. (2.5), the local thrust on the small segment, dT, is given by:

$$dT = 2\rho v(V_{INF} + v)dydz \tag{2.8}$$

Also, by expanding the concept of Eq. (2.7), the local power on the small segment, dP, is given by:

$$dP = 2\rho v(V_{INF} + v)^2 dydz \tag{2.9}$$

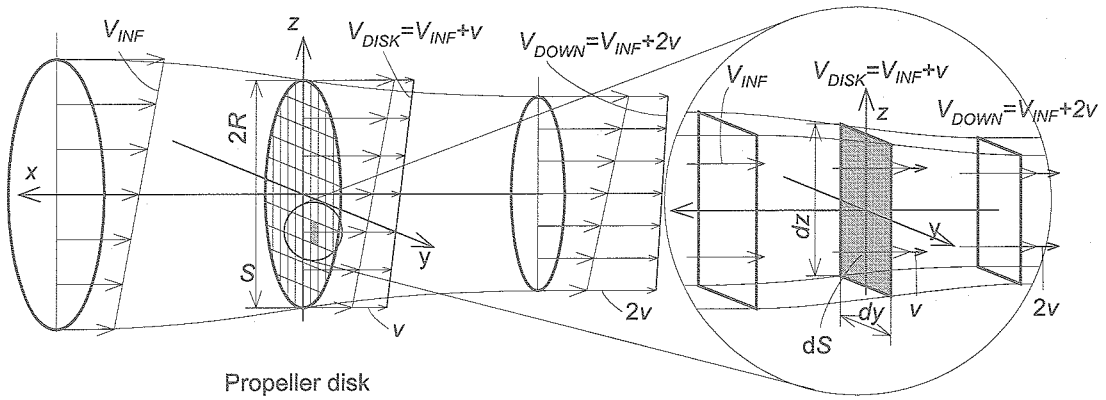

Fig. 2.3 Concept of an isolated propeller disk segment

By integrating Eq. (2.8) and (2.9), the total thrust, T, and total power, P, becomes:

$$T = \iint_S 2\rho v(V_{INF} + v)\, dydz \tag{2.10}$$

$$P = \iint_S 2\rho v(V_{INF} + v)^2 dydz \tag{2.11}$$

The problem of optimizing the thrust distribution of a propeller rotating in a wind gradient can be rewritten as follows:

Problem

maximize T

subject to $P=P_0$

where P_0 is constant. From Eqs. (2.10) and (2.11), the Hamiltonian of Problem becomes:

$$H = 2\rho v(V_{INF} + v) + \lambda\left\{2\rho v(V_{INF} + v)^2\right\} \tag{2.12}$$

where λ is Lagrange's parameter. H is a function of only v and z, thus Euler's Equation becomes:

$$\frac{\partial H}{\partial v} - \frac{d}{dz}\left(\frac{\partial H}{\partial v'}\right) = 0 \qquad (2.13)$$

where ' denotes the partial derivative with respect to z. Eq. (2.12) into Eq. (2.13) gives:

$$\frac{\partial}{\partial v}\left[2\rho v(V_{INF}+v)+\lambda\left\{2\rho v(V_{INF}+v)^2\right\}\right]=0 \quad (2.14)$$

From this we obtain:

$$v=\frac{1}{3\lambda}\left\{-(1+2\lambda V_{INF})\pm\sqrt{\lambda^2 V_{INF}{}^2+\lambda V_{INF}+1}\right\} \quad (2.15)$$

Although Eq. (2.15) has + and – signs ahead of the square root, the positive sign does not give a positive value of v. Thus only the negative sign is valid. Eq. (2.15) seems to give the value of v, but it still contains the unknown parameter λ. This must be determined by using Eq. (2.11) and the condition, $P=P_0$. However, it is almost impossible to determine λ analytically. Therefore, λ is obtained by computation.

2.4. Example

To compute Lagrange's parameter, λ, for a specific example, the following values were used: the radius of the propeller, R, is 1.0m; the velocity of flow far ahead of the propeller center, V_{AV}, is 10 m/s, the wind gradient function, $V_{GRAD}(z)$, is given by:

$$V_{GRAD}(z)=2.0z \qquad (2.16)$$

Fig. 2.4 shows the relation between λ and the total power, P, of the propeller in the wind gradient. From this figure, we obtain λ=–0.9689 for P=100W and λ=–0.9926 for P=0W. When P=100W, total thrust is 11.7N, whereas the thrust is 9.87N when P=100W with no wind gradient. Furthermore, even when P=0W, thrust has a positive value, 1.92N. That is, a propeller in a wind gradient can generate thrust without power. Fig. 2.5 shows the induced velocities, v, as functions of z, and Fig. 2.6 shows the local thrusts as functions of z. These figures show that the region where the propeller generates thrust corresponds to the region where the V_{INF} is lower than V_{AV} the region where the propeller generates drag corresponds to the region where the V_{INF} is higher than V_{AV} Fig. 2.7 shows the local powers as functions of z. This figure shows that the region where the propeller consumes the power approximately corresponds to the region where the V_{INF} is lower than V_{AV} and the region where the propeller absorbs the power from the air approximately corresponds to the region where the V_{INF} is higher than V_{AV}.

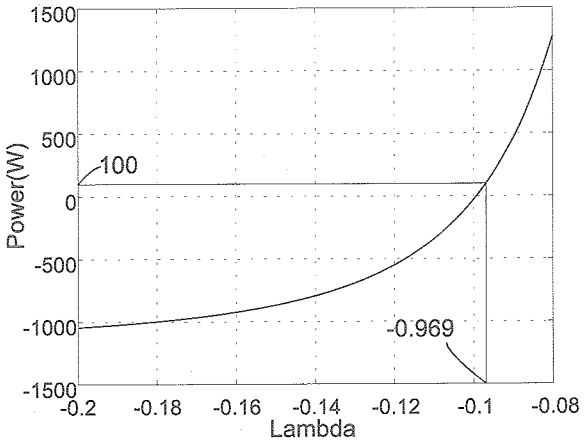

Fig. 2.4 Lambda and Power

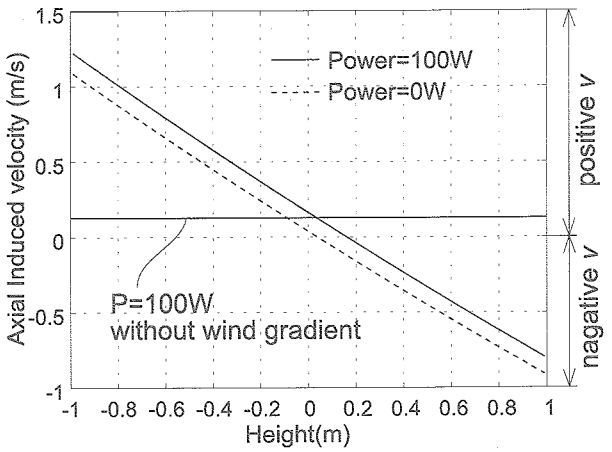

Fig 2.5 Induced Flow Distribution

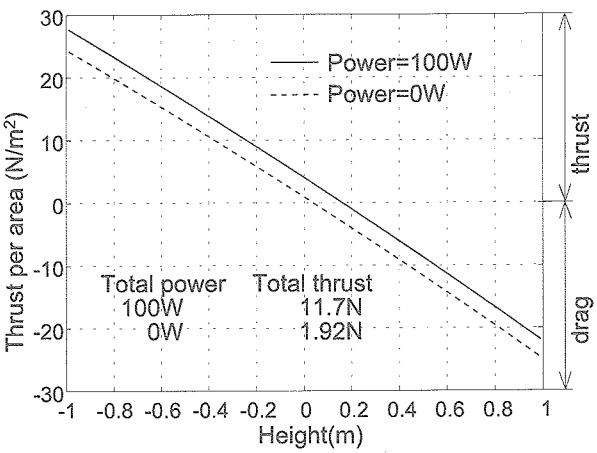

Fig. 2.6 Thrust Distribution

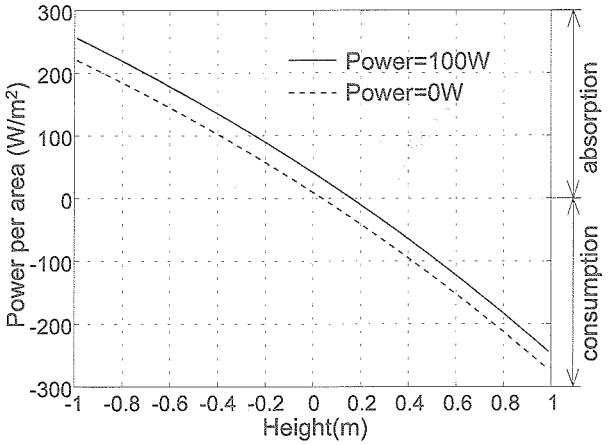

Fig. 2.7 Power Distribution

3. Analysis of Steady Propeller by Vortex Method

3.1. Propeller Model in Uniform Flow

In the previous chapter, the thrust distribution of a propeller in a wind gradient was optimized using the expanded momentum theory. The result of the previous chapter has shown that a propeller in a wind gradient generates thrust without power. This result is amazing but doubtful since the momentum theory is not exactly accurate and is valid only with strong assumptions. In this chapter, the method for calculating the performance of a propeller that works in a uniform flow is described.

Fig. 3.1 shows the propeller treated here, which has the following properties: the radius of the propeller is R(m); the number of the blades is B; the angular velocity of the propeller is Ω(rad/s); The chord length of the propeller blades is c(m); The geometrical angle of the propeller blades is θ(rad). Further, the velocity of air far ahead of the propeller, V_{INF}(m/s), is uniform and constant. The purpose of this chapter is to describe the method for calculating the thrust generated by the propeller with the effect of the profile drag, T_D(N), the power consumed by the propeller with the effect of the profile drag, P_D(W), the thrust generated by the propeller without the effect of the profile drag, T(N), and the power consumed by the propeller without the effect of the profile drag, P(W). It is assumed that the induced velocity is much lower than the wind velocity. This assumption is valid only when the disk-loading is very light. However this assumption makes it easy to use the vortex method, because the vortex method has usually an inevitable difficulty. That is, it is difficult to determine the shape of the trailing vortices because the induced velocity deforms the wake and elongates the pitch of the wake, d(m). This difficulty is very important and discussed further in Appendix A. If the induced velocity is negligible small, both the deformation of the wake and the elongation of the pitch are negligible, and the trailing vortices form an Archimedean screw like surface.

3.2. Definitions

The propeller is described by using a right-hand coordinate system as shown in Fig. 3.2: the number

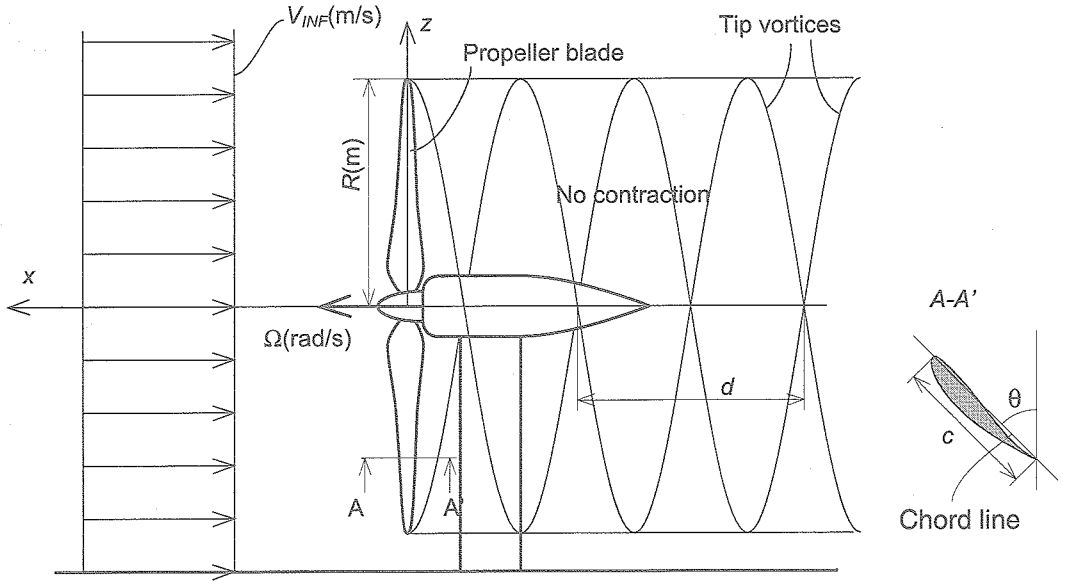

Fig. 3.1 Side view of a propeller in a uniform stream

of blades is B; Blade #1 is on the y-axis; the rotating direction of the propeller is counterclockwise; the trailing vortices form an Archimedean screw like surface with constant pitch, d(m). From the previous assumption, this d is given by:

$$d = \frac{2\pi V_{INF}}{\Omega} \qquad (3.1)$$

Further, the trailing vortices are designated by the following definition as shown in Fig. 3.3.

- Each blade is divided into N segment width of the segments is dR(m).
- The bj-th trailing vortex is released from the inner end of the j-th segment of Blade #b.
- The j-th control point, $C.P.(j)$, is located on the middle of the j-th blade segment of Blade #1.
- The current j-th dividing point, $D.P.(b, 0, j)$, is located on the inner end of the j-th segment of Blade #1.
- The bij-th dividing point, $D.P.(b, i, j)$, stands for the position of the j-th dividing point of Blade #b at the i-th time step, idt(sec).
- The b-th vortex sheet stands for the vortex sheet released from Blade #b.
- The bj-th blade segment stands for the j-th blade segment of Blade #b.
- The range of i is [-M, 0], and M is very large number
- The bj-th horse shoe vortex consists of the bj-th trailing vortex, vortex A, and the bound vortex on the bj-th blade segment, and the (b, j+1)th trailing vortex, vortex B as shown in Fig. 3.3.
- The strength of the circulation around bj-th horse shoe vortex is Γ_j, and it is assumed that the j-th horse shoe vortices of each blade are identical.

3.3. Influence Coefficients

Influence coefficients, ($\mathbb{X}_{ij}$, $\mathbb{Y}_{ij}$, $\mathbb{Z}_{ij}$), are defined as the magnitude of the induced velocities at $C.P.(i)$, (v_{Xi}, v_{Yi}, v_{Zi}), induced by the j-th horse shoe vortex with a unit circulation strength on each blade. Therefore, v_{Xi}, v_{Yi} and v_{Zi} are given by:

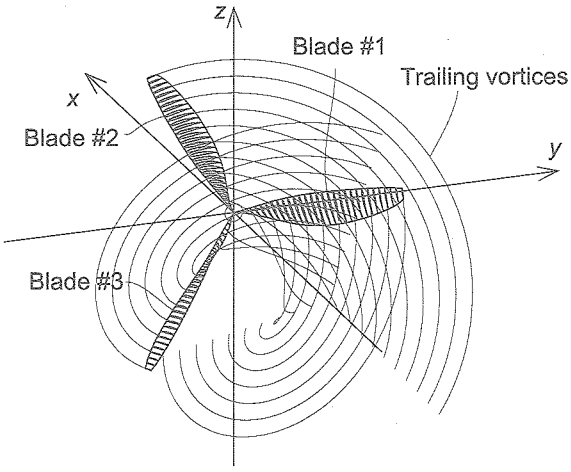

Fig. 3.2 Coordinates of propeller: B=3

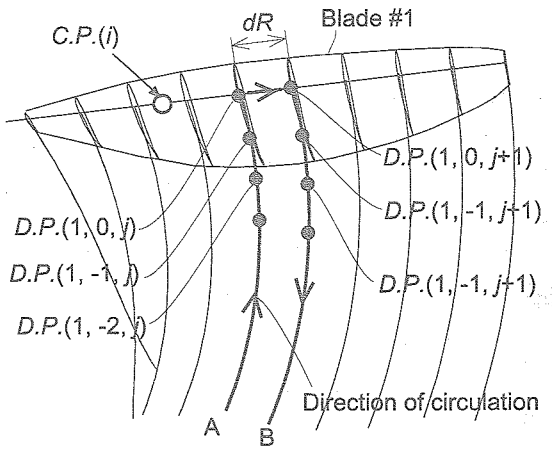

Fig. 3.3 Definition of points on the vortex sheet released from Blade #1

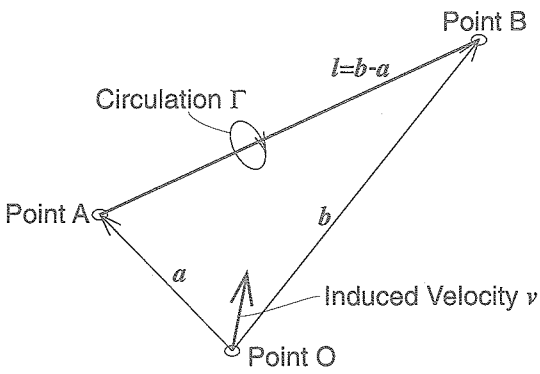

Fig. 3.4 The Biot-Savart law. The Velocity at Point O Induced by the circulation around Segment A-B.

$$v_{Xi} = \sum_{j=1}^{N} \mathbf{X}_{ij} \Gamma_j \tag{3.2}$$

$$v_{Yi} = \sum_{j=1}^{N} \mathbf{Y}_{ij} \Gamma_j \tag{3.3}$$

$$v_{Zi} = \sum_{j=1}^{N} \mathbf{Z}_{ij} \Gamma_j \tag{3.4}$$

When a trailing vortex is the straight segment between Point A and Point B, A-B, as shown in Fig. 3.4, the velocity of the flow at Point O induced by the circulation around A-B is obtained from the Biot-Savart law as:

$$v = \frac{\Gamma}{4\pi} \frac{a \times l}{|a \times l|^2} \left(\frac{b}{|b|} - \frac{a}{|a|} \right) \cdot l \tag{3.5}$$

where a and b are vectors from Point O to Point A and Point B respectively and l is b - a.

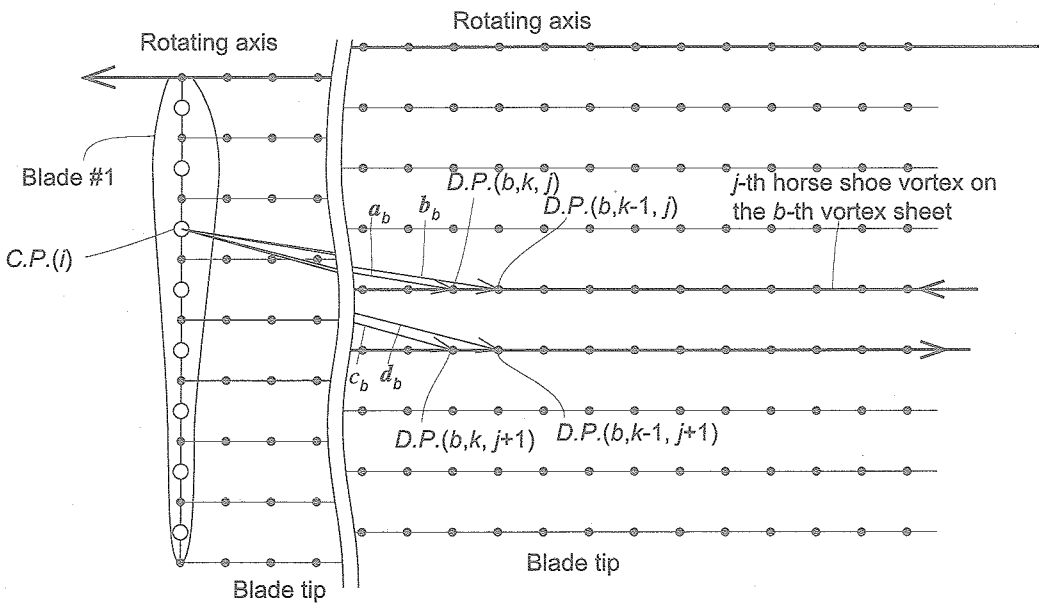

Fig. 3.5 Definition of vectors on the b-th vortex sheet.
The vortex sheet is flattened to illustrate.

In a similar fashion, the influence coefficients between $C.P.(i)$ and the j-th horse shoe vortex ($\mathbf{X}_{ij}$, $\mathbf{Y}_{ij}$, $\mathbf{Z}_{ij}$), are given by:

$$\left(\mathbf{X}_{ij}, \mathbf{Y}_{ij}, \mathbf{Z}_{ij}\right)^{\mathrm{T}} =$$

$$\frac{1}{4\pi} \sum_{b=1}^{B} \sum_{k=1}^{M} \left\{ -\frac{a_b \times l_b}{|a_b \times l_b|^2} \left(\frac{b_b}{|b_b|} - \frac{a_b}{|a_b|} \right) \cdot l_b + \frac{c_b \times l'_b}{|c_b \times l'_b|^2} \left(\frac{d_b}{|d_b|} - \frac{c_b}{|c_b|} \right) \cdot l'_b \right\} \tag{3.6}$$

where a_b, b_b, c_b and d_b are vectors from $C.P.(i)$ of Blade #1 to $D.P.(b, k, j)$, $D.P.(b, k\text{-}1, j)$, $D.P.(b, k, j\text{+}1)$ and $D.P.(b, k\text{-}1, j\text{+}1)$ respectively as shown in Fig. 3.5; l_b is the vector defined by $l_b = b_b\text{-}a_b$ and l'_b is $d_b\text{-}c_b$. In Eq. (3.6), the first term represents the influence of the circulation around the vortex segment between $D.P.(b, k, j)$ and $D.P.(b, k\text{-}1, j)$. Also, the second term represents the influence of the circulation around the vortex segment between $D.P.(b, k, j\text{+}1)$ and $D.P.(b, k\text{-}1, j\text{+}1)$.

3.4. Thrust and Power with Effect of Profile Drag

In this section the total thrust generated by the propeller with the effect of the profile drag, T_D, and the total power consumed by the propeller with the effect of the profile drag, P_D, are obtained.

The angle of attack of 1i-th blade segment, α_i (rad), and the relative velocity between this segment and the air, V_i(m/s), are given by the vector diagram shown in Fig. 3.6: where V_{Ti}(m/s) is the relative velocity at $C.P.(i)$ tangential to the rotating disk; V_{Pi}(m/s) is the relative velocity at $C.P.(i)$ perpendicular to the rotating disk; ϕ_i(rad) is the angle of flow to the rotational disk; θ_i(rad) is the geometrical angle of the 1i-th blade segment; r_i is the distance between the center of rotation and $C.P.(i)$. From this diagram, V_{Ti} and V_{Pi} are given by:

$$V_{Ti} = r_i\Omega - v_{Zi} \tag{3.7}$$

$$V_{Pi} = V_{INF} - v_{Xi} \tag{3.8}$$

and V_i is given by:

$$V_i = \sqrt{V_{Ti}^{\ 2} + V_{Pi}^{\ 2}} \tag{3.9}$$

Using V_{Ti} and V_{Pi}, ϕ_i is given by:

$$\phi_i = \tan^{-1}\left(\frac{V_{Pi}}{V_{Ti}}\right) \tag{3.10}$$

From Fig. 3.6, α_i is given by;

$$\alpha_i = \theta_i - \phi_i \tag{3.11}$$

The lift generated by the 1i-th blade segment, L_i(N), is:

$$L_i = \frac{1}{2}\rho V_i^2 C_L(\alpha_i, Re_i) c_i dR \tag{3.12}$$

where ρ(kg/m^3) is the density of air: c_i(m) is the chord length of the 1i-th blade segment; C_L is the lift coefficient that is a function of α and Reynolds number, Re. Also the drag generated by the 1i-th blade segment, D_i(N), is:

$$D_i = \frac{1}{2}\rho V_i^2 C_D(\alpha_i, Re_i) c_i dR \tag{3.13}$$

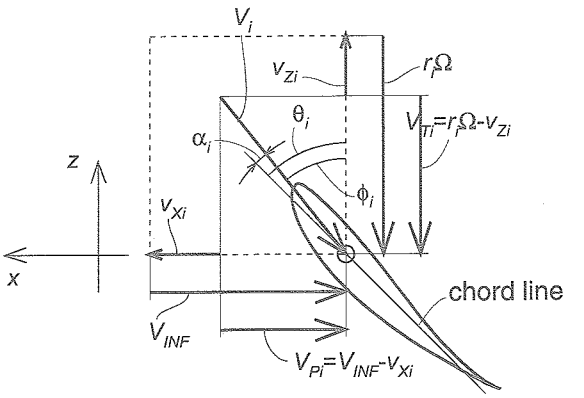

Fig. 3.6 Vector diagram of i-th blade segment of Blade #1.

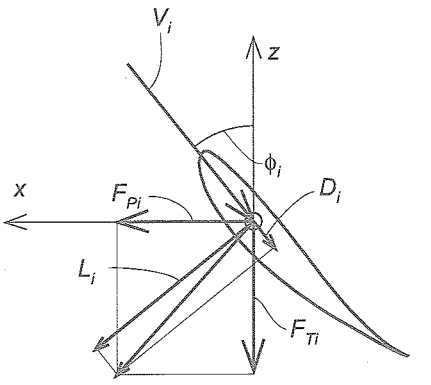

Fig. 3.7 Forces act on the i-th blade segment of Blade #1

where C_D is the drag coefficient that is a function of α and Re. From Fig. 3.7, the force of the 1i-th blade segment perpendicular to the rotating disk, F_{Pi}, is given by:

$$F_{Pi} = L_i \cos\phi_i - D_i \sin\phi_i \tag{3.14}$$

Similarly, the force of the i-th blade segment tangential to the rotating disk, F_{Ti}, is given by:

$$F_{Ti} = D_i \cos\phi_i + L_i \sin\phi_i \tag{3.15}$$

The summation of Eq. (3.14) multiplied by B gives the total thrust:

$$T_D = B\sum_{i=1}^{N} F_{Pi} \tag{3.16}$$

Similarly, Eq. (3.15) gives the total power:

$$P_D = B\sum_{i=1}^{N} F_{Ti} r_i \Omega \tag{3.17}$$

If R, V_{INF}, Ω c_i, θ_i, $C_L(\alpha)$ and $C_D(\alpha)$ are given, it seems possible to obtain T_D and P_D from the above equations. However, T_D and P_D still contain the unknown variables, Γ_i.

3.5. Thrust and Power without Effect of Profile Drag

In this section the thrust generated by the propeller without the effect of the profile drag, T(N), and the power consumed by the propeller without the effect of the profile drag, P(W), are obtained.

From the Kutta-Joukowsky theorem the thrust caused by the circulation around the 1i-th blade segment, T_i(N), is given by:

$$T_i = \rho\Gamma_i V_{Ti}\, dR \tag{3.18}$$

Similarly, the power caused by the circulation around the 1i-th blade segment, P_i(W), is given by:

$$P_i = \rho\Gamma_i V_{Pi}\, dR r_i \Omega \tag{3.19}$$

The summation of Eq. (3.18) multiplied by B gives the total thrust, T(N), caused by the circulations:

$$T = B\sum_{i=1}^{N} \rho\Gamma_i V_{Ti}\, dR \tag{3.20}$$

Further, Eqs. (3.4), (3.7) and (3.20) give:

$$T = B\sum_{i=1}^{N} \rho\Gamma_i \left(r_i\Omega - \sum_{j=1}^{N} \mathbb{Z}_{ij}\Gamma_j \right) dR \tag{3.21}$$

Similarly, the summation of Eq. (3.19) multiplied by B gives the total power, P(W), caused by the circulations:

$$P = B\sum_{i=1}^{N} \rho\Gamma_i V_{Pi}\, dR r_i\Omega \tag{3.22}$$

Further, Eqs. (3.2), (3.8) and (3.22) give:

$$P = B\sum_{i=1}^{N} \rho\Gamma_i \left(V_{INF} - \sum_{j=1}^{N} \mathbb{X}_{ij}\Gamma_j \right) dR r_i\Omega \tag{3.23}$$

3.6. Determination of Circulations

The lift from Eq. (3.12) equals the lift caused by the circulation given by:

$$L_i = \rho\Gamma_i V_i\, dR \tag{3.24}$$

Therefore, the following equation holds:

$$\frac{1}{2}\rho V_i^2 C_L(\alpha_i, Re_i) c_i\, dR = \rho\Gamma_i V_i\, dR \tag{3.25}$$

one thus obtains:

$$\Gamma_i = V_i C_L(\alpha_i, Re_i) c_i \tag{3.26}$$

where α_i is the angle of attack of 1i-th blade segment as described before. From Eqs. (3.7), (3.8), (3.10) and (3.11), α_i is given by the function of the induced velocities:

$$\alpha_i = \theta_i - \tan^{-1}\left(\frac{V_{INF} - v_{Xi}}{r_i\Omega - v_{Zi}} \right) \tag{3.27}$$

Furthermore, Eqs. (3.2) and (3.4) into Eq. (3.27) gives this as a function of the circulations:

$$\alpha_i = \theta_i - \tan^{-1}\left(\frac{V_{INF} - \sum_{j=1}^{N} \mathbb{X}_{ij}\Gamma_j}{r_i\Omega - \sum_{j=1}^{N} \mathbb{Z}_{ij}\Gamma_j} \right) \tag{3.28}$$

Eq. (3.28) into Eq. (3.26) then gives closed equations for the circulations:

$$\Gamma_i = V_i C_L\left\{ \theta_i - \tan^{-1}\left(\frac{V_{INF} - \sum_{j=1}^{N} \mathbb{X}_{ij}\Gamma_j}{r_i\Omega - \sum_{j=1}^{N} \mathbb{Z}_{ij}\Gamma_j} \right), Re_i \right\} c_i \tag{3.29}$$

It is very difficult to solve Eq. (3.29) analytically because of its nonlinearity. However, the following iteration procedure may be used to solve Eq. (3.29):

Step 1: Select the initial values of Γ_i, $\Gamma_i^{(1)}$; where $^{()}$ indicates the iterating number. For example $\Gamma_i^{(1)}$=0.

Step 2: Calculate the values of $\Gamma_i^{(N+1)}$ using $\Gamma_i^{(N)}$ and Eq. (3.29)

Step 3: Calculate the index of error, $\varepsilon^{(N+1)}$, defined by:

$$\varepsilon^{(N+1)} = \sum_{i=1}^{N} \left\{ \Gamma_i^{(N+1)} - \Gamma_i^{(N)} \right\}^2 \qquad (3.30)$$

Step4: Evaluate $\varepsilon^{(N+1)}$. If $\varepsilon^{(N+1)} < \varepsilon_0$ (where ε_0 is a small number) then stop, otherwise repeat Step2:

Once the circulations are obtained, induced velocities are given by Eqs. (3.2), (3.3) and (3.4). Further, T_D and P_D are given by Eqs. (3.7) through (3.17), and T and P are given by Eqs. (3.21) and (3.23).

3.7. Procedure of Steady Propeller Analysis

T_D and P_D have been obtained. The procedures to calculate them is as follows:

1. Specify the propeller, V_{INF}, Ω, R, M, N, dt, c_i and θ_i.
2. Determine the position of $C.P.(i)$ and $D.P.(b, i, j)$.
3. Calculate $\mathbb{X}_{ij}$, $\mathbb{Y}_{ij}$ and $\mathbb{Z}_{ij}$ from Eq. (3.6)
4. Determine Γ_i by using the iterative procedure described in Section 6.
5. Calculate v_{Xi} and v_{Zi} using Eqs. (3.2) and (3.4)
6. Calculate T_D and P_D using Eqs. (3.7) through (3.17)

T and P have been also obtained here for the convenience in the later chapters. The procedure to calculate them is the same procedure described above except Procedures 5 and 6. Instead of Procedures 5 and 6, the following procedure is used:

5. Calculate T and P using Eqs. (3.21) and (3.23)

Note that the light disk-loading assumption in which v_{Xi} and v_{Zi} are negligible small compared with V_{INF} is employed here in order to make it possible to determine the shape of the trailing vortices. Hence, T_D, P_D, T and P obtained by the above procedure are not reliable, if v_{Xi} and v_{Zi} are not negligibly small compared with V_{INF}.

4. Analysis of Unsteady Propeller by Vortex Method

4.1. Propeller Model without Effect of Vortex Shear

In the previous chapter the method for calculating the thrust and the power of a propeller in a uniform wind has been described. In this chapter, the method for calculating the thrust and the power of a propeller that works in a wind gradient is described. At first, the trailing vortices and the shed vortices are assumed to form an Archimedean screw-like surface instead of a sheared Archimedean screw surface.

Fig. 4.1 shows the propeller treated here, which has the following properties: the radius of the propeller is R(m); the number of the blades is B; the angular velocity of the propeller is Ω(rad/s); the

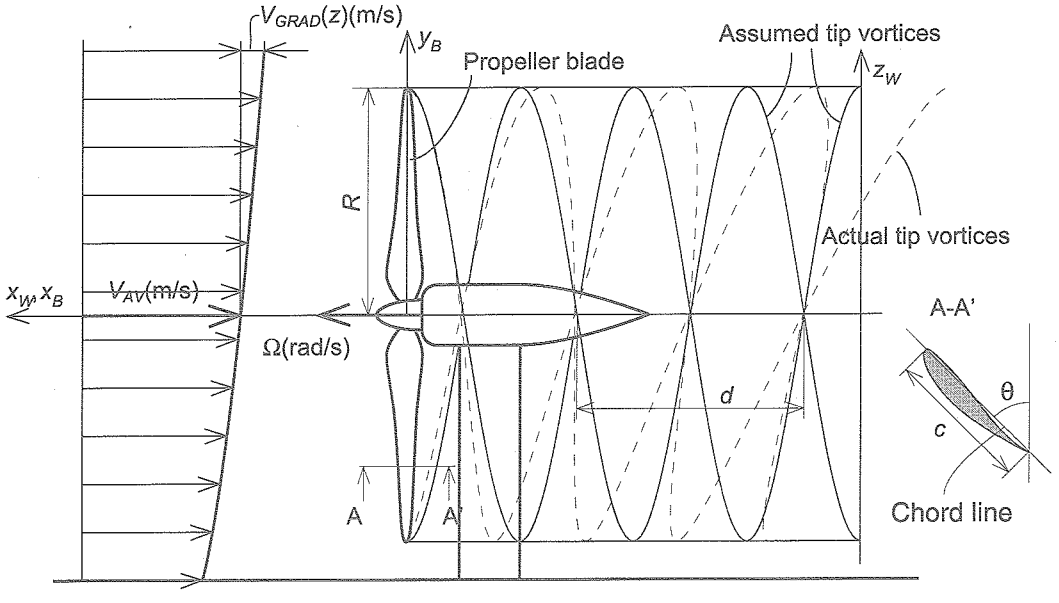

Fig. 4.1 Side view of the propeller in a wind gradient.

chord length of the propeller blades is c(m); the geometrical angle of the propeller blades is θ(rad). Further, the velocity of air ahead of the propeller, V_{INF}(m/s), is the function of the height given by:

$$V_{INF} = V_{AV} + V_{GRAD}(z) \tag{4.1}$$

where V_{AV} is the velocity of the air far ahead of the propeller center and V_{GRAD} is a wind gradient function. The purpose of this chapter is to describe the method for calculating the thrust generated by this propeller with the effect of the profile drag, T_D(N), the power consumed by the propeller with the effect of the profile drag, P_D (W), the thrust generated by this propeller without the effect of the profile drag, T(N), and the power consumed by the propeller without the effect of the profile drag, P(W).

As in Chapter 3, it is assumed that the induced velocity is much lower than the wind velocity. Also it is assumed that the trailing vortices and the shed vortices form an Archimedean screw-like surface instead of a sheared Archimedean screw surface.

4.2. Definitions

The control points and the dividing points are described by using a x_W-y_W-z_W coordinate system that is conveyed by the wind with the velocity, V_{AV}, but does not rotate as shown in Fig. 4.2. On the contrary, x_{Bb}-y_{Bb}-z_{Bb} coordinate systems are fixed on Blade #b, and rotate with Blade #b, and are used to describe the flow around the blade segments. The rotating direction of the propeller is counterclockwise. The trailing vortices and the shed vortices form an Archimedean screw-like surface with con stant pitch, d(m). From the previous assumption, this d is given by:

$$d = \frac{2\pi V_{AV}}{\Omega} \tag{4.2}$$

In contrast with the development in Chapter 3, vortex rings are used here instead of trailing vortices and shed vortices in order to satisfy the Helmholtz's theorem automatically. The vortex sheets are specified by the following definitions:

- The number of the rotating cycle is L.
- The number of time steps in one cycle is M.
- One blade is divided into N blade segments.
- The width of the blade segments is dR(m).
- The length of the time step is dt(sec).
- The initial position of Blade #1 is on the y_W-axis.

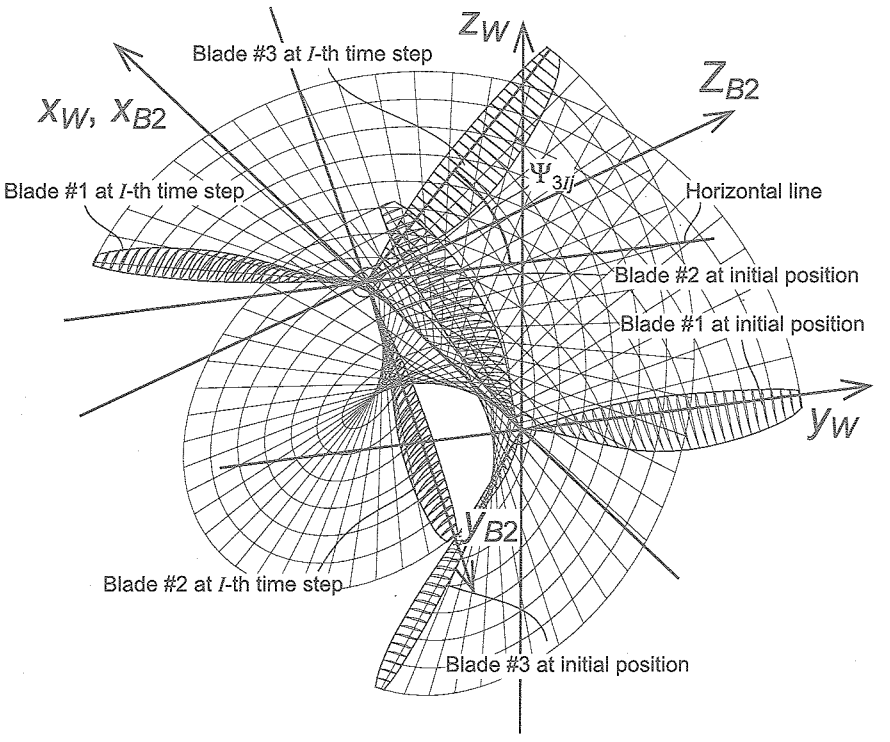

Fig. 4.2 Coordinates of the propeller; B=3. x_W-y_W-z_W coordinates systemare conveyed by the wind but does not rotate, while x_{Bb}-y_{Bb}-z_{Bb} coordinates systems are fixed on Blade #b.

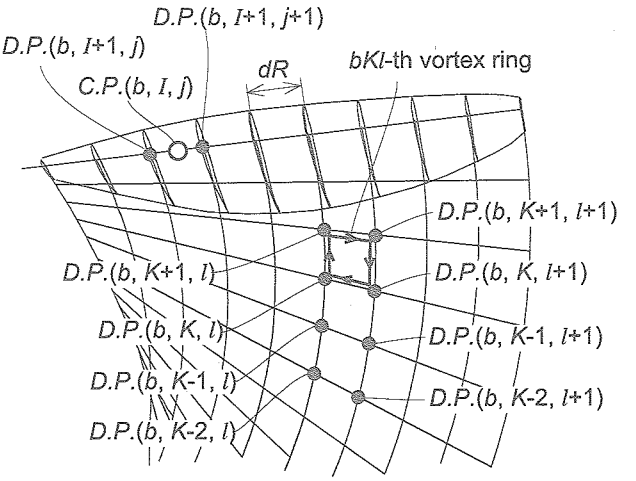

Fig.4.3 Definition of points on the *b*-th vortex sheet.

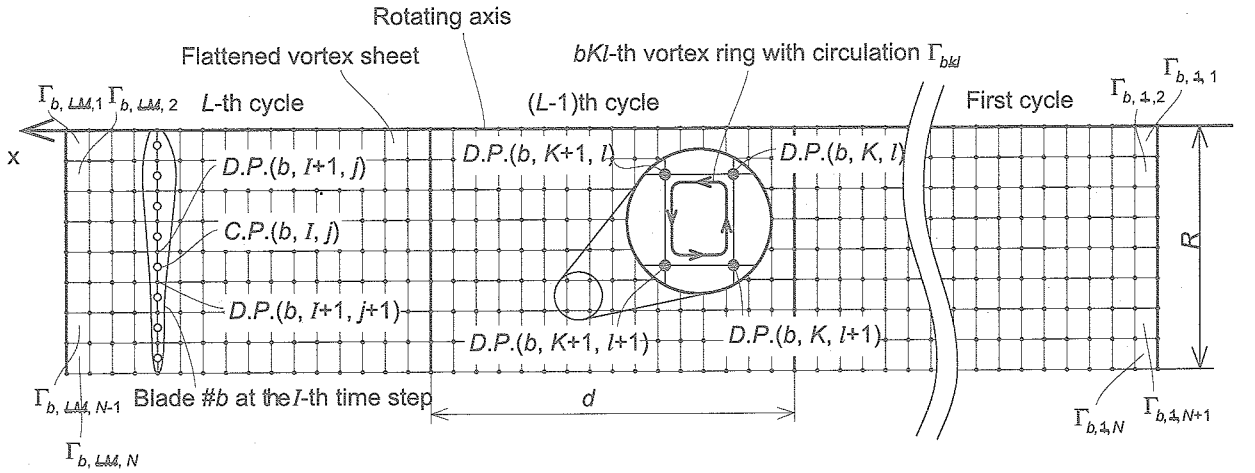

Fig. 4.4 Definition of points on the *b*-th vortex sheet. The vortex sheet is flattened to illustrate.

- *I* and *K* are variables for the time step from the initial time (instead of using *i* and *k* for the sake of the later convenience).
- A number with an underscore represents that the number is counted from the initial time.
- The circulation around the bound vortex on the *j*-th blade segment of Blade #*b* at the *I*-th time step is represented by Γ_{bIj}.
- Suffix *bIj* represents a physical value of the *j*-th blade segment of Blade #*b* at the *I*-th time step.
- The *bIj*-th blade segment stands for the *j*-th blade segment of Blade #*b* at the *I*-th time step.
- The *bIj*-th vortex ring stands for the vortex ring released from the *j*-th blade segment of Blade #*b* at the *I*-th time step.
- The *b*-th vortex sheet represents the vortex sheet released from Blade #*b*.
- The *cKl*-th dividing point, *D.P.*(*c, K, l*), is located on the inner end of the *cKl*-th blade segment.
- The *bIj*-th control point, *C.P.*(*b, I, j*), is located on the middle of the *bIj*-th blade segment, which is positioned between *D.P.*(*b, I*+1, *j*) and *D.P.*(*b, I*+1, *j*+1) as shown Figs. 4.3 and 4.4.
- The *bKl*-th vortex ring forms the rectangle consisting of *D.P.*(*b, K*+1, *l*), *D.P.*(*b, K*+1, *l*+1) , *D.P.*(*b, K, l*+1) and *D.P.*(*b, K, l*).
- The strength of the circulation around the *bKl*-th vortex ring is equal to that of the circulation around the bound vortex on the *bKl*-th segment at the *K*-th time step.

4.3. Influence Coefficients

Influence coefficients, ($\mathbb{X}_{bIjcKl}$, $\mathbb{Y}_{bIjcKl}$, $\mathbb{Z}_{bIjcKl}$), are defined as the magnitude of the velocity at *C.P.*(*b, I, j*), (v_{XbIj}, v_{YbIj}, v_{ZbIj}), induced by a unit circulation strength around the *cKl*-th vortex ring. Upon using these influence coefficients, v_{XbIj}, v_{YbIj}, v_{ZbIj} are given by:

$$v_{XbIj} = \sum_{c=1}^{B}\sum_{K=1}^{LM}\sum_{l=1}^{N} \mathbb{X}_{bIjcKl}\Gamma_{cKl} \tag{4.3}$$

$$v_{YbIj} = \sum_{c=1}^{B}\sum_{K=1}^{LM}\sum_{l=1}^{N} \mathbb{Y}_{bIjcKl}\Gamma_{cKl} \tag{4.4}$$

$$v_{ZbIj} = \sum_{c=1}^{B}\sum_{K=1}^{LM}\sum_{l=1}^{N} \mathbb{Z}_{bIjcKl}\Gamma_{cKl} \tag{4.5}$$

Also, the tangential component of the induced velocity, $v_{\theta Ij}$, is given by:

$$v_{\theta bIj} = -v_{YbIj}\sin\Psi_{bIj} + v_{ZbIj}\cos\Psi_{bIj} \tag{4.6}$$

where Ψ_{bIj} is the azimuth angle of the *bIj*-th blade segment as shown in Fig. 4.2. The above equation is also expressed as:

$$v_{\theta bIj} = \sum_{c=1}^{B}\sum_{K=1}^{LM}\sum_{l=1}^{N} \Theta_{bIjcKl}\Gamma_{cKl} \tag{4.7}$$

where Θ_{bIjcKl} is defined by:

$$\Theta_{bIjcKl} = -\mathbb{Y}_{bIjcKl}\sin\Psi_{bIj} + \mathbb{Z}_{bIjcKl}\cos\Psi_{bIj} \tag{4.8}$$

In a similar fashion to Eq. (2.6), the influence coefficients between *C.P.*(*b, I, j*) and the *cKl*-th vortex ring, ($\mathbb{X}_{bIjcKl}$, $\mathbb{Y}_{bIjcKl}$, $\mathbb{Z}_{bIjcKl}$), are given by:

$$\begin{aligned}
&\left(\mathbb{X}_{bIjcKl}, \mathbb{Y}_{bIjcKl}, \mathbb{Z}_{bIjcKl}\right)^T \\
&= \frac{1}{4\pi}\left\{\frac{\mathbf{a}\times\mathbf{l}_1}{|\mathbf{a}\times\mathbf{l}_1|^2}\left(\frac{\mathbf{b}}{|\mathbf{b}|}-\frac{\mathbf{a}}{|\mathbf{a}|}\right)\cdot\mathbf{l}_1 + \frac{\mathbf{b}\times\mathbf{l}_2}{|\mathbf{b}\times\mathbf{l}_2|^2}\left(\frac{\mathbf{c}}{|\mathbf{c}|}-\frac{\mathbf{b}}{|\mathbf{b}|}\right)\cdot\mathbf{l}_2\right. \\
&\quad \left. + \frac{\mathbf{c}\times\mathbf{l}_3}{|\mathbf{c}\times\mathbf{l}_3|^2}\left(\frac{\mathbf{d}}{|\mathbf{d}|}-\frac{\mathbf{c}}{|\mathbf{c}|}\right)\cdot\mathbf{l}_3 + \frac{\mathbf{d}\times\mathbf{l}_4}{|\mathbf{d}\times\mathbf{l}_4|^2}\left(\frac{\mathbf{a}}{|\mathbf{a}|}-\frac{\mathbf{d}}{|\mathbf{d}|}\right)\cdot\mathbf{l}_4\right\} \quad K\le I \\
&\left(\mathbb{X}_{bIjcKl}, \mathbb{Y}_{bIjcKl}, \mathbb{Z}_{bIjcKl}\right)^T = (0 \quad 0 \quad 0)^T, \quad K>I
\end{aligned} \tag{4.9}$$

where ***a***, ***b***, ***c*** and ***d*** are vectors from *C.P.*(*b, I, k*) to *D.P.*(*c, K*+1, *l*), *D.P.*(*c, K*+1, *l*+1), *D.P.*(*c, K, l*+1) and *D.P.*(*c, K, l*) respectively as shown in Fig. 4.5. $\boldsymbol{l}_1$, $\boldsymbol{l}_2$, $\boldsymbol{l}_3$ and $\boldsymbol{l}_4$ are the vectors defined by ***b-a***, ***c-b***, ***d-c***, ***a-d*** respectively. When *K*>*I*, the first expression of Eq. (4.9) does not have physical meaning. Thus the second expression is necessary.

For example, $\mathbb{X}_{bIjcKl}$ is calculated by using Eq (4.9) as shown in Table 3.1. The numerical example is as follows: *R*=1.0m, V_{AV}=10.0m/s, Ω=5.0π rad/s, *B*=2, *L*=2, M=4, N=3.

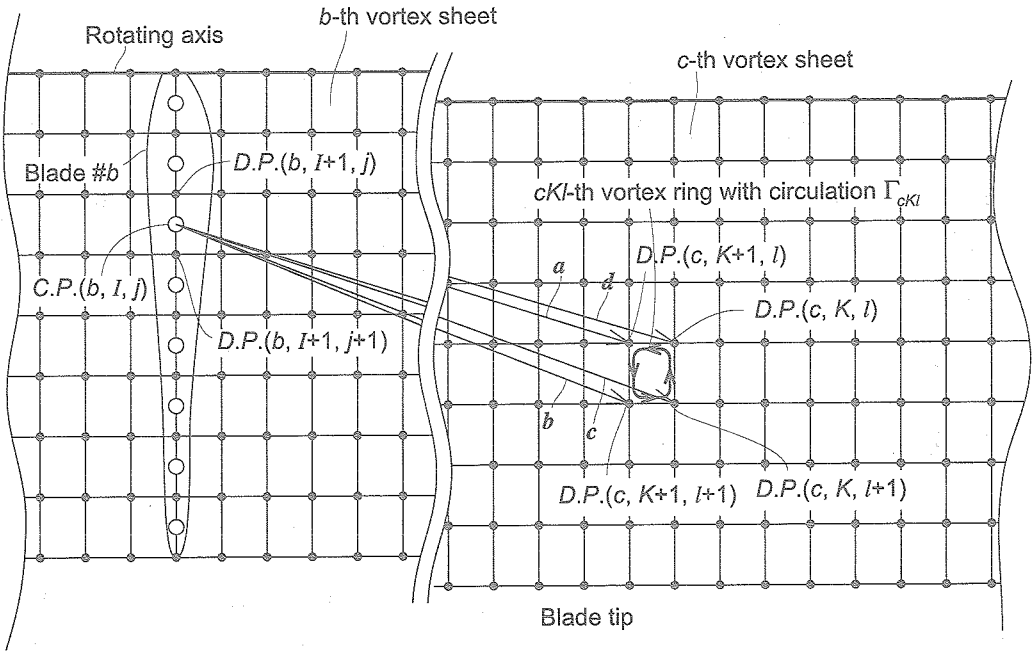

Fig. 4.5 Definition of vectors for the definition of the influence coefficients. Vortex sheets are flattened to illustrate.

Table 3.1

Influence coefficient, $X_{1,10,2,c,K,l}$ calculated by Eq.(3.9). B=2, L=3, M=4, N=3. $X_{1,10,2,c,K,l}$ stands for the magnitude of the x_W-component of the velocity at C.P.(1, 10, 2) induced by a unit circulation strength around the cKl-th vortex ring.

		3rd cycle				2nd cycle				1st cycle			
Blade #1							K						
		12	11	10	9	8	7	6	5	4	3	2	1
	1	0	0	0.1167	0.0105	-0.0043	-0.0025	-0.0004	-0.0002	-0.0003	-0.0002	-0.0001	-0.0001
l	2	0	0	-0.9616	0.0037	-0.0056	-0.0052	-0.0019	-0.0008	-0.0007	-0.0005	-0.0003	-0.0002
	3	0	0	0.4707	0.0034	-0.0046	-0.007	-0.0032	-0.0013	-0.001	-0.0008	-0.0005	-0.0003
Blade #2							K				$X_{1,10,2,2,3,1}$		
		12	11	10	9	8	7	6	5	4	3	2	1
	1	0	0	-0.0174	-0.0267	-0.0011	-0.0002	-0.0009	-0.0006	-0.0002	-0.0001	-0.0001	-0.0001
l	2	0	0	0.004	-0.0406	-0.0095	-0.002	-0.0018	-0.0014	-0.0007	-0.0004	-0.0003	-0.0003
	3	0	0	0.0099	-0.0397	-0.0149	-0.0026	-0.0023	-0.002	-0.0011	-0.0006	-0.0005	-0.0004

4.4. Thrust and Power with Effect of Profile Drag

In this section the total thrust generated by the propeller at the *I*-th time step with the effect of the profile drag, T_{DI}, and the total power consumed by the propeller at the *I*-th time step with the effect of the profile drag, P_{DI}, are obtained.

The angle of attack of the *bIj*-th blade segment, α_{bIj} (rad), and relative velocity between this segment and air, V_{bIj}(m/s), are given by the vector diagram shown in Fig. 4.6: V_{TbIj}(m/s) is the relative velocity at *C.P.*(*b, I, j*) tangential to the rotating disk; V_{PbIj}(m/s) is the relative velocity at *C.P.*(*b, I, j*) perpendicular to the rotating disk; ϕ_{bIj}(rad) is angle of the flow to the rotational disk; θ_{bIj}(rad) is the geometrical angle of the *bIj*-th blade segment; r_{bIj} is the distance between the center of rotation and *C.P.*(*b, I, j*). From Fig. 4.6, V_{TbIj}, V_{PbIj} are given by:

$$V_{TbIj} = r_{bIj}\Omega - v_{\theta bIj} \tag{4.10}$$

$$V_{PbIj} = V_{INFbIj} - v_{XbIj} \tag{4.11}$$

where V_{INFbIj} is obtained from Eq. (4.1). Further V_{bIj} is given by:

$$V_{bIj} = \sqrt{V_{TbIj}^{\ 2} + V_{PbIj}^{\ 2}} \tag{4.12}$$

Using V_{TbIj} and V_{PbIj}, ϕ_{bIj} is given by:

$$\phi_{bIj} = \tan^{-1}\left(\frac{V_{PbIj}}{V_{TbIj}}\right) \tag{4.13}$$

From Fig. 4.6, α_{bIj} is given by:

$$\alpha_{bIj} = \theta_{bIj} - \phi_{bIj} \tag{4.14}$$

The lift generated by the *bIj*-th blade segment, L_{bIj}, is:

$$L_{bIj} = \frac{1}{2}\rho V_{bIj}^{\ 2} C_L(\alpha_{bIj}, Re_{bIj}) c_{bIj} dR \tag{4.15}$$

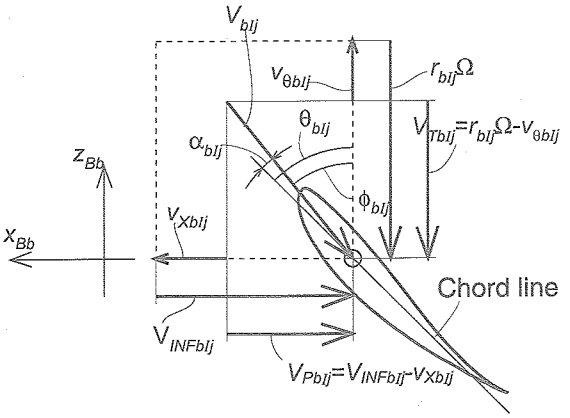

Fig. 4.6 Vector diagram of the *bIj*-th blade segment. From x_B-y_B-z_B coordinates system fixed on Blade *#b*.

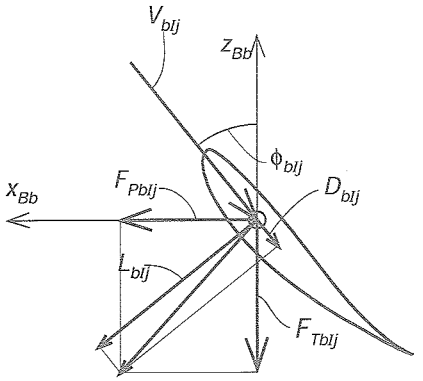

Fig. 4.7 Forces of the *bIj*-th blade segment. From x_B-y_B-z_B coordinates system fixed on Blade *b#*

where ρ(kg/m^3) is the density of air: c_{bIj} is the chord length of the *bIj*-th blade segment; C_L is the lift coefficient that is a function of α. Also the drag generated by the *bIj*-th blade segment, D_{bIj}, is:

$$D_{bIj} = \frac{1}{2}\rho V_{bIj}^{\ 2} C_D(\alpha_{bIj}, Re_{bIj}) c_{bIj} dR \tag{4.16}$$

where C_D is the drag coefficient that is a function of α. From Fig. 4.7, the force of the *bIj*-th blade segment perpendicular to the rotating disk, F_{PbIj}, is given by:

$$F_{PbIj} = L_{bIj}\cos\phi_{bIj} - D_{bIj}\sin\phi_{bIj} \tag{4.17}$$

Similarly, the force of the *bIj*-th blade segment tangential to the rotating disk, F_{TbIj}, is given by:

$$F_{TbIj} = D_{bIj}\cos\phi_{bIj} + L_{bIj}\sin\phi_{bIj} \tag{4.18}$$

The summation of Eq. (4.17) gives the total thrust at the I-th time step, T_{DI}:

$$T_{DI} = \sum_{b=1}^{B}\sum_{j=1}^{N} F_{PbIj} \tag{4.19}$$

Similarly, (4.18) gives the total power at the I-th time step, P_{DI}:

$$P_{DI} = \sum_{b=1}^{B}\sum_{j=1}^{N} F_{TbIj} r_{bIj}\Omega \tag{4.20}$$

If R, V_{AV}, V_{GRAD}, Ω, c_{bIj}, θ_{bIj}, $C_L(\alpha)$ and $C_D(\alpha)$ are given, it seems possible to obtain T_{DI} and P_{DI} from the above equations. However, T_{DI} and P_{DI} still contain the unknown variables, Γ_{bIj}.

4.5. Thrust and Power without Effect of Profile Drag

In this section the thrust at the I-th time step without the effect of profile drag, T_I(N), and the power at I-th time step without the effect of profile drag, P_I (W), are obtained.

From the Kutta-Joukowsky theorem, the thrust caused by the circulation around the bound vortex on the bIj-th blade segment, T_{bIj}(N), is given by:

$$T_{bIj} = \rho\Gamma_{bIj} V_{TbIj}\, dR \tag{4.21}$$

Similarly, the power caused by the circulation around the bound vortex on the bIj-th blade segment, P_{bIj}(W), is given by:

$$P_{bIj} = \rho\Gamma_{bIj} V_{PbIj}\, dR r_{bIj}\Omega \tag{4.22}$$

The summation of Eq. (4.21) gives the total thrust, T_I(N), at the I-th time step caused by the circulations:

$$T_I = \sum_{b=1}^{B}\sum_{j=1}^{N} \rho\Gamma_{bIj} V_{TbIj} dR \tag{4.23}$$

Eqs. (4.7), (4.10) and (4.23) give:

$$T_I = \sum_{b=1}^{B}\sum_{j=1}^{N} \rho\Gamma_{bIj}\left(r_{bIj}\Omega - \sum_{c=1}^{B}\sum_{K=1}^{LM}\sum_{l=1}^{N} \Theta_{bIjcKl}\Gamma_{cKl}\right) dR \tag{4.24}$$

Similarly, the summation of Eq. (4.22) gives the total power, P_I (W), at the I-th time step caused by the circulations:

$$P_I = \sum_{b=1}^{B}\sum_{j=1}^{N} \rho\Gamma_{bIj} V_{PbIj} dR r_{bIj}\Omega \tag{4.25}$$

Eqs. (4.3), (4.11) and (4.25) give:

$$P_I = \sum_{b=1}^{B}\sum_{j=1}^{N} \rho\Gamma_{bIj}\left(V_{INFbIj} - \sum_{c=1}^{B}\sum_{K=1}^{LM}\sum_{l=1}^{N} \mathbb{X}_{bIjcKl}\Gamma_{cKl}\right) dR r_{bIj}\Omega \tag{4.26}$$

4.6. Determination of Circulations

In a similar fashion to the development in Chapter 3, the Circulations, Γ_{bIj}, can be determined. The lift from Eq. (4.15) equals the lift caused by the circulation and is given by:

$$L_{bIj} = \rho\Gamma_{bIj} V_{bIj}\, dR \tag{4.27}$$

Therefore, the following equation holds:

$$\frac{1}{2}\rho V_{bIj}{}^2 C_L(\alpha_{bIj}) C_{bIj}\, dR = \rho\Gamma_{bIj} V_{bIj}\, dR \tag{4.28}$$

and one thus obtains:

$$\Gamma_{bIj} = V_{bIj} C_L(\alpha_{bIj}) C_{bIj} \tag{4.29}$$

where α_{bIj} is the angle of attack of the bIj-th blade section as described before. From Eqs. (4.10), (4.11), (4.13) and (4.14), α_{bIj} is given by a function of the induced velocities as follows:

$$\alpha_{bIj} = \theta_{bIj} - \tan^{-1}\left(\frac{V_{INFbIj} - v_{XbIj}}{r_{bIj}\Omega - v_{\theta bIj}} \right) \tag{4.30}$$

Furthermore, Eqs. (4.3) and (4.7) into Eq. (4.30) gives this as a function of the circulations:

$$\alpha_{bIj} = \theta_{bIj} - \tan^{-1}\left(\frac{V_{INFbIj} - \sum_{c=1}^{B}\sum_{K=1}^{LM}\sum_{l=1}^{N} \mathbb{X}_{bIjcKl}\Gamma_{cKl}}{r_{bIj}\Omega - \sum_{c=1}^{B}\sum_{K=1}^{LM}\sum_{l=1}^{N} \Theta_{bIjcKl}\Gamma_{cKl}} \right) \tag{4.31}$$

Eq. (4.31) into Eq. (4.29) then gives closed equations for the circulations:

$$\Gamma_{bIj} = V_{bIj} C_L \left\{ \theta_{bIj} - \tan^{-1} \left(\frac{V_{INFbIj} - \sum_{c=1}^{B} \sum_{K=1}^{LM} \sum_{I=1}^{N} \mathbf{X}_{bIjcKI} \Gamma_{cKI}}{r_{bIj}\Omega - \sum_{c=1}^{B} \sum_{K=1}^{LM} \sum_{I=1}^{N} \Theta_{bIjcKI} \Gamma_{cKI}} \right), Re_{bIj} \right\} c_{bIj} \qquad (4.32)$$

It is almost impossible to solve Eq. (4.32) analytically because of its non-linearity. However, the following iteration procedure may be used to solve Eq. (4.32):

Step 1: Select initial values of the circulations around the bound vortex on the $b\underline{1}j$-th blade segment, $\Gamma_{b\underline{1}j}{}^{(1)}$; where $(\,)$ indicates the iterating number. For example, $\Gamma_{b\underline{1}j}{}^{(1)}=0$. Note that the subscript is not bIj, but $b\underline{1}j$ which means the j-th blade segment of Blade #b is at the first time step.

Step 2: Let I=1 and N=1.

Step 3: Calculate the new values of $\Gamma_{bIj}{}^{(N+1)}$ using $\Gamma_{bIj}{}^{(N)}$ and Eq. (4.32)

Step 4: Calculate the index of errors, $\varepsilon_I{}^{(N+1)}$, defined by:

$$\varepsilon_I{}^{(N+1)} = \sum_{b=1}^{B} \sum_{j=1}^{N} \left\{ \Gamma_{bIj}{}^{(N+1)} - \Gamma_{bIj}{}^{(N)} \right\}^2 \qquad (4.33)$$

Step 5: Evaluate $\varepsilon_I{}^{(N+1)}$. If $\varepsilon_I{}^{(N+1)} < \varepsilon_0$ (where ε_0 is a small number) then go to Step 6; otherwise repeat Step 3.

Step 6: Let I=I+1 and N=1.

Step 7: If I>LM then stop, otherwise repeat Step 3.

Once Γ_{bIj} are obtained, induced velocities are given by Eqs. (4.3) and (4.7), T_D and P_D are given by Eqs. (4.10) through (4.20), T and P are given by Eqs. (4.24) and (4.26)

4.7. Reduction of Variable Number

So far, the method for calculating the thrust and the power of the propeller in the wind gradient from the first cycle to the L-th cycle has been described. Also, the previous section has shown the most laborious procedure in this method is the procedure to determine the circulations. Thus the problem of calculating the thrust and power is almost identical to the problem for calculating the circulations. From now on, the problem for calculating the thrust and power is expressed as the problem for calculating the circulations.

By the way, it is only the converged periodical set of the circulations in the last full cycle that this paper intends to obtain. Note that "set of circulation" stands for the MN circulations on a vortex sheet in one cycle. However the solution obtained by the method described above contains not only this, but also the transitional sets of the circulations in the early cycles as shown in Fig. 4.8-a. Furthermore, every previous set of the circulations must have been obtained in order to calculate the set of circulations in the last full cycle, because the induced velocity in the last full cycle is produced by every vortex ring that the blades have left previously. Of course, it is not meaningless to calculate every set of the circulations from the initial cycle to the last cycle. However, it is not efficient to calculate the sets of circulations in every cycle in order to obtain the converged periodical set of the circulations in the last full cycle. This inefficiency is solved in this section.

If the calculation of the circulations converges, it is expected that the last few sets of the circulations should be almost periodical as shown in the gray region of Fig. 4.8-a. That is to say:

$$\Gamma_{bIj} \approx \Gamma_{b,\, I-nM,\, j},\ (L\text{-}1)M \le I \le LM \qquad (4.34)$$

where n is an arbitrary natural number that is not large. To solve the inefficiency stated above, the following approximation is introduced here.

Approximation

The every set of circulation in every cycle is identical to the set of circulations in the last full cycle. That is:

$$\Gamma_{b,\, I-nM,\, j} = \Gamma_{bIj},$$

$$1 \le b \le B,\ (L\text{-}1)M+1 \le I \le LM,\ 1 \le j \le N,\ 1 \le n \le L\text{-}1$$

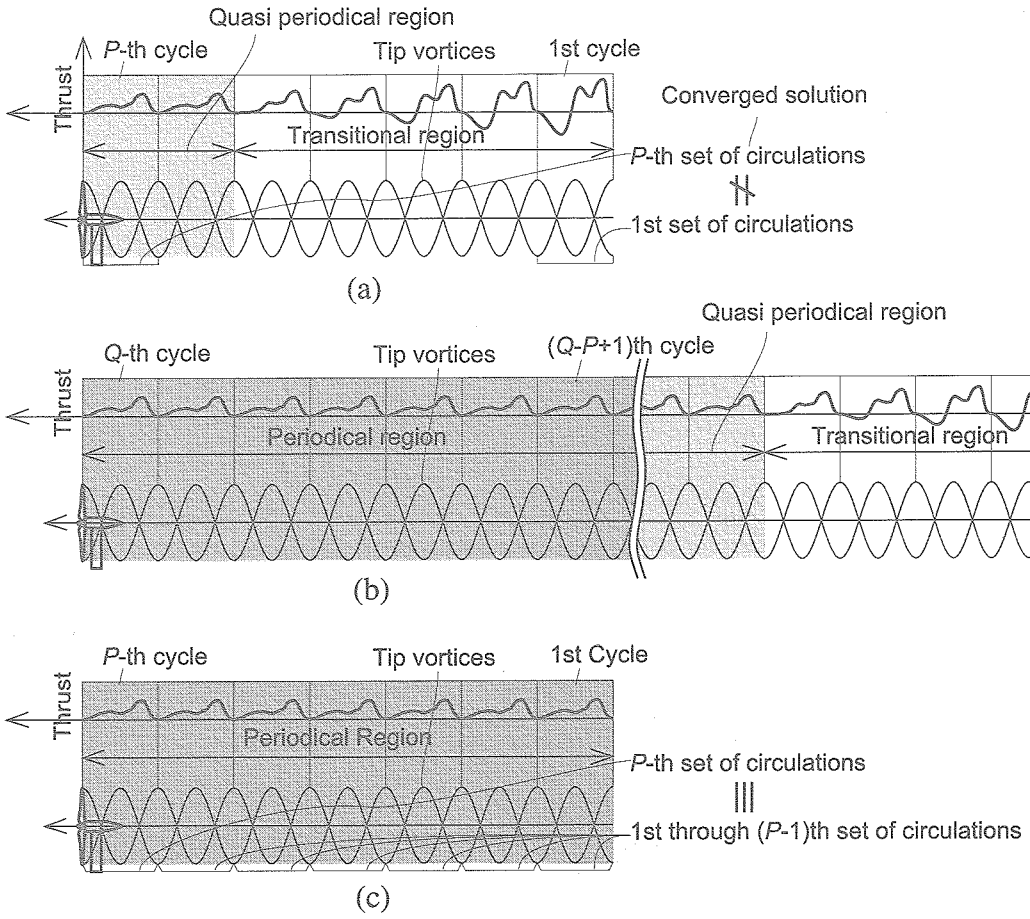

Fig. 4.8 Sets of circulations obtained by Eq. (3.35): (a) change of thrust in P-th cycle (b) change of thrust in Q-th cycle; (c) change of thrust in P-th cycle using Eq. (3.35).

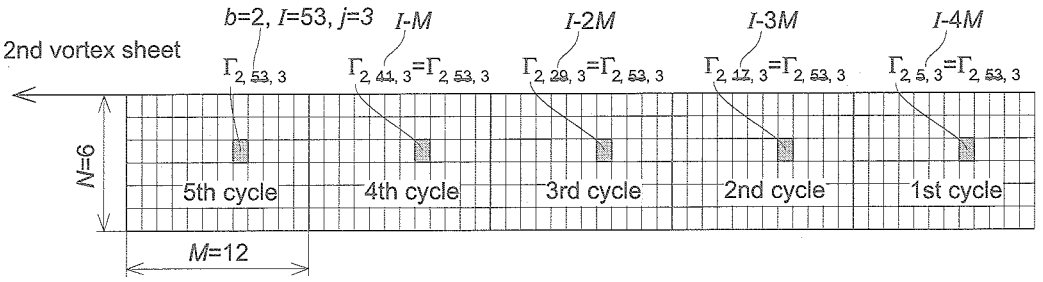

Fig. 4.9 Basic concept of Eq. (3.35): L=5, M=12, N=6, b=2, I=53, j=3.

The basic concept of this approximation is shown in Fig. 4.9. In other words, only the set of circulations in the last cycle is the object of the calculation, and every set of circulations in every previous cycle is supposed to be identical to the set of circulations in the last one cycle. This approximation reduces the number of the circulations tremendously, but it may seem that it also reduces the accuracy of the circulations. On the contrary, however, this approximation can increase the accuracy of the circulations. This reason is described as follows. The most important factor for obtaining an accurate solution is the accuracy of the induced velocities in the last cycle. Further, to increase the accuracy of the induced velocities, very long vortex sheet must be used. However this means the number of cycles, L, must be vast value, which is not dealt with by actual calculations. Let this vast value be Q and the value that can be dealt by actual calculations be P. Of course, $P<<Q$. If the calculation using $L=Q$

could be executed, Eq. (4.35) should hold in the last P cycles very well, as shown in Fig. 4.8-b. Additionally, the influence of the vortex rings is proportional to the inverse-square of the distance. Hence, at the last cycle, the influence of the vortex rings released from the initial time step to $(Q\text{-}P)$th time step is negligibly small. Therefore the accuracy of solution of the calculation neglecting these vortex rings is still good as shown in Fig. 4.8-c. That is, Eq. (4.35) works well.

Eq. (4.35) into Eq. (4.7) gives:

$$v_{\theta bIj} = \sum_{c=1}^{B} \sum_{K=(L-1)M+1}^{LM} \sum_{I=1}^{N} \Theta_{bIjcKI} \Gamma_{cKI} \qquad (4.36)$$

where Θ'_{bIjcKl} is defined by:

$$\Theta'_{bIjcKl} = \sum_{n=0}^{L-1} \Theta_{b,I,j,c,K-nM,l}$$

$$1 \le b \le B,\ 1 \le c \le B,\ 1 \le j \le N,\ 1 \le l \le N,$$
$$(L\text{-}1)M+1 \le K \le LM,\ (L\text{-}1)M+1 \le I \le LM \qquad (4.37)$$

This summation is illustrated in Fig. 4.10. The range of I and K in Eq. (4.36) is $[(L\text{-}1)M+1, LM]$. Thus, the number of variables has been reduced from $BLMN$ to BMN.

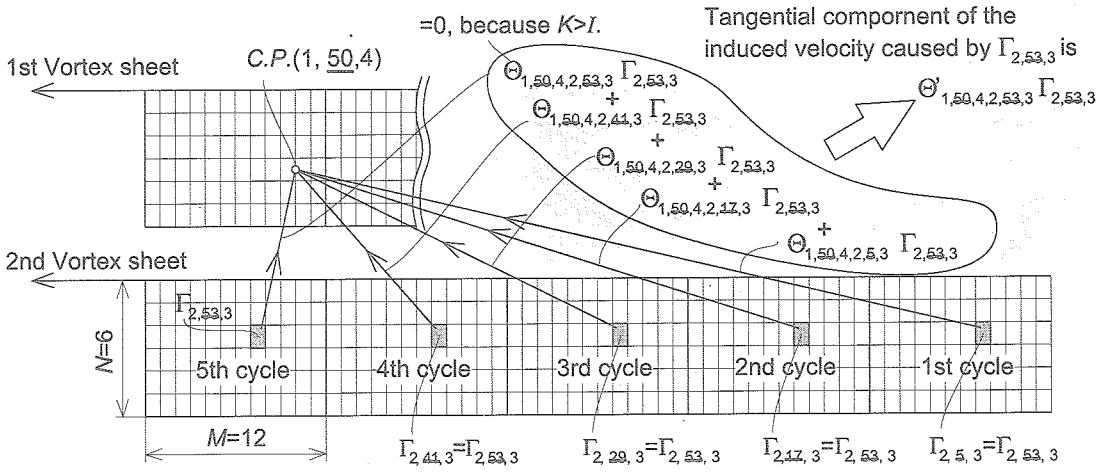

Fig. 4.10 Basic concept of redefinition (3.37): L=5, M=12, N=6, b=1, I=50, j=4, c=2, K=53, l=3. Tangential compornent of the induced velocity at $C.P.(1, 50, 4)$ caused by $\Gamma_{2,53,3}$ is $\Theta'_{1,50,4,2,53,3}\Gamma_{2,53,3}$.

However it is inconvenient to use these large numbers for the range of I and K. Therefore, the circulations are redefined as follows.

$$\Gamma_{bij} = \Gamma_{b,I-(L-1)M,j} \qquad (4.38)$$

This equation means that the ranges of I are converted from $[(L\text{-}1)M+1, LM]$ into $[1, M]$ by using i. In other words, i is the number of time steps from the start of the last cycle, while I is the number of time steps from the initial time. Also, k is the number of time steps from the start of the last cycle

Thus Θ'_{bijckl} is redefined as follows.

$$\Theta'_{bijckl} = \Theta'_{b,I-(L-1)M,j,c,K-(L-1)M,l} \qquad (4.39)$$

By this redefinition, the range of I and K of Θ'_{bijckl} is converted from $[(L\text{-}1)M+1, LM]$ to $[1, M]$, and Eq. (4.36) can be expressed by the simple form as follows:

$$v_{\theta bij} = \sum_{c=1}^{B} \sum_{k=1}^{M} \sum_{l=1}^{N} \Theta'_{bijckl} \Gamma_{ckl} \qquad (4.40)$$

In a similar fashion, Eq. (4.35) into Eq. (4.3) gives:

$$v_{Xbij} = \sum_{c=1}^{B} \sum_{k=1}^{M} \sum_{l=1}^{N} \mathbb{X}'_{bijckl} \Gamma_{ckl} \qquad (4.41)$$

where $\mathbb{X}'_{bijckl}$ is defined by:

$$\mathbb{X}'_{bijckl} = \mathbb{X}'_{b,I-(L-1)M,j,c,K-(L-1)M,l} \qquad (4.42)$$

and $\mathbb{X}'_{bljcKl}$ is defined by:

$$\mathbb{X}'_{bljcKl} = \sum_{n=0}^{L-1} \mathbb{X}_{b,I,j,c,K-nM,l}$$

$$1 \le b \le B,\ 1 \le c \le B,\ 1 \le j \le N,\ 1 \le l \le N,$$
$$(L\text{-}1)M+1 \le K \le LM,\ (L\text{-}1)M+1 \le I \le LM \qquad (4.43)$$

For example, $\mathbb{X}'_{bljcKl}$ are calculated by Eq. (4.43) as shown in Table 3.2. The numerical example is the same as that of Table 3.1. Furthermore, there is a simple relation among Γ_{1ij}, Γ_{2ij}, ... and Γ_{Bij} as shown in Fig. 4.11. This relation can be expressed as follows:

$$\Gamma_{b,i-bM/B,j} = \Gamma_{ij},\ i\text{-}bM/B > 0$$

$$\Gamma_{b,i+M-bM/B,j} = \Gamma_{ij},\ i\text{-}bM/B \le 0 \qquad (4.44)$$

Table 3.2

Influence coefficient, $\mathbb{X}'_{1,2,2,c,k,l}$ transformed from Table 3.1 by using Eq.(3.43)

Blade #1		k = 4	3	2	1
l	1	-0.0046	-0.0027	0.1162	0.0102
	2	-0.0063	-0.0057	-0.9638	0.0027
	3	-0.0056	-0.0078	0.467	0.0018

Blade #2		k = 4	3	2	1
l	1	-0.0013	-0.0003	-0.0184	-0.0274
	2	-0.0102	-0.0024	0.0019	-0.0423
	3	-0.016	-0.0032	0.0071	-0.0421

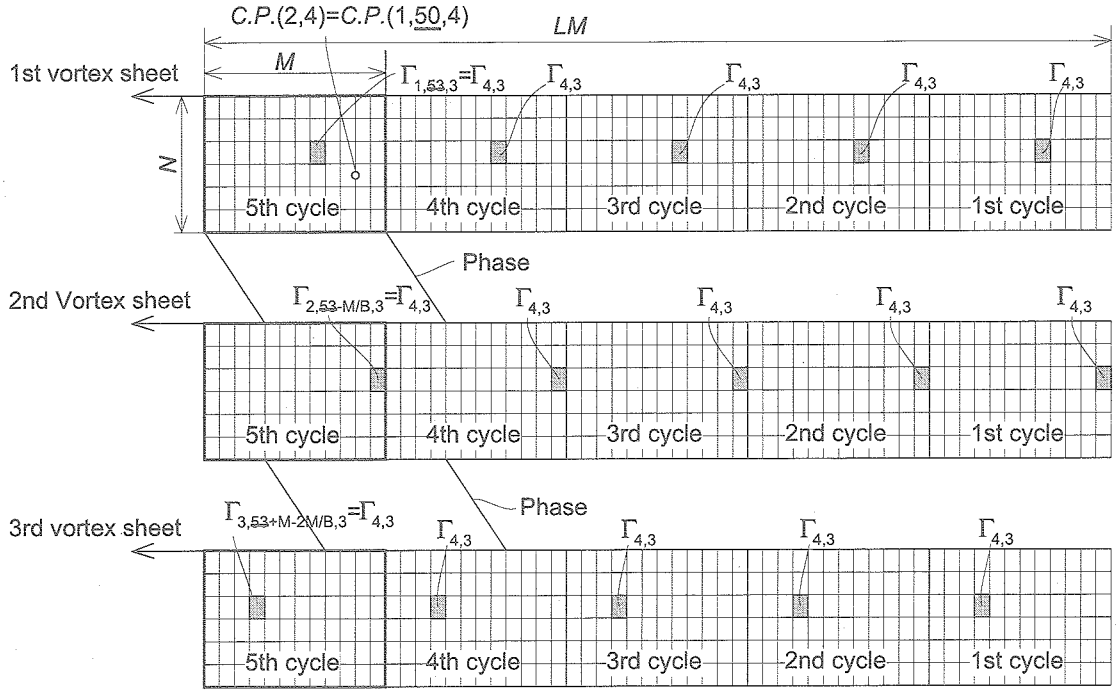

Fig. 4.11 Map of circulations with same strength: B=3, L=5, M=12, N=6

where Γ_{ij} is identical to Γ_{1ij}. From now on, Γ_{ij} is used instead of Γ_{1ij}. Note that the difference of expression between Γ_{ij} and Γ_{bij} is only the number of the subscripts, however the difference of the meaning is very large. By Eq. (4.42), the number of variables has been reduced from *BMN* to *MN*. Further, Eq. (4.44) into Eq. (4.40) gives:

$$v_{\theta ij} = \sum_{k=1}^{M}\sum_{l=1}^{N} \Theta'_{ijkl}\,\Gamma_{kl} \tag{4.45}$$

where Θ'_{ijkl} is defined by:

$$\Theta'_{ijkl} = \sum_{c=1}^{B} \Theta'_{1,i,j,c,f(c,k),l} \tag{4.46}$$

and $f(c, k)$ is the function of c and k given by:

$$f(c,k) = k-(c-1)M/B,\ k-(c-1)M/B > 0$$

$$f(c,k) = k+M-(c-1)M/B,\ k-(c-1)M/B \le 0 \tag{4.47}$$

Similarly, Eq. (4.44) into Eq. (4.10) gives:

$$v_{Xij} = \sum_{k=1}^{M}\sum_{l=1}^{N} \mathbb{X}'_{ijkl}\Gamma_{kl} \tag{4.48}$$

where $\mathbb{X}'_{ijkl}$ is defined by:

$$\mathbb{X}'_{ijkl} = \sum_{c=1}^{B} \mathbb{X}'_{1,i,j,c,f(c,k),l} \tag{4.49}$$

For example, $\mathbb{X}'_{ijkl}$ are calculated by Eq. (4.49) as shown in Table 3.3. The numerical example is the same as that of Table 3.1.

Table 3.3
Influence coefficient, $\mathbb{X}'_{2,2,k,l}$ transformed from Table 3.2 by using Eq.(3.49)

		k			
		4	3	2	1
l	1	-0.023	-0.0301	0.1149	0.0099
	2	-0.0044	-0.048	-0.974	0.0003
	3	0.0015	-0.0499	0.451	-0.0014

4.8. Redefinition of T_D, P_D, T and P

In the previous section, the number of the circulations is reduced from BLMN to MN, which reduces the labor of the calculation tremendously. Before the reduction of the number of the circulations, *BLMN* circulations must be treated. By the reduction, however, only *MN* circulations on the first vortex sheet at the last cycle need to be treated. While the circulations on the *b*-th vortex sheet at the last cycle are expressed as Γ_{bij}, the circulations on the first vortex sheet at the last cycle are expressed as the simplified expression, Γ_{ij}, which is introduced in the previous section. To use Γ_{ij} efficiently, equations in the section 4 and 5 must be redefined. In this chapter T_D, P_D, T and P are redefined.

Using the same procedure of the reduction of variables, Eqs. (4.10) through (4.20) are transformed and the suffixes are simplified as follows:

$$V_{Tij} = r_{ij}\Omega - v_{\theta ij} \tag{4.50}$$

$$V_{Pij} = V_{INFij} - v_{Xij} \tag{4.51}$$

$$V_{ij} = \sqrt{V_{Tij}^{\ 2} + V_{Pij}^{\ 2}} \tag{4.52}$$

$$\phi_{ij} = \tan^{-1}\left(\frac{V_{Pij}}{V_{Tij}}\right) \tag{4.53}$$

$$\alpha_{ij} = \theta_{ij} - \phi_{ij} \tag{4.54}$$

$$L_{ij} = \frac{1}{2}\rho V_{ij}^{\ 2} C_L(\alpha_{ij}, Re_{ij})\,c_{ij}\,dR \tag{4.55}$$

$$D_{ij} = \frac{1}{2}\rho V_{ij}^{\ 2} C_D(\alpha_{ij}, Re_{ij})\,c_{ij}\,dR \tag{4.56}$$

$$F_{Pij} = L_{ij}\cos\phi_{ij} - D_{ij}\sin\phi_{ij} \tag{4.57}$$

$$F_{Tij} = D_{ij}\cos\phi_{ij} + L_{ij}\sin\phi_{ij} \tag{4.58}$$

$$T_{Di} = \sum_{j=1}^{N} F_{Pij} \tag{4.59}$$

$$P_{Di} = \sum_{j=1}^{N} F_{Tij} r_{ij}\Omega \tag{4.60}$$

where T_{Di} in Eq. (4.59) is the thrust generated by Blade #1 at the i-th time step, while T_{DI} in Eq. (4.19) is the total thrust at the I-th time step. Also P_{Di} in Eq. (4.60) is the power consumed by Blade #1 at the i-th time step, while P_{DI} in Eq. (4.20) is the total power at the I-th time step.

Similarly, Eqs. (4.21) and (4.22) are transformed and the suffixes are simplified as follows:

$$T_{ij} = \rho\Gamma_{ij}\left(r_{ij}\Omega - \sum_{k=1}^{M}\sum_{l=1}^{N}\Theta'_{ijkl}\,\Gamma_{kl}\right)dR \qquad (4.61)$$

$$P_{ij} = \rho\Gamma_{ij}\left(V_{INFij} - \sum_{k=1}^{M}\sum_{l=1}^{N}\mathbb{X}'_{ijil}\Gamma_{kl}\right)dRr_{ij}\Omega \qquad (4.62)$$

Also, Eqs. (4.24) and (4.25) are transformed and the suffixes are simplified as follows:

$$T_i = \sum_{j=1}^{N}\rho\Gamma_{ij}\left(r_{ij}\Omega - \sum_{k=1}^{M}\sum_{l=1}^{N}\Theta'_{ijkl}\,\Gamma_{kl}\right)dR \qquad (4.63)$$

$$P_i = \sum_{j=1}^{N}\rho\Gamma_{ij}\left(V_{INFij} - \sum_{k=1}^{M}\sum_{l=1}^{N}\mathbb{X}'_{ijil}\Gamma_{kl}\right)dRr_{ij}\Omega \qquad (4.64)$$

where T_i in Eq. (4.63) is the thrust generated by Blade #1 at the i-th time step, while T_I in Eq. (4.24) is the total thrust at the I-th time step. Also P_i in Eq. (4.64) is the power consumed by Blade #1 at the i-th time step, while P_I in Eq. (4.25) is the total power at the I-th time step.

Furthermore, Eq. (4.32), which is the closed equations for the circulations, is also transformed as follows:

$$\Gamma_{ij} = V_{ij}C_L\left\{\theta_{ij} - \tan^{-1}\left(\frac{V_{INFij} - \sum_{k=1}^{M}\sum_{l=1}^{N}\mathbb{X}'_{ijkl}\Gamma_{kl}}{r_{ij}\Omega - \sum_{k=1}^{M}\sum_{l=1}^{N}\Theta'_{ijkl}\,\Gamma_{kl}}\right), Re_{ij}\right\}c_{ij} \qquad (4.65)$$

Using this transformation, the iteration procedure in the section 6 is written as:

Step 1:Select initial values for every circulation, $\Gamma_{ij}^{(1)}$; where $()$ indicates the iterating number. For example $\Gamma_{ij}^{(1)}=0$.

Step 2:Calculate new values of $\Gamma_{ij}^{(N+1)}$ using $\Gamma_{ij}^{(N)}$ and Eq. (4.65)

Step 3:Calculate the index of error, $\varepsilon^{(N+1)}$, defined by:

$$\varepsilon^{(N+1)} = \sum_{i=1}^{M}\sum_{j=1}^{N}\left\{\Gamma_{ij}^{(N+1)} - \Gamma_{ij}^{(N)}\right\}^2 \qquad (4.66)$$

Step 4:Evaluate $\varepsilon^{(N+1)}$. If $\varepsilon^{(N+1)} < \varepsilon_0$ (where ε_0 is a small number) then stop, otherwise repeat Step 2.

4.9. Procedure of Unsteady Propeller Analysis without Effect of Vortex Shear

T_{Di}, P_{Di}, T_i and P_i have been obtained. The procedure to calculate T_{Di}, P_{Di} is as follows:

1. Specify the propeller, V_{INF}, Ω, R, M, N, dt, c_{ij} and θ_{ij}.
2. Determine the position of *C.P.*(b, I, l) and *D.P.* (b, I, l).
3. Calculate $\mathbb{X}_{bIjcKl}$ and Θ_{bIjcKl} using Eqs. (4.8) and (4.9).
4. Redefine $\mathbb{X}'_{bijckl}$ and Θ'_{bijckl} using Eqs. (4.37), (4.39), (4.42) and (4.43).
5. Redefine $\mathbb{X}'_{ijkl}$ and Θ'_{ijkl} using Eqs. (4.46) and (4.49)
6. Determine Γ_{ij} by using the iterative procedure described in Section 9.
7. Calculate v_{Xij} and $v_{\Theta ij}$ using Eqs. (4.41) and (4.40).
8. Calculate T_{Di} and P_{Di} using Eqs. (4.50) through (4.60).

T_i and P_i have been also obtained here for the convenience of the later chapters. The procedure to calculate them is the same procedure described above except Procedures 7 and 8. Instead of Procedures 7 and 8, the following procedure is used:

7. Calculate T_i and P_i using Eqs. (4.63) and (4.64)

Note that the assumption that v_{Xij} and $v_{\Theta ij}$ are negligible small compared with V_{INF} is employed here in order to make it possible to determine the shape of the trailing vortices. Hence, T_{Di}, P_{Di}, T_i and P_i obtained by the above procedure are not reliable, if v_{Xij} and $v_{\Theta ij}$ are not negligibly small compared with V_{INF}.

5. Effect of Vortex Shear

5.1. Propeller Model with Effect of Vortex Shear

The effect of vortex shear was not treated in the previous chapter in order to simplify the problem. In this chapter, the method for calculating the thrust and power of a propeller in a wind gradient, with the effect of vortex shear, is described.

Fig. 5.1 shows the propeller treated here, which has the same properties as described in the previous chapter. The purpose of this chapter is to describe the method for calculating the thrust generated by this propeller with the effect of the profile drag, T_D(N), the power absorbed by the propeller with the effect of the profile drag, P_D (W), the thrust generated by this propeller without the effect of the profile drag, T(N), and the power absorbed by the propeller without the effect of the profile drag, P(W), considering the effect of the vortex sheets shear.

As in Chapter 4, it is assumed that the induced velocity is much lower than the wind velocity.

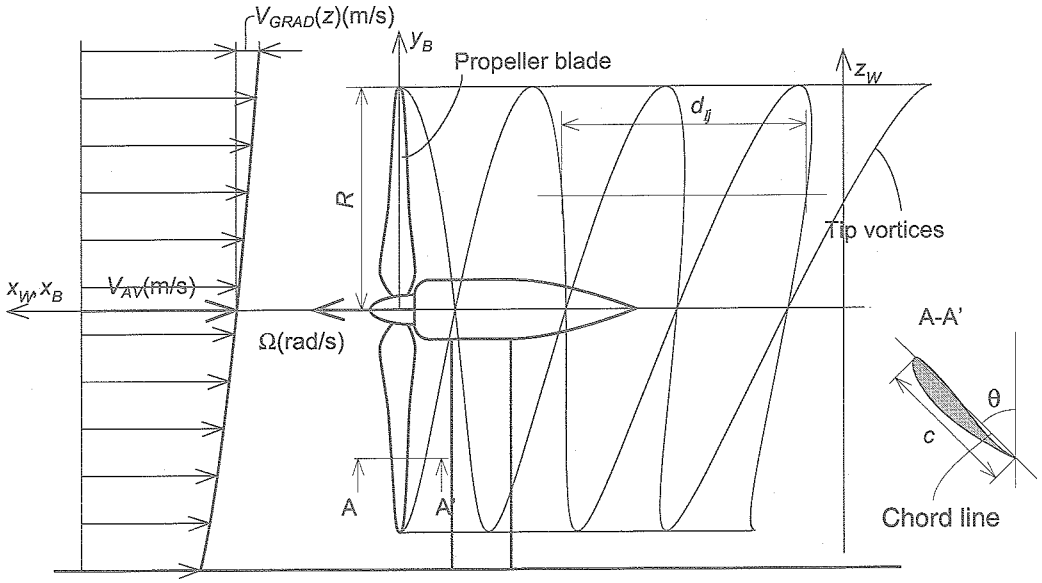

Fig. 5.1 Side view of the propeller in a wind gradient.

5.2. Definitions

The control points and the dividing points are described by using a x_W-y_W-z_W coordinate system that is conveyed by the wind with the velocity, V_{AV}, but does not rotate. Furthermore almost all definitions are the same as in the previous chapter.

However, vortex sheets are conveyed by the velocity, V_{INF}, that is a function of the height given by Eq. (4.1). Thus the pitch of the vortex sheet, d_{Ij}, is given by:

$$d_{Ij} = \frac{2\pi}{\Omega} V_{INFIj} \tag{5.1}$$

This equation means that the pitch of the vortex sheet is also a function of the height. Thus, the shear of the Archimedean screw-like vertex sheet increases as time lapses as shown in Fig. 5.2. Hence the absolute position of the dividing points described by the wind coordinate system is a function of the time step. That is:

- $D.P.(c, K, I)$ at the I-th time step is expressed by $D.P.(I, c, K, I)$.

The definitions of the points are shown in Fig. 5.3. Although the shape of the vortex ring varies, the Kelvin's theorem requires the strength of the circulation around a vortex ring to not vary. Thus Γ_{bIj} has the same value at any time step.

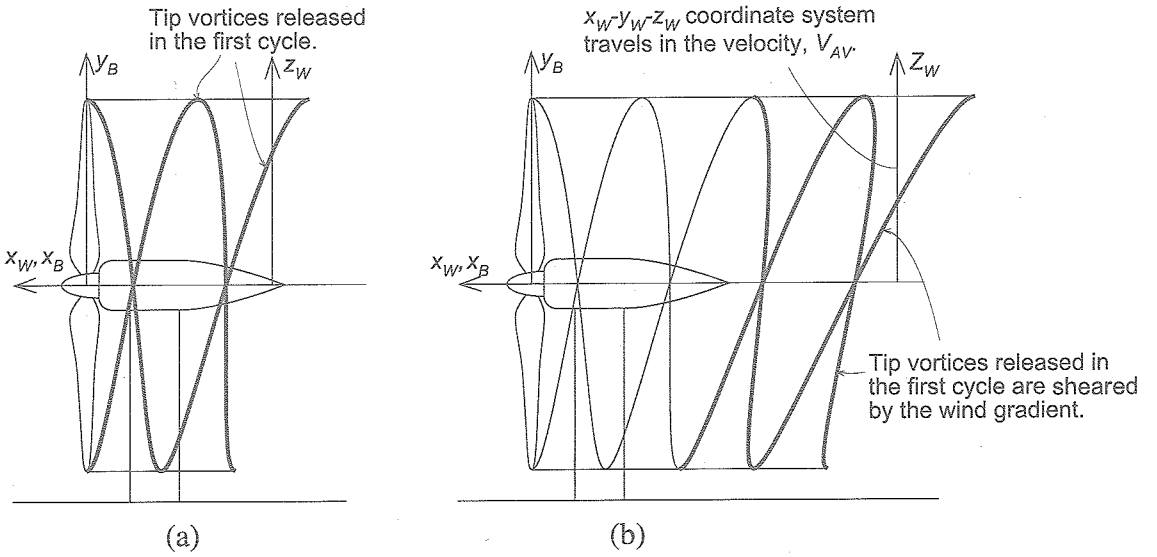

Fig. 5.2 The deformation of the vortex sheets caused by the wind gradient. (a) The shape of the vortex sheets at the end of the first cycle. (b) The shape of the vortex sheets at the end of the second cycle.

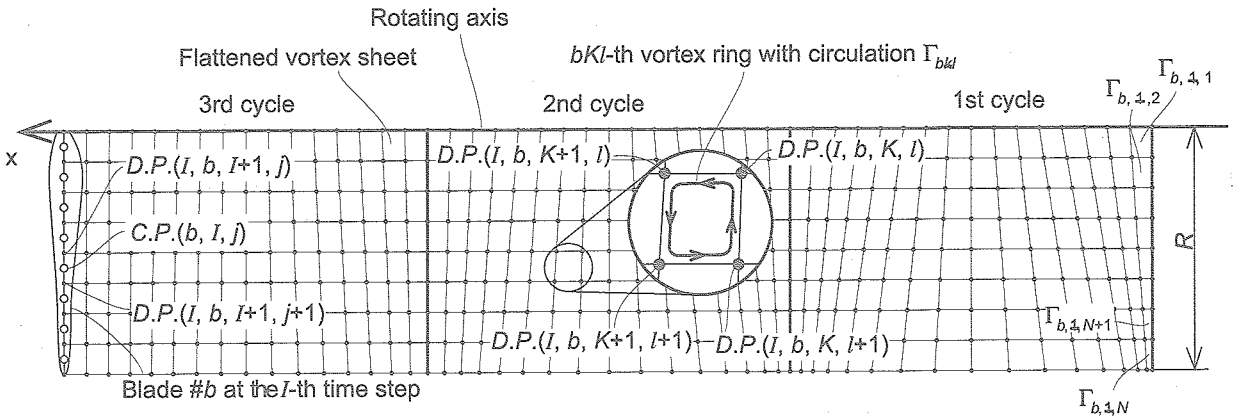

Fig. 5.3 Definition of points on the b-th vortex sheet at the I-th time step. The vortex sheet is flattened to illustrate.

5.3. Influence Coefficients

The influence coefficients, ($\mathbb{X}_{bljcKl}$, $\mathbb{Y}_{bljcKl}$, $\mathbb{Z}_{bljcKl}$), are defined in a similar way to the previous chapter. The only difference is the use of *D.P.*(*I*, *c*, *K*, *l*) instead of *D.P.*(*c*, *K*, *l*). In this chapter, ($\mathbb{X}_{bljcKl}$, $\mathbb{Y}_{bljcKl}$, $\mathbb{Z}_{bljcKl}$) is also defined by Eq. (3.9). However the definitions of $\boldsymbol{a}$, $\boldsymbol{b}$, $\boldsymbol{c}$ and $\boldsymbol{d}$ are different from the previous definitions: $\boldsymbol{a}$, $\boldsymbol{b}$, $\boldsymbol{c}$ and $\boldsymbol{d}$ are defined as the vectors from *C.P.*(*b*, *I*, *l*) to *D.P.*(*I*, *c*, *K*+1, *l*), *D.P.*(*I*, *c*, *K*+1, *l*+1), *D.P.*(*I*, *c*, *K*, *l*+1) and *D.P.*(*I*, *c*, *K*, *l*), respectively, as shown in Fig. 5.4.

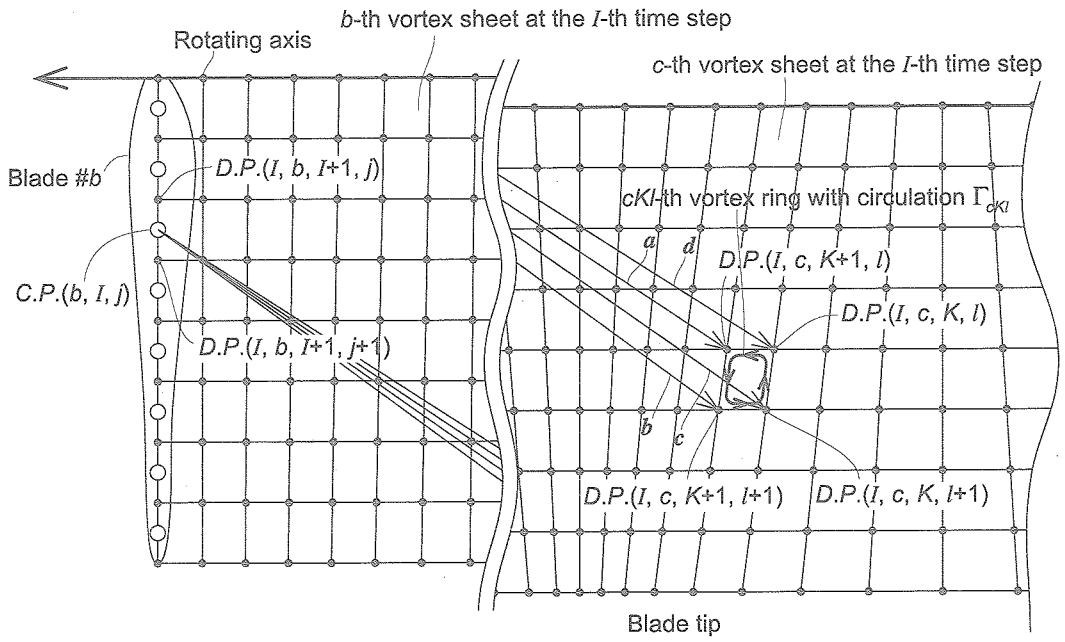

Fig. 5.4 Definition of vectors for the definition of the influence coefficients. Vortex sheets are flattened to illustrate.

5.4. Procedure of Unsteady Propeller Analysis with Effect of Vortex Shear

The influence coefficients that account for the effect of the vortex-sheet shear are obtained. The procedures to calculate T_{Di}, P_{Di}, T_i and P_i are almost the same procedures as described in Section 9 of Chapter 4. The procedure to calculate T_{Di}, P_{Di} is as follows:

1. Specify the propeller, V_{INF}, Ω, R, M, N, dt, c_{ij} and θ_{ij}.
2. Determine the position of $C.P.(b, I, l)$ and $D.P.(I, c, K, l)$.
3. Calculate $\mathbf{X}_{bIjcKl}$ and Θ_{bIjcKl} using Eqs. (3.8) and (3.9).
4. Redefine $\mathbf{X}'_{bijckl}$ and Θ'_{bijckl} using Eqs. (3.37), (3.39), (3.42) and (3.43).
5. Redefine $\mathbf{X}'_{ijkl}$ and Θ'_{ijkl} using Eqs. (3.46) and (3.49)
6. Determine Γ_{ij} by using the iterative procedure described in Section 9 of Chapter 4.
7. Calculate v_{Xij} and $v_{\Theta ij}$ using Eqs. (3.41) and (3.40).
8. Calculate T_{Di} and P_{Di} using Eqs. (3.50) through (3.60).

The difference between the above procedures and the procedures described in Section 9 of Chapter 4 is only Procedure 2.

T_i and P_i are also obtained by the same procedures as described in Section 9 of Chapter 4. Note that the assumption that v_{Xij} and $v_{\Theta ij}$ are negligible small compared with V_{INF} is employed here in order to make it possible to determine the shape of the trailing vortices. Hence, T_{Di}, P_{Di}, T_i and P_i obtained by the above procedure are not reliable, if v_{Xij} and $v_{\Theta ij}$ are not negligibly small compared with V_{INF}.

6. Propeller Design as Optimization Problem

6.1. Optimization Problem

So far, the method for calculating the thrust and the power of a propeller in a wind gradient has been described. However, the purpose of this paper is to describe the method for optimizing the circulation distribution that minimizes the energy loss of the propeller. In this chapter, using the equations and symbols that are defined in the previous chapters, the problem for optimizing the propeller is transformed into a minimizing problem of a quadratic objective function with a quadratic constraint function.

Usually, it is not easy to obtain even the local optimal solution of an optimization problem because of the high nonlinearity of the objective function and the constraint functions. Fortunately, however, the objective function and the constraint function of this problem can be described by quadratic functions whose Hessian matrices are positive definite. Thus, this problem is classified as a convex programming problem, which has been investigated very well[8]. Usually, it is not easy to solve a convex programming problem. However the convex programming problem treated here is solved easily, since the convex programming problem is consists of one quadratic objective function and one quadratic constraint function. Therefore, by transforming the problem for optimizing the propeller into the minimizing problem of a quadratic objective function with a quadratic constraint function, the problem can be easily solved. The procedure to solve this problem is described in Appendix B briefly.

6.2. Classification of Problems

There are two kinds of optimization problems that correspond to the problems in the previous chapters:

1. The optimization problem of circulation distribution of the propeller in a uniform wind. This problem corresponds to the problem in Chapter 3.
   - 1-1. without the effect of the profile drag.
   - 1-2. with the effect of the profile drag.
2. The optimization problem of circulation distribution of the propeller in a wind gradient with the effect of shear of the vortex sheets. This problem corresponds to the problem in Chapter 5.
   - 2-1. without the effect of the profile drag.
   - 2-2. with the effect of the profile drag.

The first problem is named Problem 1 and the second problem is named Problem 2, for convenience. Problem 1 and Problem 2 have two important differences. One is the optimization problem without the effect of the profile drag, and another is the optimization problem with the effect of the profile drag. The former is named Problem X-1 and the latter is named Problem X-2. Though Problem X-2 can be transformed into the convex programming problem consists of the quadratic functions, the derivation of the quadratic function is quite complex and needs numbers of pages. Therefore, transformation of Problem X-2 is not described in this paper.

6.3. Quadratic Objective Function of Problem 1-1

In this section, Problem 1-1 is transformed into a minimizing problem of a quadratic objective function with a quadratic constraint function.

The total thrust without the effect of the profile drag, T, given by Eq. (2.21), can be rewritten as:

$$T = \sum_{i=1}^{N} B\rho\Omega r_i dR\Gamma_i - \sum_{i=1}^{N}\sum_{j=1}^{N} B\rho dR\mathbb{Z}_{ij}\Gamma_i\Gamma_j \quad (6.1)$$

Upon introducing the Einstein's notation, Eq. (6.1) can be rewritten as:

$$T = -\mathbb{A}_{ij}\Gamma_i\Gamma_j - \mathbb{B}_i\Gamma_i \quad (6.2)$$

where Einstein's notation omits the symbol Σ if, in the same term, a suffix occurs twice.
and $\mathbb{A}_{ij}$ and $\mathbb{B}_i$ are:

$$\mathbb{A}_{ij} = B\rho dR\mathbb{Z}_{ij} \quad (6.3)$$

$$\mathbb{B}_i = -B\rho\Omega r_i dR \quad (6.4)$$

Eq. (6.2) is a typical quadratic function. Thus, it has been shown that the thrust of a propeller in a uniform wind can be expressed by a quadratic function. Further, the total power without the effect of the profile drag, P, given by Eq. (2.23) can be rewritten as:

$$P = \sum_{i=1}^{N} B\rho V_{INF} dR r_i\Omega\Gamma_i - \sum_{i=1}^{N}\sum_{j=1}^{N} B\rho dR r_i\Omega\mathbb{X}_{ij}\Gamma_i\Gamma_j \quad (6.5)$$

which can be expressed as:

$$P = \mathbb{C}_{ij}\Gamma_i\Gamma_j + \mathbb{D}_i\Gamma_i \quad (6.6)$$

where $\mathbb{C}_{ij}$ and $\mathbb{D}_i$ are:

$$\mathbf{C}_{ij} = -B\rho dRr_i\Omega\mathbf{X}_{ij} \tag{6.7}$$

$$\mathbf{D}_i = B\rho V_{INFi}\, dRr_i\Omega \tag{6.8}$$

That is, Problem 1-1 can be transformed into the following problem:

Problem 1-1'

$$\begin{aligned} &\text{minimize} && \mathbf{A}_{ij}\Gamma_i\Gamma_j + \mathbf{B}_i\Gamma_i, \\ &\text{subject to} && \mathbf{C}_{ij}\Gamma_i\Gamma_j + \mathbf{D}_i\Gamma_i - P_0 \le 0. \end{aligned}$$

where, P_0 is the value of the designated power. Problem 1-1' is classified as a convex programming problem. Note that the constraint condition is not an equation, since the constraint condition of the convex programming problem must be the form shown above. Furthermore, Problem 1-1' is expressed by quadratic functions only. Thus, It is easy to solve Problem 1-1'.

6.4. Quadratic Objective Function of Problem 2-1

In this section, Problem 2-1 is transformed into a minimizing problem of a quadratic objective function with a quadratic constraint function.

T_i given by Eq. (3.61) is the thrust generated by Blade #1 at the i-th time step without the effect of the profile drag. T_i is not adequate for the objective function since T_i is not a scalar but a vector. One of the scalars adequate for the objective function is the average thrust generated by the propeller in one cycle without the effect of the profile drag, T_{AV}, derived from Eq. (3.61):

$$T_{AV} = \frac{B}{M}\sum_{i=1}^{M}\sum_{j=1}^{N}\rho\Gamma_{ij}\left(r_{ij}\Omega - \sum_{k=1}^{M}\sum_{l=1}^{N}\Theta'_{ijkl}\Gamma_{kl}\right)dR \tag{6.9}$$

where Θ'_{ijkl} is defined in Chapter 5. This may be rewritten as:

$$T_{AV} = \sum_{i=1}^{M}\sum_{j=1}^{N}\frac{B}{M}\rho dRr_{ij}\Omega\Gamma_{ij} - \sum_{i=1}^{M}\sum_{j=1}^{N}\sum_{k=1}^{M}\sum_{l=1}^{N}\frac{B}{M}\rho dR\Theta'_{ijkl}\Gamma_{ij}\Gamma_{kl} \tag{6.10}$$

Upon introducing Einstein's notation, Eq. (6.10) becomes:

$$T_{AV} = -\mathbf{A}_{ijkl}\Gamma_{ij}\Gamma_{kl} - \mathbf{B}_{ij}\Gamma_{ij}$$

where $\mathbf{A}_{ijkl}$ and $\mathbf{B}_{ij}$ are:

$$\mathbf{A}_{ijkl} = \frac{B}{M}\rho dR\Theta'_{ijkl} \tag{6.11}$$

$$\mathbf{B}_{ij} = -\frac{B}{M}\rho dRr_{ij}\Omega \tag{6.12}$$

P_i given by Eq. (3.62) is also a vector. A constraint condition can be a vector form. However, one scalar constraint condition is more easily solved. Thus, the following scalar is used for the constraint condition in this paper: the average power absorbed by the propeller in one cycle without the effect of the profile drag, P_{AV}, derived from Eq. (3.62):

$$P_{AV} = \frac{B}{M}\sum_{i}^{M}\sum_{j=1}^{N}\rho\Gamma_{ij}\left(V_{INFij} - \sum_{k=1}^{M}\sum_{l=1}^{N}\mathbf{X}'_{ijil}\Gamma_{kl}\right)dRr_{ij}\Omega R \tag{6.13}$$

This may be expressed as:

$$P_{AV} = \sum_{i=1}^{M}\sum_{j=1}^{N}\frac{B}{M}\rho V_{INFij}dRr_{ij}\Omega\Gamma_{ij} - \sum_{i=1}^{M}\sum_{j=1}^{N}\sum_{k=1}^{M}\sum_{l=1}^{N}\frac{B}{M}\rho dRr_{ij}\Omega\mathbf{X}'_{ijil}\Gamma_{ij}\Gamma_{kl} \tag{6.14}$$

Similarly, Eq.(6.14) can be rewritten as:

$$P_{AV} = \mathbf{C}_{ijkl}\Gamma_{ij}\Gamma_{kl} + \mathbf{D}_{ij}\Gamma_{ij} \tag{6.15}$$

where $\mathbf{C}_{ijkl}$ and $\mathbf{D}_{ij}$ are:

$$\mathbf{C}_{ijkl} = -\frac{B}{M}\rho dRr_{ij}\Omega\mathbf{X}'_{ijil} \tag{6.16}$$

$$\mathbf{D}_{ij} = \frac{B}{M}\rho V_{INFij}dRr_{ij}\Omega \tag{6.17}$$

That is, Problem 2-1 can be transformed into the following problem:

Problem 2-1'

$$\text{minimize} \quad \mathbb{A}_{ijkl}\Gamma_{ij}\Gamma_{kl} + \mathbb{B}_{ij}\Gamma_{ij},$$
$$\text{subject to} \quad \mathbb{C}_{ijkl}\Gamma_{ij}\Gamma_{kl} + \mathbb{D}_{ij}\Gamma_{ij} - P_0 \le 0.$$

Also, Problem 2-1' is classified as a convex programming problem. Furthermore, Problem 2-1' is expressed by quadratic functions only. Thus, Problem 2-1' is also easily solved.

7. Solution Evaluation of Steady Propeller Design

7.1. Outline of Evaluation

So far, the method for optimizing the circulation distribution that minimizes the energy loss of a propeller in a wind gradient has been developed. In this chapter, the following are described: First, Prandtl's approximate solution[1] is introduced in order to be used as a reference for the accuracy of the solutions of Problem 1-1', and the concepts of v' and F are also introduced for the later convenience. Second, based on Prandtl's approximate solution, the validity and accuracy of the solution of Problem 1-1' are evaluated and the adequate values for the number of blade segments and the number of the time steps are determined, which are used in the later calculations. Third, based on the solution of Problem 1-1', the validity and accuracy of the solution of Problem 2-1' without wind gradient are also evaluated.

7.2. Prandtl's Approximate Solution

Prior to evaluations of the validity and the accuracy of the present method, Prandtl's approximate solution is introduced. The main purpose of this section is the introduction of v' and F that are defined by Betz and Prandtl[1]. The precise description of Prandtl's approximate solution is not shown here, since it is beyond the scope of this paper. However, this solution has been precisely described by Larrabee[9), 10), 11)].

Though Prandtl's approximate solution is used as a reference for the accuracy of the proposed method in this paper, it is an approximate solution because of the following two reasons. First, Prandtl modeled the effect of the blade tips by using an analogy with the flow about an infinite array of semi-infinite plates. Second, Prandtl used vortex sheets with a constant pitch that does not take the effect of the induced velocity into consideration. The second approximation is only valid when a propeller is 'lightly loaded'. Goldstein[2] has established a propeller theory without the first approximation, however, the second approximation is also necessary in his theory. Even though Goldstein's solution is more accurate than Prandtl's approximate solution, Prandtl's approximate solution is used in this paper because of its simplicity and applicability.

Betz has defined v' in his propeller theory as follows:

$$v' = w / \cos \phi_V \tag{7.1}$$

where w is the induced velocity on the vortex sheet far behind the propeller and exactly normal to the vortex sheet, when the vortex sheet consists of the trailing vortices only.
The helical angle, ϕ_V, is defined by:

$$\tan \phi_V = \frac{V_{INF} + w_X}{r\Omega - w_\theta} \tag{7.2}$$

where w_X is the axial component of w, and is defined by:

$$w_X = w \cos \phi_V \tag{7.3}$$

and w_θ is the tangential component of w, and is defined by:

$$w_\theta = w \sin \phi_V \tag{7.4}$$

These definitions are illustrated in Fig. 7.1. Betz has also shown that in the optimized propeller, the vortex sheets far behind the propeller are conveyed backward with a uniform velocity. Further, Betz has shown that for a coordinate system fixed to the air, that uniform velocity is v'. This is called Betz condition. Furthermore, it can be easily seen that there is no flow that crosses the vortex surface. As a result, the flow far behind the propeller is identical to the flow generated by the rigid helical surfaces that are conveyed backward in the air with the velocity, v'. Thus v' is called vortex displacement velocity. As mentioned above, Prandtl modeled the flow by using an analogy with the flow about an infinite

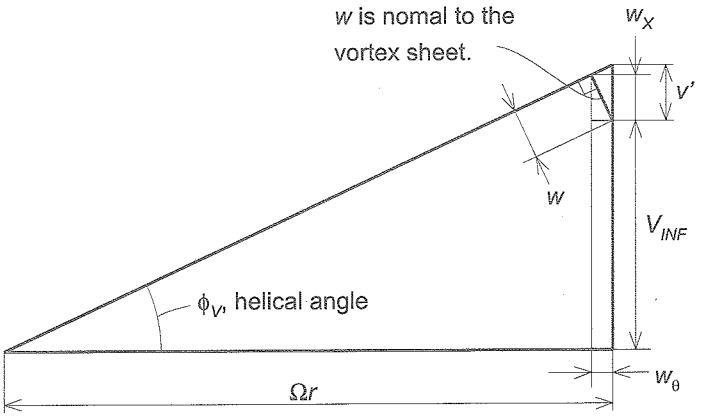

Fig. 7.1 Vector diagram of the flow on the surface of a vortex sheet far behind the propeller. w is induced velocity.

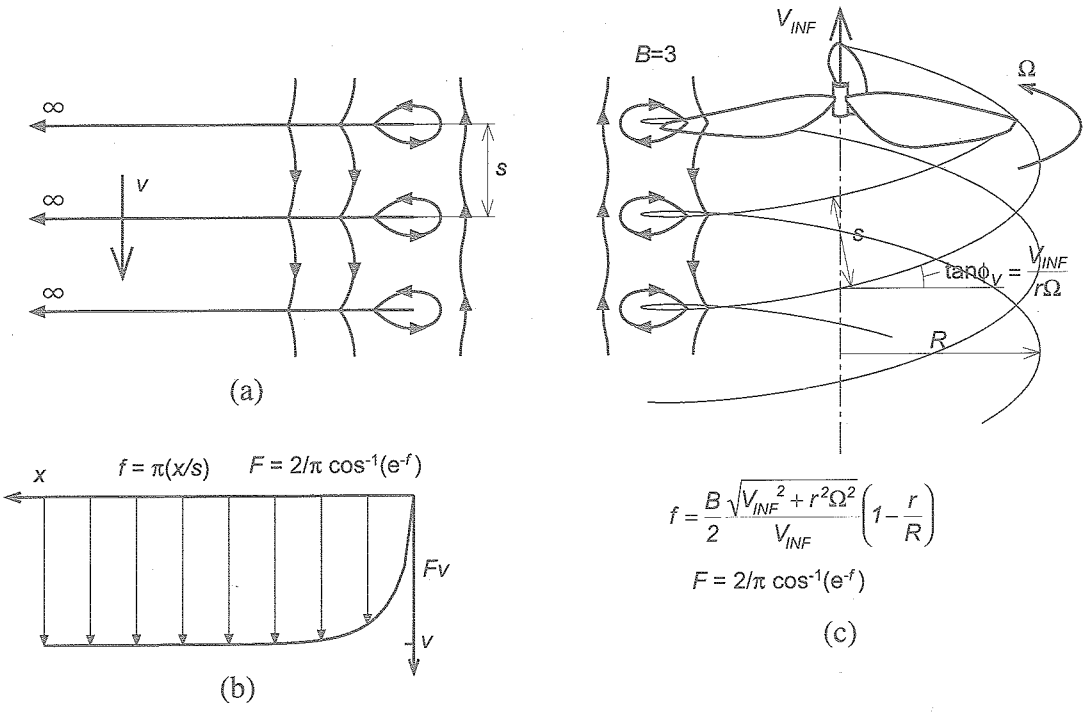

Fig.7.2 Principle concept of function F.(a) Flow about an infinite array of semi-infinite Plates. (b) Average axial velocity y of Fig.1-(a). This velocity is given by Fv.(c) Flow aboutvortex sheets.

array of semi-infinite plates as shown in Fig. 7.2-(a). In Fig. 7.2-(a) plates are traveling with velocity, v. Fig. 7.2-(a) shows that there is a flow that rounds the tip of the plates. By this flow, the average axial flow is reduced as shown in Fig. 7.2-(b), and the average axial flow is given by Fv; where F is a function introduced by Prandtl and defined by:

$$F = \frac{2}{\pi}\cos^{-1}\left(e^{-f}\right) \tag{7.5}$$

and f is given by:

$$f = \pi\frac{x}{s} \tag{7.6}$$

where x is the distance from the plate tip and s is the distance between the plates. Prandtl considered that the average axial flow about the propeller shown in Fig. 7.2-(c) is also given by Eq. (7.5). However, the value of s must be modified because of the effect of the vortex sheet helical angle, ϕ_V.

Thus, in the model shown in Fig. 7.2-(c), Eq. (7.6) is modified as:

$$f = \frac{B}{2}\frac{\sqrt{{V_{INF}}^2 + r^2\Omega^2}}{V_{INF}}\left(1-\frac{r}{R}\right) \qquad (7.7)$$

Prandtl has shown that the circulation distribution of an optimized propeller is given by:

$$\Gamma = \frac{2\pi}{B\Omega}V_{INF}v'\frac{\Omega^2 r^2}{{V_{INF}}^2+\Omega^2 r^2}F \qquad (7.8)$$

In Eq. (7.8), v' is an unknown variable that is determined by the designated consumed power, P_0. To obtain the value of v', Larrabee's method[4] is convenient.

7.3. Solution Accuracy of Problem 1-1'

In this section, the validity and accuracy of the solution of Problem 1-1' are evaluated. The numerical example is as follows: R=1.0m, V_{INF}=10m/s, Ω=10π rad/s, B=2, ρ=1.225kg/m^3, P_0=100W, the length of vortex sheets, L_V, is 10m. The number of the time steps in one cycle, M_C, and the number of the blade segments, N, are parameters. The following cases are selected for calculations:

Case 1, N=10, M_C=18, 36, 180,

Case 2, N=30, M_C=18, 36, 180.

v_i' is calculated in each case, and the results are shown in Figs. 7.3 and 7.4. As mentioned above, the Betz condition requires v_i' to be constant. As seen in both figures, the values of v_i's are almost constant and approximately equal to that of Prandtl's approximate solution. This means that solutions given by the proposed method have good accuracy. Further, it can be seen that the more M_C increases, the more constant v_i' becomes. Thus, an increase of M_C effectively improves the accuracy of the calculation. Though Case 2 uses more N than Case 1, the values of v_i's of Case 2 are not more constant than those of Case 1. This means that there is an appropriate ratio between N and M_C. The propulsive efficiencies, ηs, as functions of N and M_C are plotted in Fig. 7.5. This shows that η in each case agrees well with η of Prandtl's approximate solution, and η in each case approaches that of Prandtl's approximate solution as M_C increases. This tendency is appropriate for a computational result. In addition, it should be noted that the results of Case 1 are more accurate than those of Case 2 in spite of the small number of N.

Also, the distributions of Γ_is are shown in Fig. 7.6. Since every result is very similar to each other, only the results of the two extreme cases and Prandtl's approximate solution are shown. One is the case that the number of the variables is the smallest: N=10 and M_C=18.

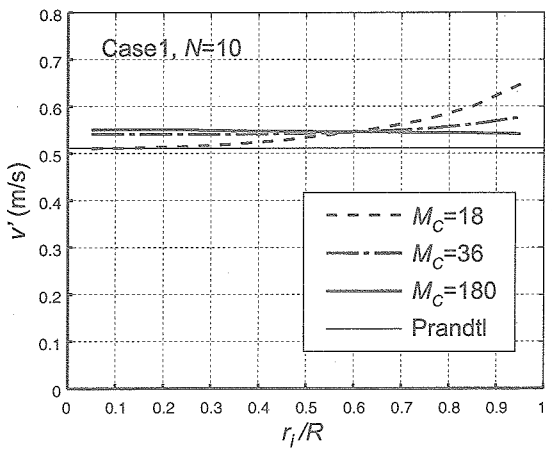

Fig. 7.3 Distribution of v'. N=10.

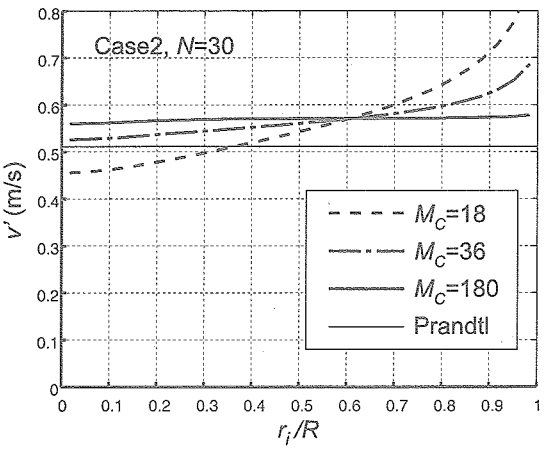

Fig. 7.4 Distribution of v'. N=30.

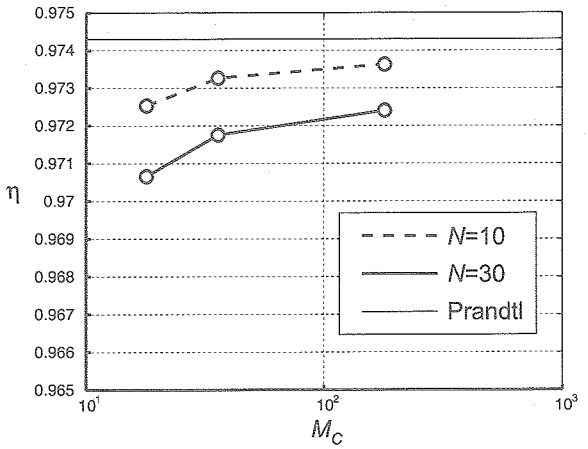

Fig. 7.5 η as a function of N and M_C.

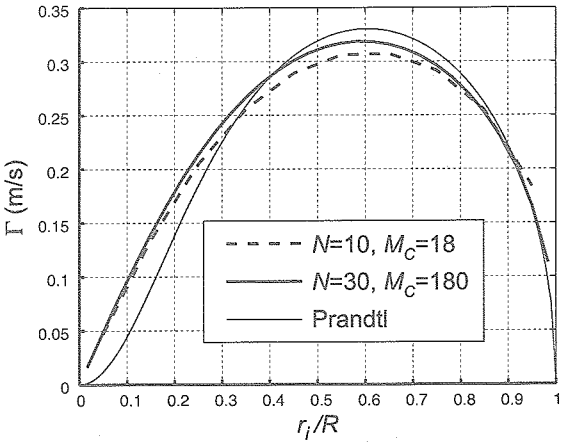

Fig. 7.6 Distribution of Γ_i.

Another is the case that the number of the variables is the largest: N=30 and M_C=180. Both distributions of the circulation are similar to that of Prandtl's approximate solution and much more similar to that of Goldstein's exact solution[5]. In addition, it should be noted that the results of Case 1 is more accurate than those of Case 2 in spite of the small number of N. This is probably caused by the improper ratio between N and M_C.

To sum up the above evaluations, the accuracy of the solution of Problem 1-1' is acceptable and greatly depends on the number of M_C, but is not very dependant on the number of N. Hence, it is desirable to use a large number of M_C in order to obtain an accurate solution. However, the number of operations to solve this optimization problem is proportional to the cube of the number of the decision variables, in the worst case. Therefore, from now on, 10 and 38 are used as the numbers of N and M respectively from a standpoint of the cost performance.

7.4. Solution Accuracy of Problem 2-1' without wind gradient

In this section the validity and accuracy of the solution of Problem 2-1' without wind gradient, which must agree with the solution of Problem 1-1', are evaluated.

The numerical example is the same as that used in the previous section; R=1.0m, V_{AV}=10m/s, Ω=10π rad/s, B=2, ρ=1.225kg/m^3, P_0=100W, the number of the cycle, L, is 5. The number of the time steps in one cycle, M, and the number of the blade segments, N, are 38 and 10 respectively, as determined in the previous section. Though Problem 2-1' is an optimization problem of a propeller in a wind gradient, the magnitude of wind gradient is chosen as 0m/s/m in order to compare this solution with the solution of Problem 1-1'.

The thrust obtained is 9.733N. Hence, η is 0.9733 that agrees with η plotted in Fig. 7.5. Further, the distribution of Γ_{ij} is shown in Fig. 7.7. The distribution of Γ_{ij} is steady as shown in Fig. 7.7, since the wind is uniform.

Also, the Γ_i distribution of the solution of Problem 1-1' in the previous section is shown by the bold line. The Γ_{ij} distribution of Problem 2-1' and that of Problem 1-1' are exactly same, as seen in Fig. 7.7. Furthermore, v'_{ij} distribution of the solution is shown in Fig. 7.8. Also, v'_i distribution of the solution of Problem 1-1' in the previous section is shown by the bold line. This shows that v'_{ij} of Problem 2-1' is constant and steady, and exactly agrees with that of Problem 1-1'. From these results, it is shown that the solution of Problem 2-1' without wind gradient is valid and accurate.

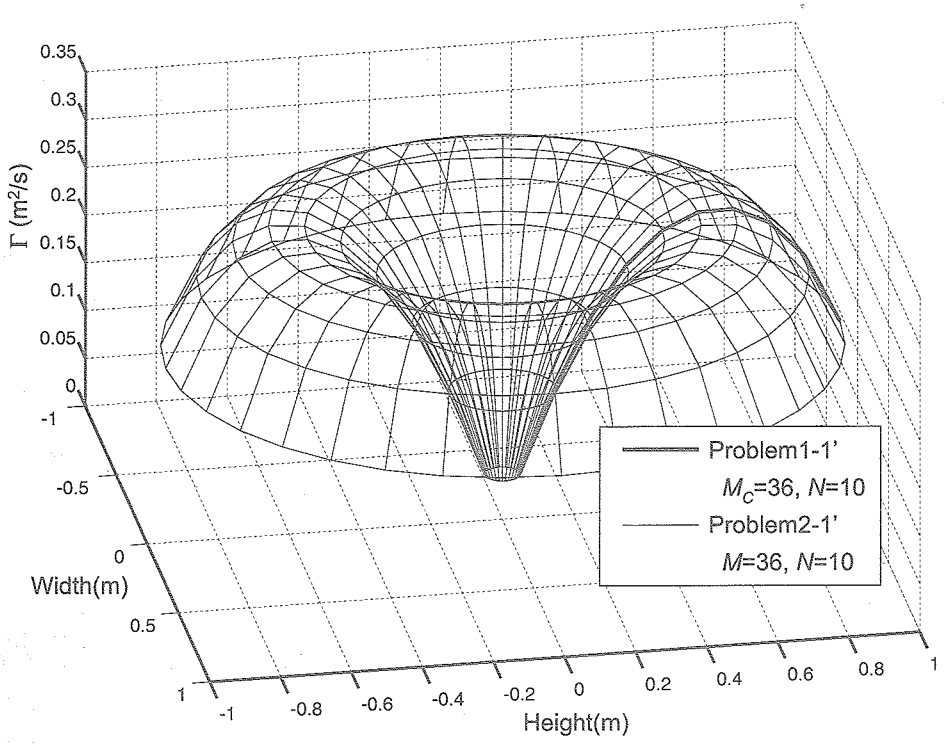

Fig.7.7 Distribution of Γ_{ij} of the solution of Problem 2-1' without t wind gradient.

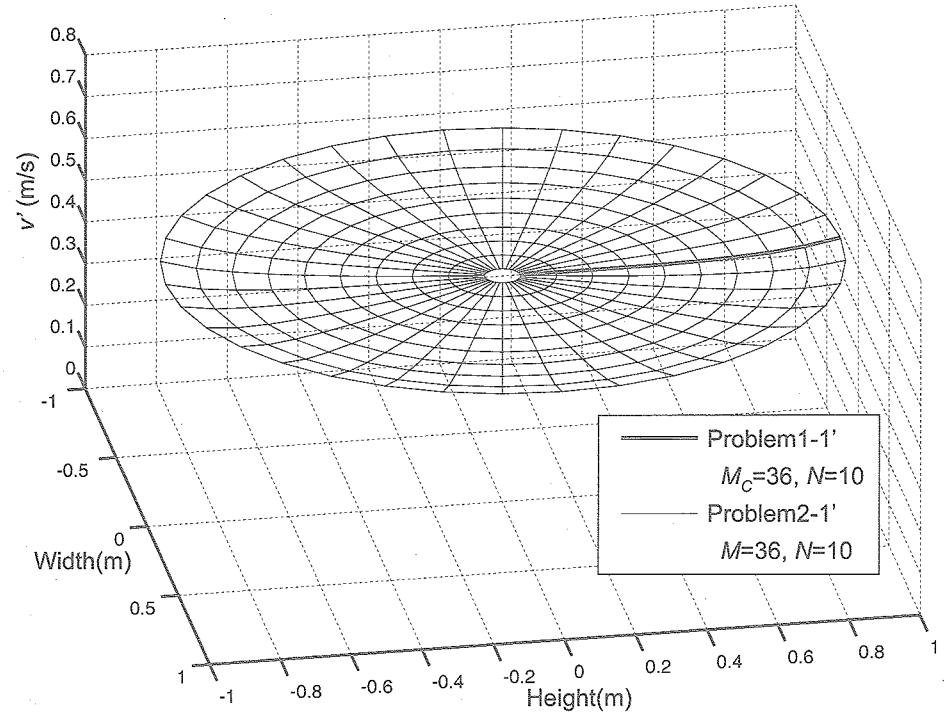

Fig.7.8 Distribution of v_i' of the solution of Problem 2-1' without t wind gradient.

8. Solution Evaluation of Unsteady Propeller Design

8.1. Solution Accuracy of Problem 2-1' with Wind Gradient

In the previous chapter, the validity and accuracy of the solutions of Problem 1-1' and Problem 2-1' without the wind gradient are shown. In this chapter, based on the results of the expanded momentum theory described in Chapter 2, the validity and accuracy of the solutions of Problem 2-1' with the wind gradient are evaluated.

The numerical example is almost the same as that used in the previous chapter; R=1.0m, V_{AV}=10m/s, Ω=10π rad/s, B=2, ρ=1.225kg/m^3, P_0=100W, L=5, M=36, N=10. The difference between this condition and the previous condition is the existence of the wind gradient. The magnitude of the wind gradient is 2m/s/m. Hence, the wind velocity, V_{INFij}, given by Eq. (4.1) becomes:

$$V_{INFij} = 10 + 2.0 z_{ij} \tag{8.1}$$

The thrust value of the solution obtained here is 10.56N. Hence, η is 1.056, while η obtained by the extended momentum theory is 1.17 and η of the normal propeller obtained in the previous chapter is 0.973. That is, though η of the solution obtained here is less than η of the expanded momentum theory, it is greater than η of the normal propeller and even greater than 1.0.

The distribution of Γ_{ij} obtained here is shown in Fig. 8.1. As seen in the figures, although the distribution of Γ_{ij} is unsteady because of the existence of the wind gradient, the distribution of Γ_{ij} is almost symmetrical about the z-axis. Further, it is seen from Fig. 8.1-b that the value of Γ_{ij} at each radius is almost proportional to the height, z_{ij}. Furthermore, the absolute values of Γ_{ij} shown in Fig. 8.1 are much larger than those of Γ_{ij} shown in Fig. 7.7. Thus, the induced velocities, which are assumed to be much smaller than V_{INFij}, must be evaluated in order to confirm that the induced velocities satisfy the light disk-loading assumption. Fig. 8.2 shows the distribution of the axial induced velocity at the propeller disk, $-v_{Xij}$ and the axial induced velocity obtained by the expanded momentum theory. Fig. 8.2-a shows that $-v_{Xij}$ obtained by the present method agrees well with the induced velocity obtained by the expanded momentum theory. Further Fig. 8.2-a shows that the maximum absolute value of $-v_{Xij}$ exceeds 1.0, which is 10% of V_{INFij}. Thus, the light disk-loading assumption does not hold properly.

8.2. Correction of Influence Coefficients

However, the gradient of $-v_{Xij}$ in Fig. 8.2-b is about -1m/s/m, which means that the gradient of the axial induced velocity at the vortex sheet far behind the propeller disk is about –2m/s/m, since the induced velocity at the propeller disk is half the value of that far behind the propeller disk. Thus the axial induced velocity at the vortex sheet, far behind the propeller disk, almost cancels the wind gradient shown Fig. 8.3. That is, the wind gradient in the propeller wake disappears and the vortex sheet travels with approximately uniform velocity if the effect of the rotating component of the induced velocity is negligible.

Note that although the vortex sheets travels with uniform velocity, a small amount of vortex shear exists. The reason is that the induced velocity near the propeller is half the value of that far behind the propeller disk, and the wind gradient does not disappear near the propeller disk as shown in Fig. 8.3. Furthermore, as mentioned in the previous chapter, the vortex sheet travels with the vortex displacement velocity, v'_{ij}, because of the existence of the rotating component of the induced velocity. Therefore, a more precise discussion of vortex shear must be done by using v'_{ij}, not by using $-v_{Xij}$.

The vortex displacement velocity v'_{ij} is defined by Eq. (6.1) and Betz condition requires v'_{ij} to be constant when the vortex sheet consists of only the trailing vortices. In this problem, however, the vortex sheet consists of not only trailing vortices but also shed vortices. Thus, the Betz condition does not make sense and the induced velocity, w_{ij}, shown in Fig. 8.4 is not normal to the vortex sheet. From Fig. 8.4 v'_{ij} may be written as:

$$v'_{ij} = \frac{V_{INFij} + w_{Xij}}{r_{ij}\Omega - w_{\theta ij}} r_{ij}\Omega - V_{INFij} \tag{8.2}$$

Fig. 8.5 shows the distribution of $v'_{ij}+V_{INFij}$. This shows that although there is a singular point at the center, the vortex sheet travels with an almost uniform velocity, 10.7m/s. Hence, it can be seen that the influence coefficients with the effect of vortex shear are not proper for the optimum propeller designs, and those without the effect of the vortex shear is proper for the optimum propeller designs.

8.3. Solution Accuracy of Problem 2-1' without Wind Gradient

So far, it is shown that the influence coefficients without the effect of the vortex shear, defined in Chapter 4, are proper for optimum propeller designs. Thus, the calculation for the same case is executed again by using the influence coefficients without the effect of the vortex shear. η of this solution is 1.059, which agrees very well with η of the previous solution, 1.056. Further, the distribution of Γ_{ij} is shown in Fig. 8.6. The figures show that the difference between Γ_{ij} shown in Fig. 8.1 and Γ_{ij} shown in Fig. 8.6 is very small. Hence, it is seen that the effect of the vortex shear is small. From now on, every calculation is executed by using the influence coefficients without the effect of the vortex shear. Also, the distributions of $-v_{Xij}$ of the solution and that given by the expanded momentum theory are shown in Fig. 8.7. This shows that the distribution of $-v_{Xij}$ is similar to that of Fig. 8.2. That is, the effect of the vortex shear is small.

8.4. Local Propulsive Efficiency

Although the gradient of $-v_{Xij}$ is approximately the same as the induced velocity derived from the expanded momentum theory, $-v_{Xij}$ is not the average axial induced velocity but the axial induced velocity on the blade. The average axial induced velocity near the propeller disk, $-\bar{v}_{Xij}$, is given by:

$$-\bar{v}_{Xij} = -Fv_{Xij} \tag{8.3}$$

where F is given by Fig. 6.5. Hence, there are two kinds of the induced velocities. One is the axial induced velocity on the blade, $-v_{Xij}$, and the other is the average axial induced velocity near the propeller disk, $-\bar{v}_{Xij}$.

It is also important to compare the thrust distribution of the solution and that given by the expanded momentum theory. For the convenience of comparison with the expanded momentum theory, the thrust per unit area, t_{ij}, is defined as follows:

$$t_{ij} = \frac{BT_{ij}}{2\pi r_{ij}} \tag{8.4}$$

where T_{ij} is the thrust of the ij-th blade segment given by Eq. (3.61). The t_{ij} distribution of the solution and the thrust per unit area given by the expanded momentum theory are shown in Fig. 8.8. This shows that the former is not similar to the latter, while the distribution of $-v_{Xij}$ is similar to that of the axial induced velocity given by the expanded momentum theory. It is, however, not $-v_{Xij}$ but $\bar{v}_{Xij}$ that should be compared with the induced velocity given by the expanded momentum theory. Here, the thrust per unit area derived from $\bar{v}_{Xij}$, t'_{ij}, is defined as:

$$t'_{ij} = -2\rho\left(V_{INF} - \bar{v}_{Xij}\right)\bar{v}_{Xij} \tag{8.5}$$

The distribution of t'_{ij} is shown in Fig. 8.9. Although the distribution of t'_{ij} is not symmetrical about z-axis, the shape of the distribution of t'_{ij} is similar to that of t_{ij}. Thus, the relation between t_{ij} and $-v_{Xij}$ is rational. Also, the power per unit area, p_{ij}, is defined as follows:

$$p_{ij} = \frac{BP_{ij}}{2\pi r_{ij}} \tag{8.6}$$

where P_{ij} is the power consumed by the ij-th blade segment given by Eq. (3.62). The distribution of p_{ij} of the solution and the power per unit area derived from the expanded momentum theory are shown in Fig. 8.10. This also shows that the former is not similar to the latter. However, the shape of the distribution of p_{ij} is quite similar to that of t_{ij}. Thus, it is expected that t_{ij}/p_{ij} is constant. By the way, the local propulsive efficiency, η_{ij}, can be defined by:

$$\eta_{ij} = \frac{V_{INFij}\,t_{ij}}{p_{ij}} \tag{8.7}$$

That is, η_{ij} is V_{INFij} times t_{ij}/p_{ij}. Therefore, it is also expected that η_{ij} is proportional to V_{INFij}. However, the distribution of η_{ij} shown in Fig. 8.11 is not regular. The propulsive efficiency can be also derived from the vector diagram at the propeller disk shown in Fig. 8.12 as follows. From Kutta-Joukowsky theorem, T_{ij} and P_{ij} are given by:

$$T_{ij} = \rho\left(r_{ij}\Omega - v_{\theta ij}\right)\Gamma_{ij}dR \tag{8.8}$$

$$P_{ij} = \rho\left(V_{INFij} - v_{Xij}\right)\Gamma_{ij}r_{ij}\Omega dR \tag{8.9}$$

The local propulsive efficiency, η'_{ij}, is given by:

$$\eta'_{ij} = \frac{V_{INFij}T_{ij}}{P_{ij}} \tag{8.10}$$

Eqs. (8.8) and (8.9) into Eq. (8.10) gives:

$$\eta'_{ij} = \frac{V_{INFij}\left(r_{ij}\Omega - v_{\theta ij}\right)}{\left(V_{INFij} - v_{Xij}\right)r_{ij}\Omega} \tag{8.11}$$

From Fig. 8.12, the following equation is obtained:

$$\frac{r_{ij}\Omega - v_{\theta ij}}{V_{INFij} - v_{Xij}} = \frac{r_{ij}\Omega}{V_{INFij} + v'_{Dij}} \tag{8.12}$$

where v'_{Dij} is the vortex displacement velocity at the propeller disk. Eq. (8.12) into Eq. (8.11) gives:

$$\eta'_{ij} = \frac{V_{INFij}}{V_{INFij} + v'_{Dij}} \tag{8.13}$$

Eq. (8.13) shows that η'_{ij} given by this very simple equation consists of V_{INFij} and v'_{Dij}. Also, the distribution of η'_{ij} is shown in Fig. 8.13. Fig. 8.13 agrees with Fig. 8.11 exactly. This means that both η_{ij} and η'_{ij} is correct and v'_{Dij} can be an index of η_{ij}.

8.5. Energy Flow

In Fig. 8.7-b, the region where $-v_{Xij}$ is negative is indicated by the gray regions. In this region, the air is not accelerated but decelerated. Further, this region approximately corresponds to the region where the wind velocity is higher than the average velocity. Also, in Figs. 8.8-b and 8.10-b, the regions where t_{ij} and p_{ij} are negative value are indicated by the gray regions respectively. These regions also approximately correspond to the region where the wind velocity is higher than the average velocity. Thus, the optimum propeller in the wind gradient absorbs the energy of the air whose velocity is higher than the average velocity and consumes the energy by accelerating the air whose velocity is lower than the average velocity.

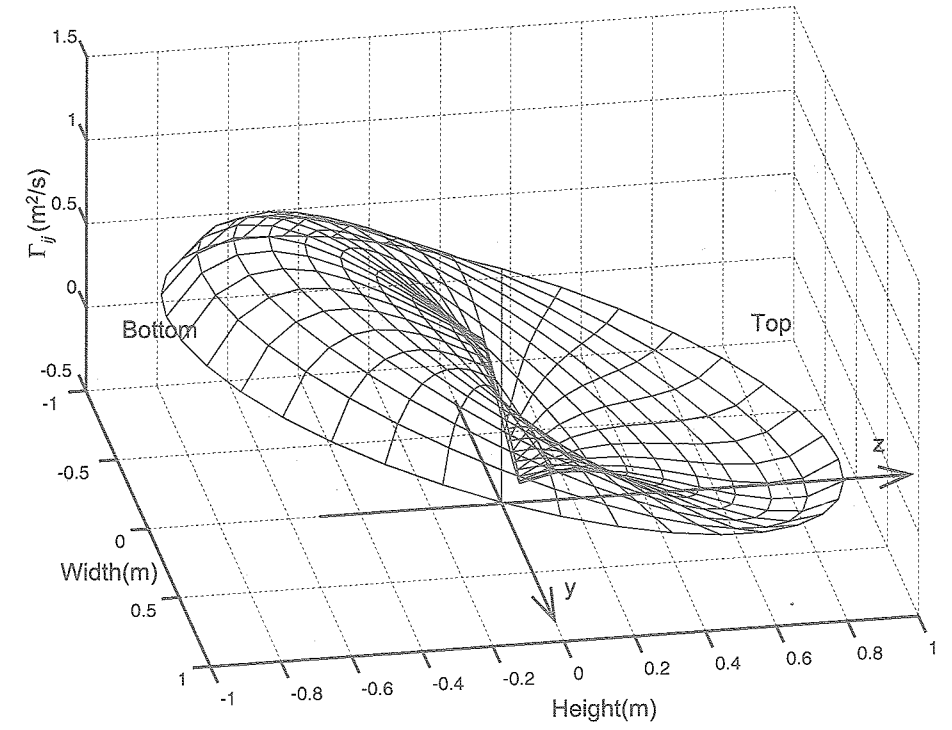

(a)

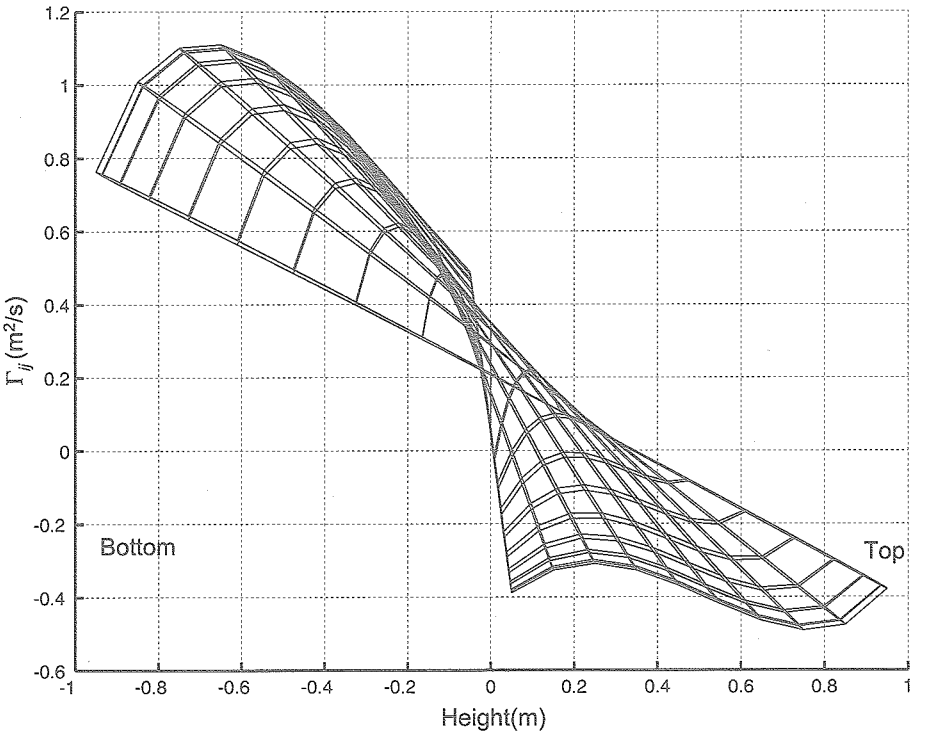

(b)

Fig. 8.1 Γ_{ij} distribution of Problem 2-1': (a) bird's-eye view; (b) side view. The wind gradient is 2m/s/m.

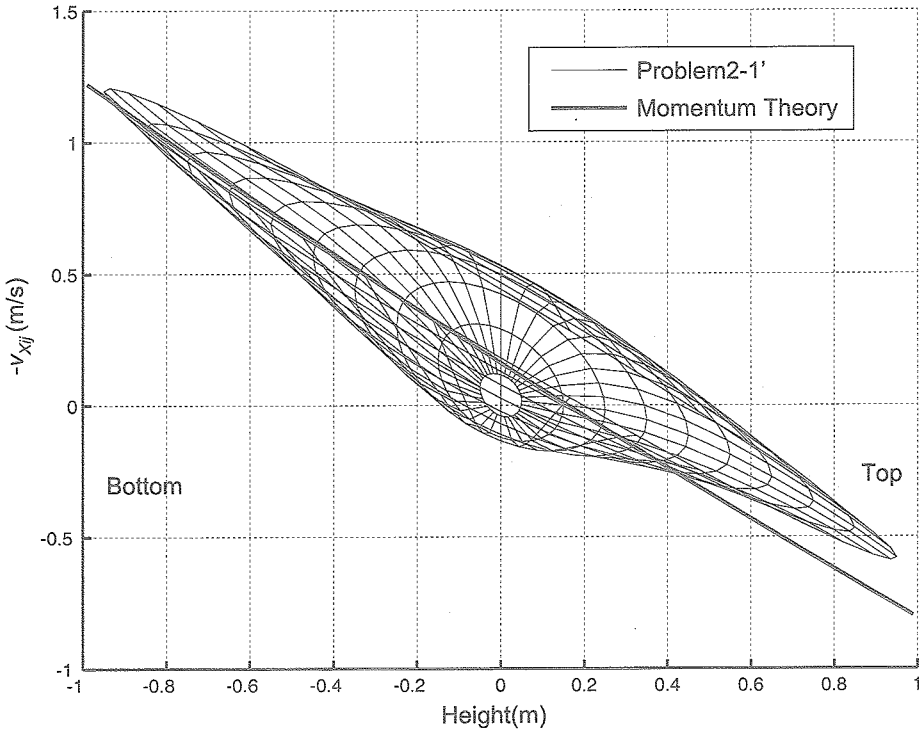

(a)

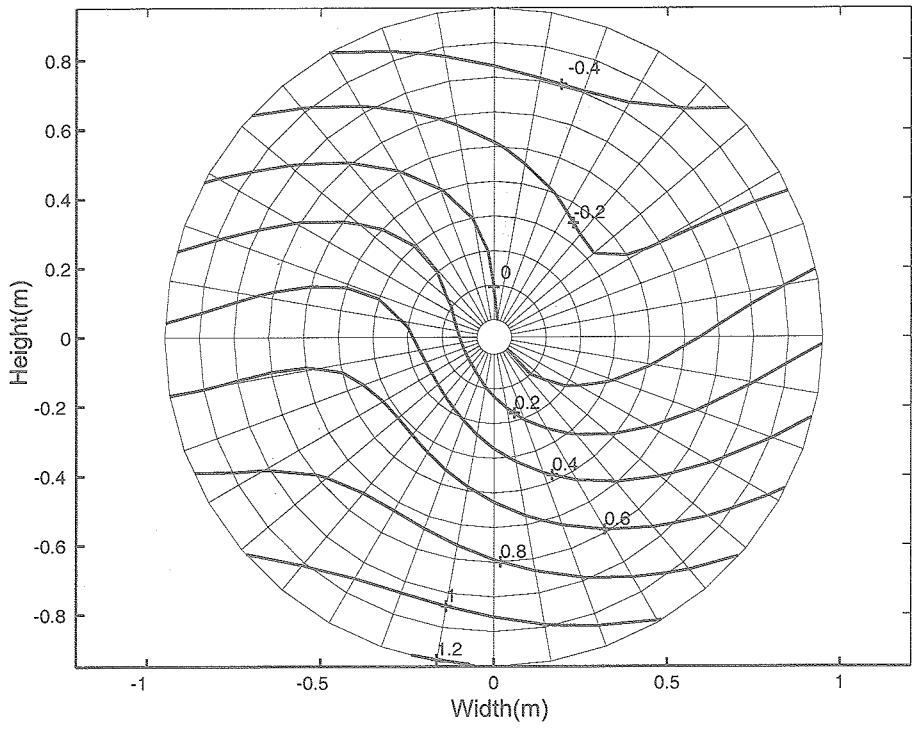

(b)

Fig. 8.2 $-v_{Xij}$ distribution of Problem 2-1': (a) bird's-eye view; (b) front view. The wind gradient is 2m/s/m. Note that positive direction of v_{Xij} is forward

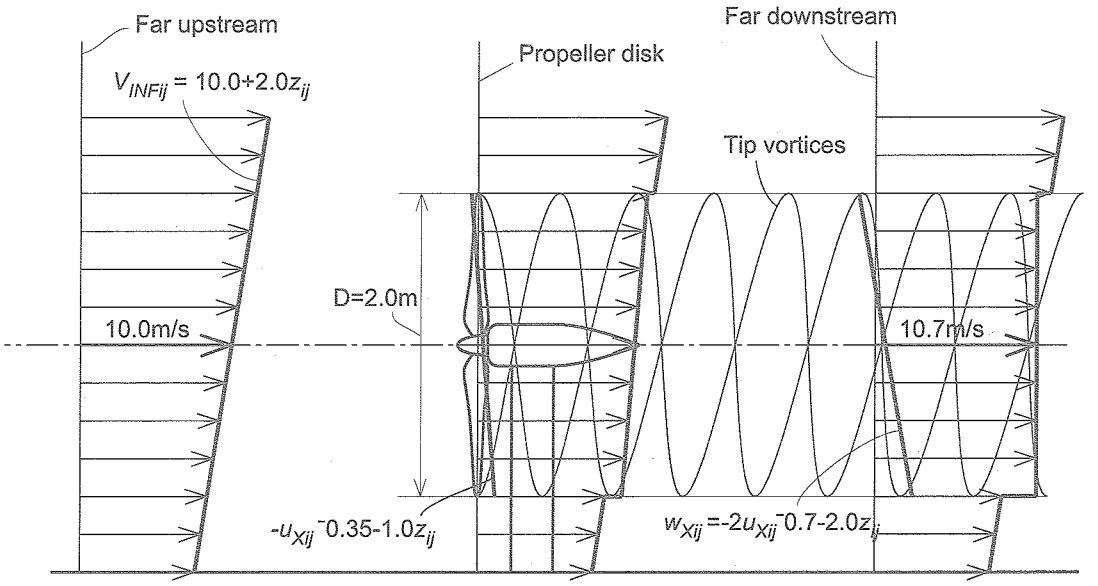

Fig.8.3 Side view of the simplified wind profile. The effect of rotating component of the induced velocity is ignored. The wind gradient far downstream disappears because of the inverted gradient of the induced velocity.

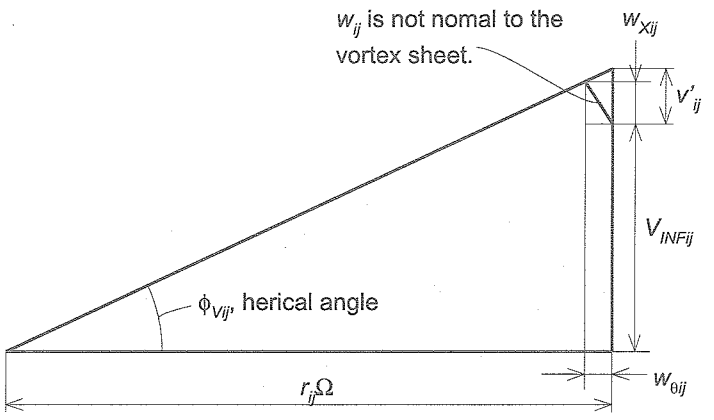

Fig. 8.4 Vector diagram of the flow on the surface of a vortex sheet far behind the propeller. w_{ij} is not normal to the vortex sheet, when the vortex sheet consists of not only the trailing vortices but also shed vortices.

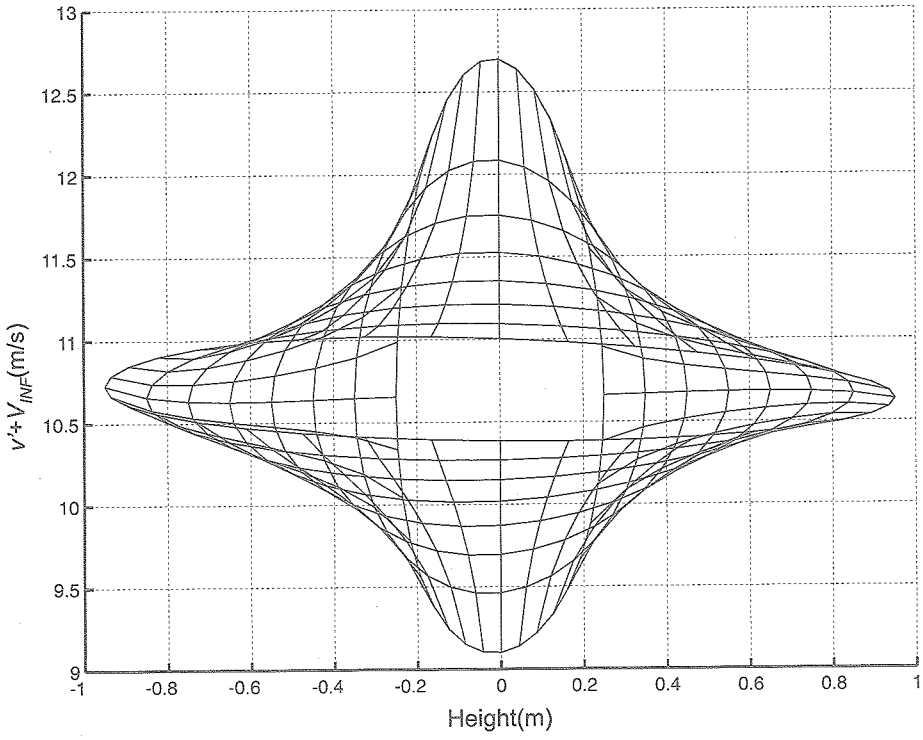

(a)

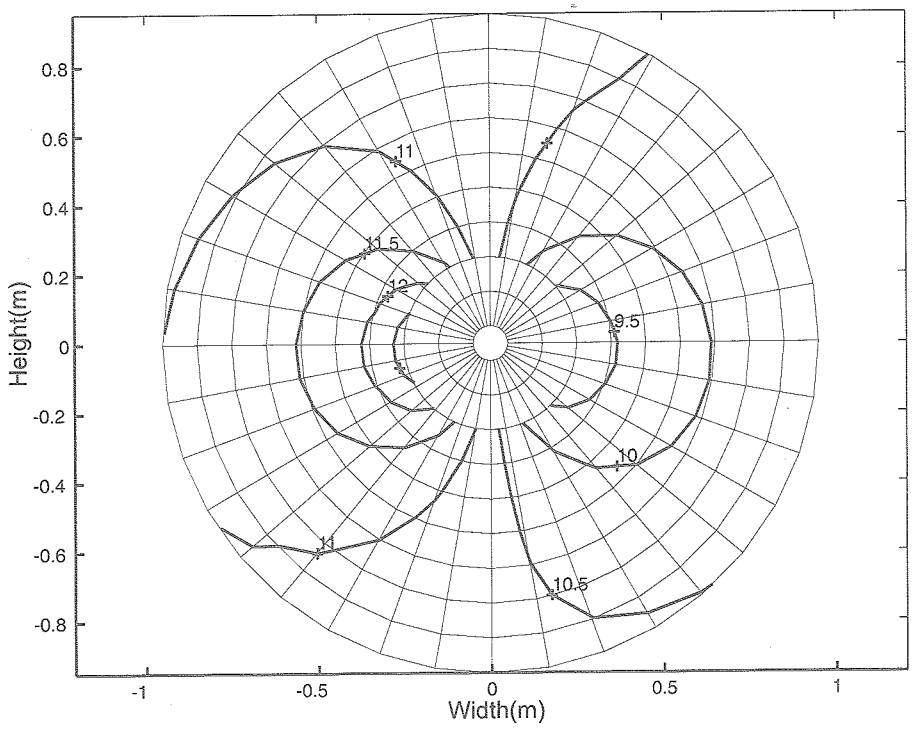

(b)

Fig. 8.5 $v'_{ij} + V_{INFij}$ distribution of Problem 2-1': (a) side view; (b) front view. The wind gradient is 2m/s/m. There is a singular point at the center. Thus $v'_{ij} + V_{INFij}$ at j=1 and 2 are not illustrated.

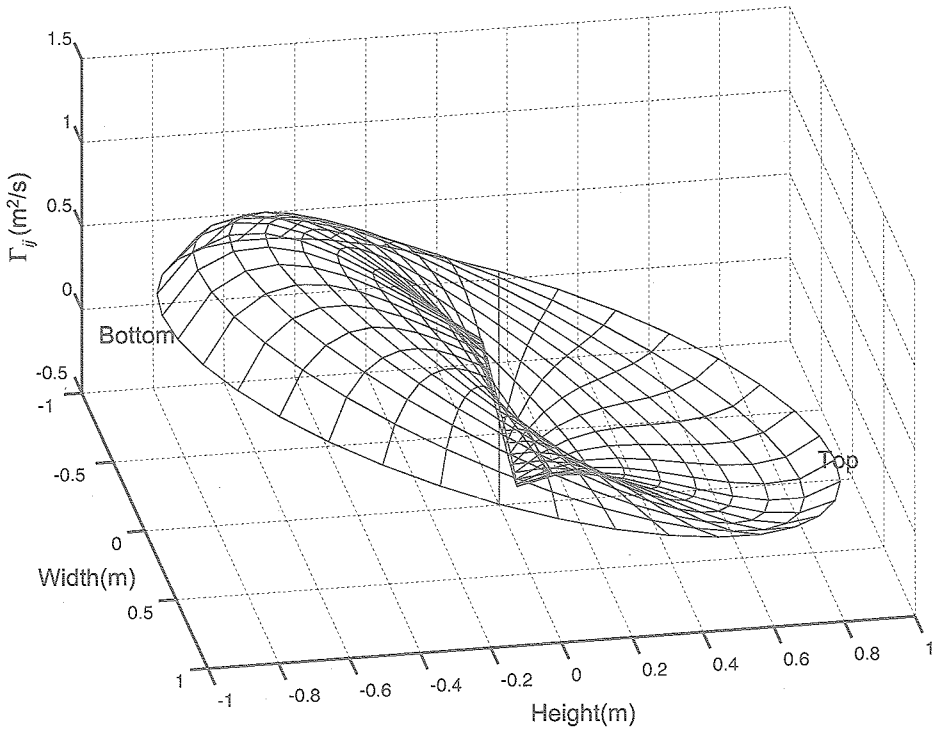

(a)

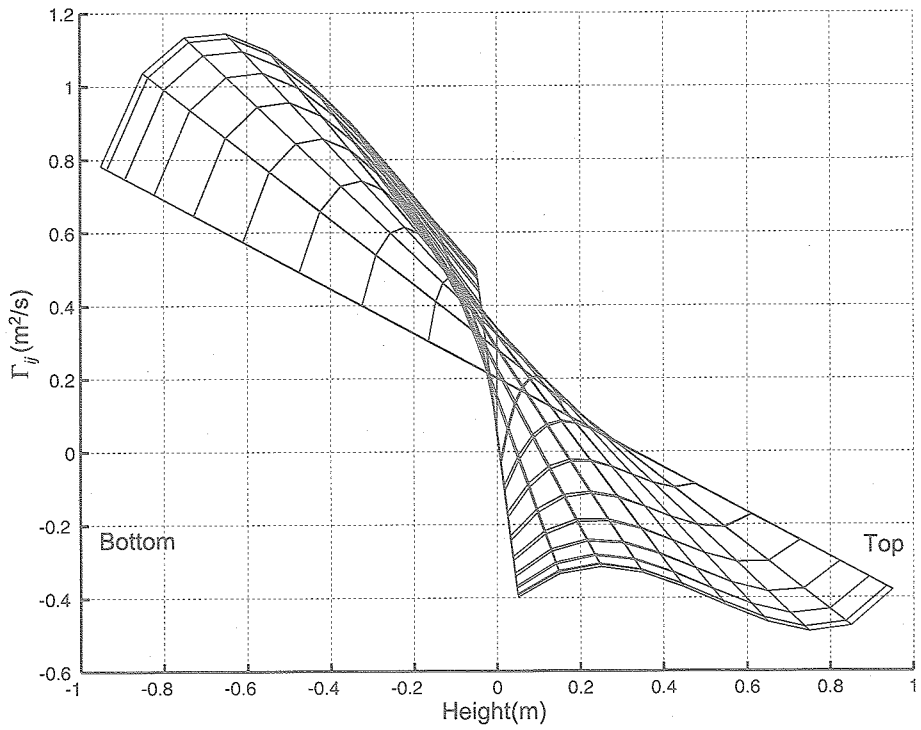

(b)

Fig.8.6 Γ_{ij} distribution of Problem 2-1'(a) bird's-eye view;(b) front view. The wind gradient is 2m/s/m. The infruence coefficients are calculated without the effect of the vortex shear.

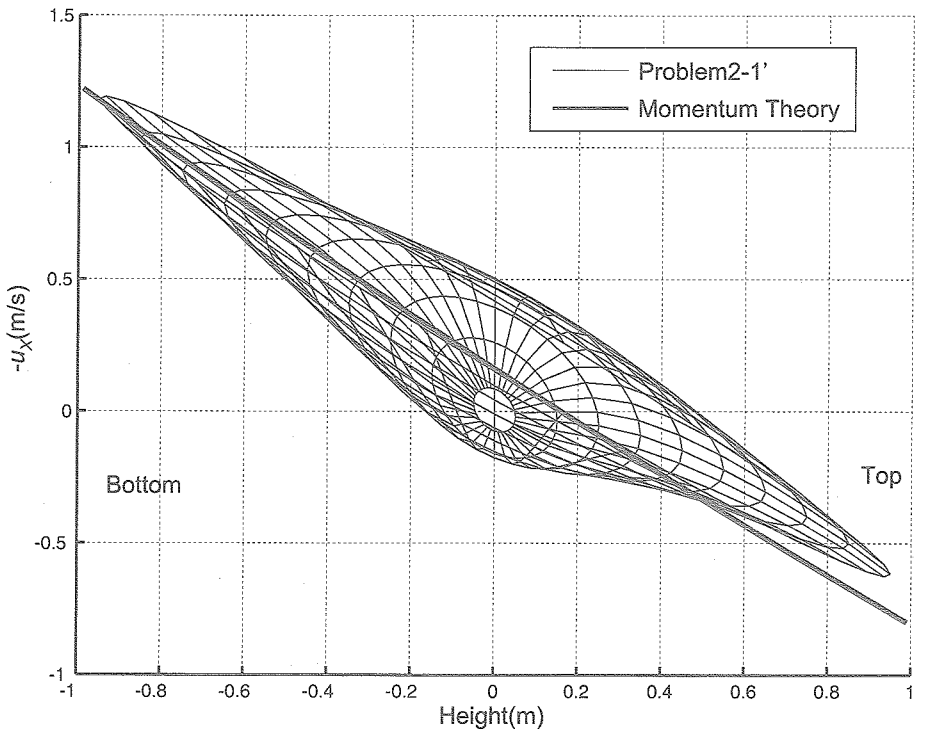

(a)

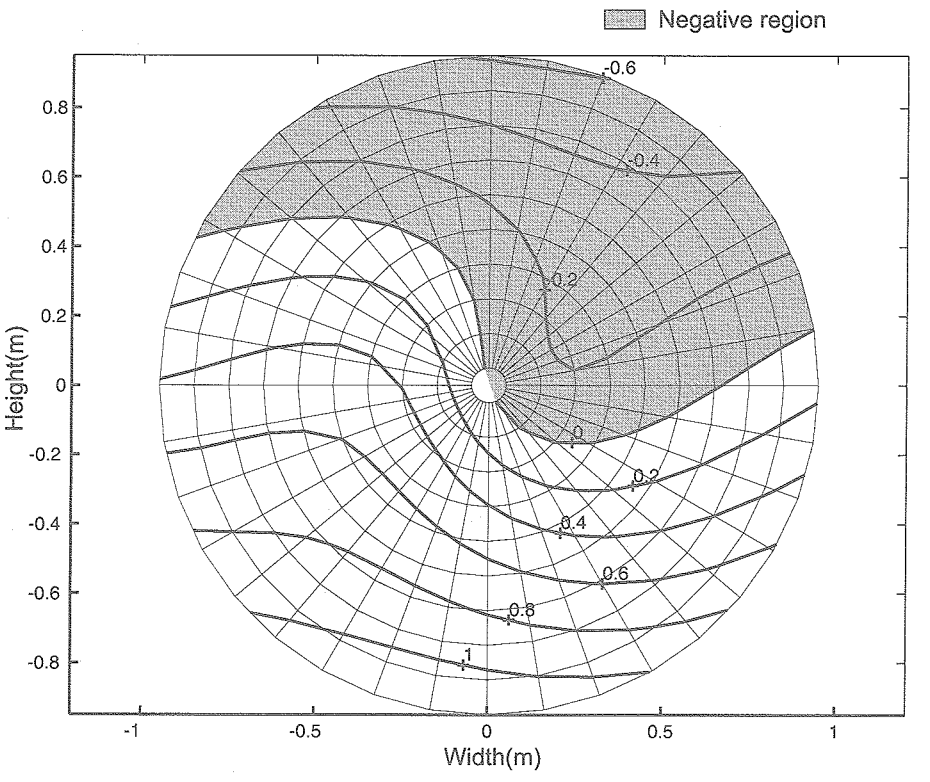

(b)

Fig.8.7 $-v_{Xij}$ distribution of Problem 2-1'(a) bird's-eye view;(b) front view. The wind gradient is 2m/s/m. The infruence coefficients are calculated without the effect of the vortex shear.

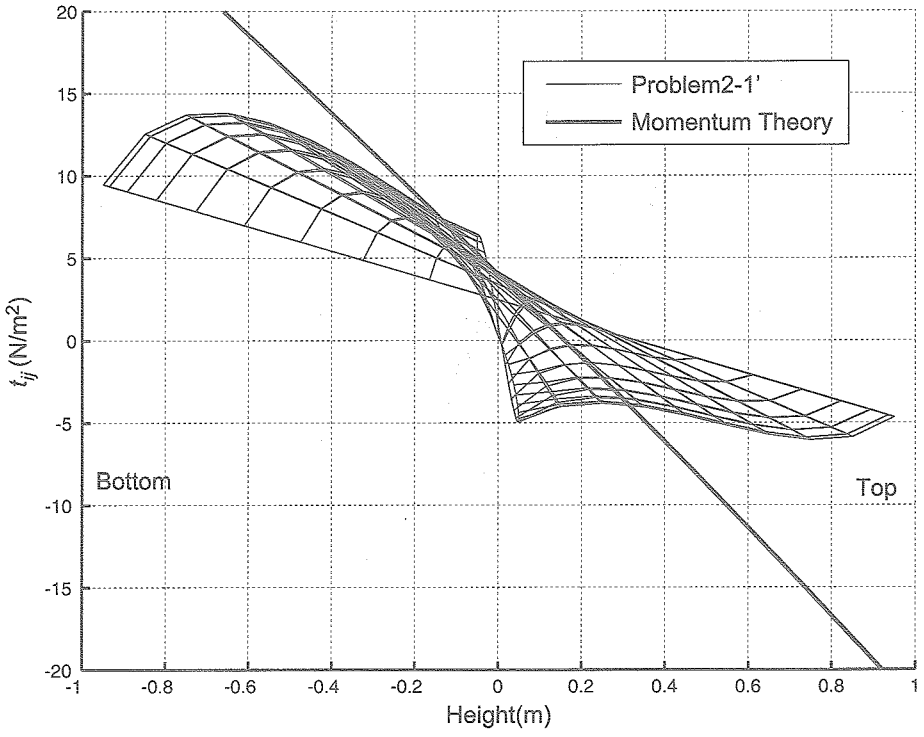

(a)

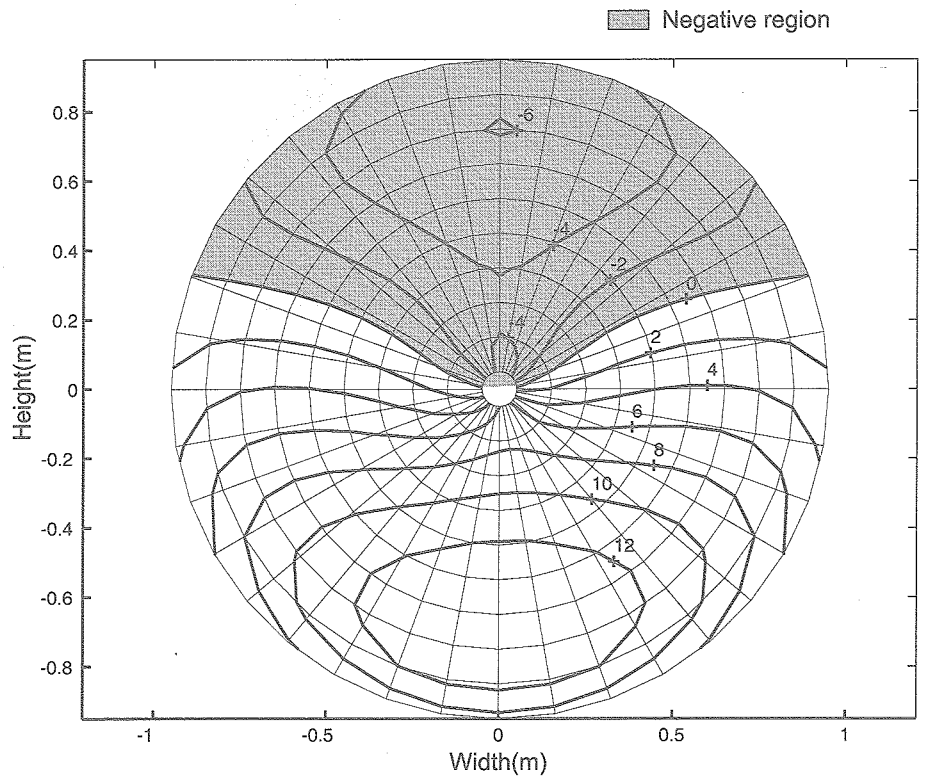

(b)

Fig.8.8 t_{ijj} distribution of Problem 2-1'(a) bird's-eye view;(b) front view. The wind gradient is 2m/s/m

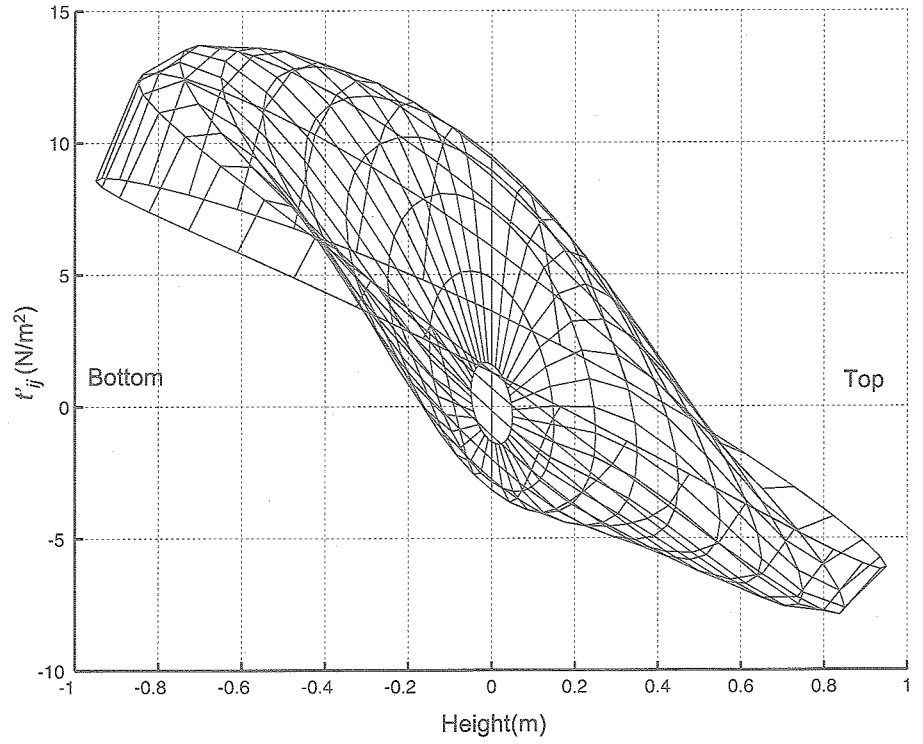

(a)

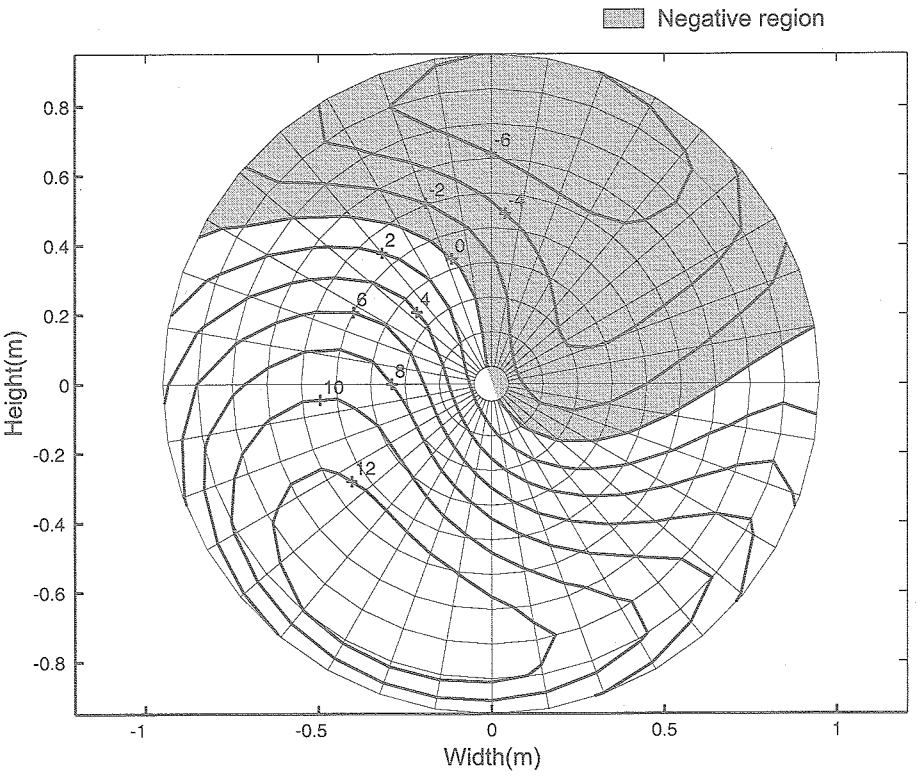

(b)

Fig. 8.9 t'_{ij} distribution of Problem 2-1': (a) bird's-eye view; (b) front view. The wind gradient is 2m/s/m.

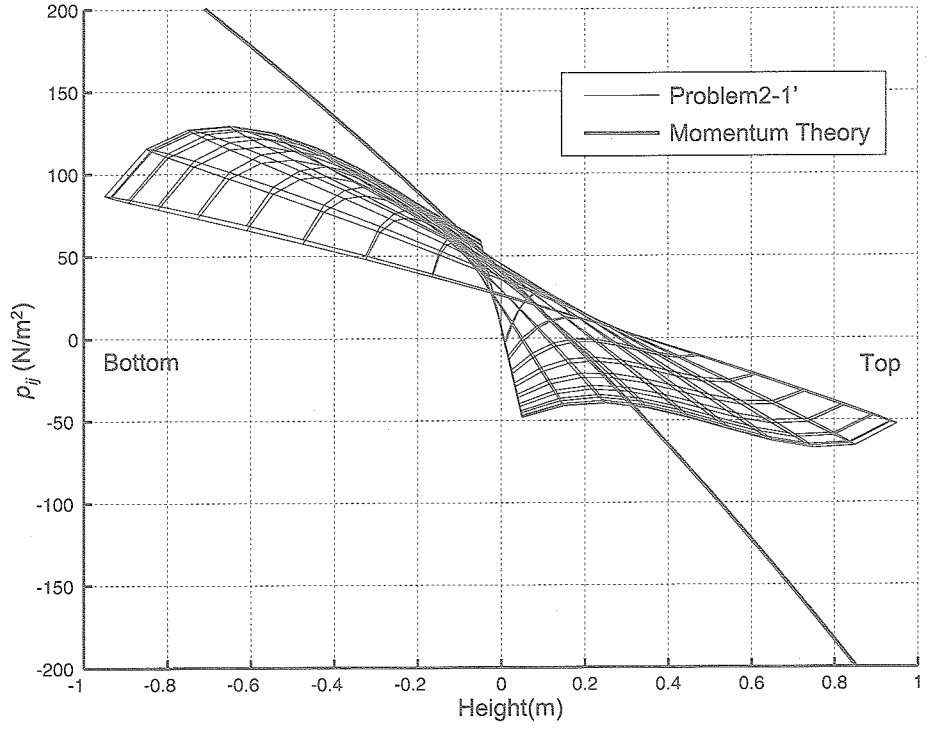

(a)

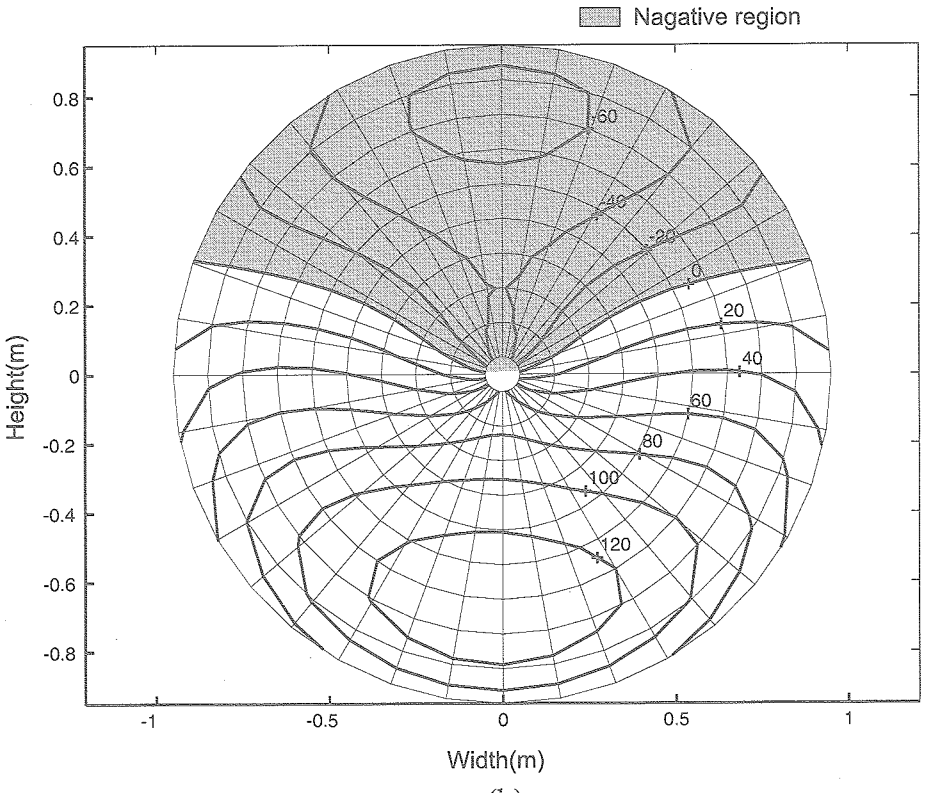

(b)

Fig.8.10 p_{ijj} distribution of Problem 2-1': (a) bird's-eye view; (b) front view. The wind gradient is 2m/s/m. The propeller absorbs energy from the air in the gray region.

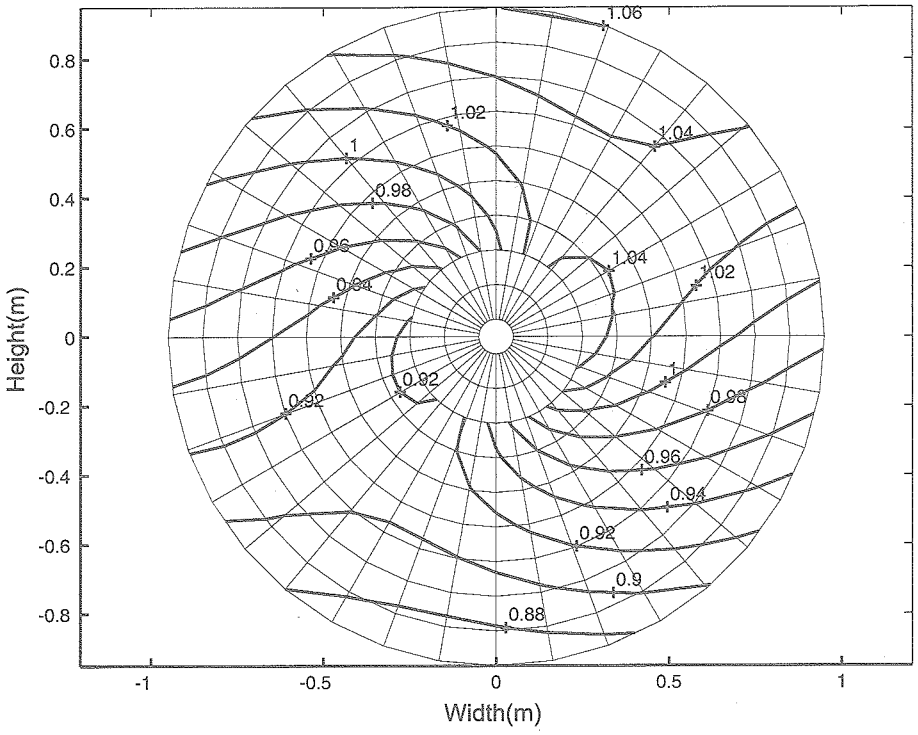

Fig. 8.11 η_{ij} distribution of Problem 2-1'.The wind gradient is 2m/s/m. There is a singular point at the center. Thus η_{ij} at j=1 and 2 are not illustrated.

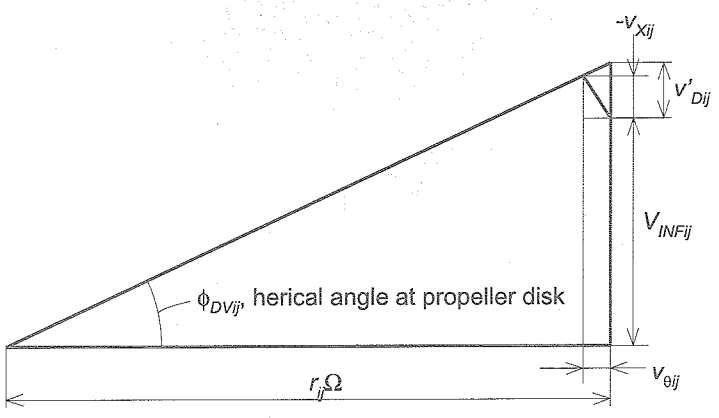

Fig.8.12 Vector diagram of the flow on the surface of a vortex sheet at the propeller disk. Though this figure is similar to Fig.6.1, the induced velocities are as half as those of Fig.6.1

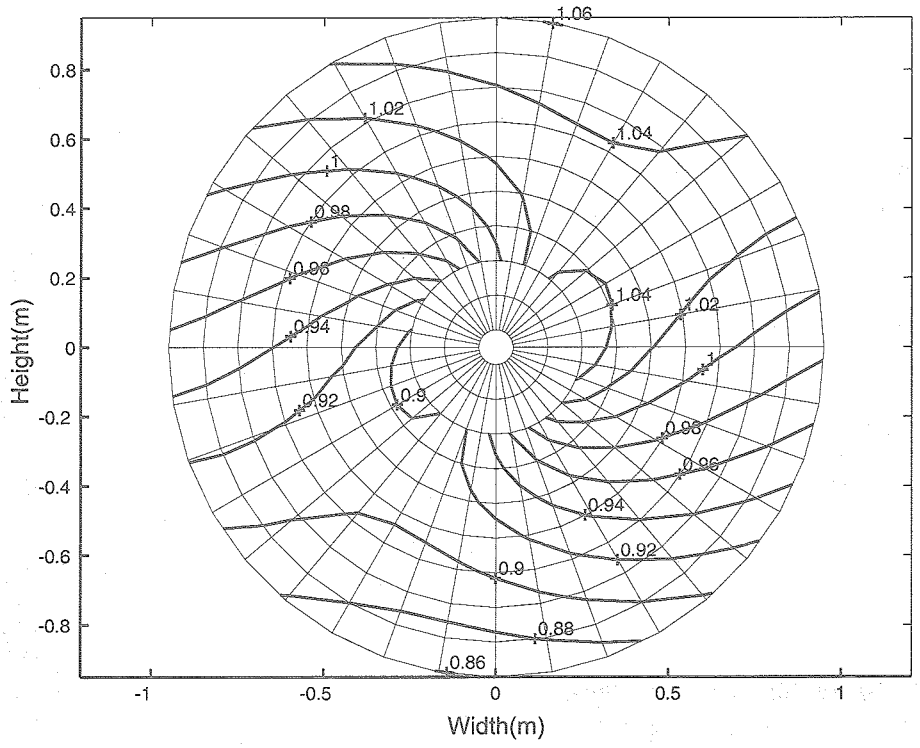

Fig. 8.13 η'_{ij} distribution of Problem 2-1'.The wind gradient is 2m/s/m. There is a singular point at the center. Thus η'_{ij} at j=1 and 2 are not illustrated.

9. Solutions to Various Conditions

9.1. Calculation Conditions

In the previous chapter, the validity and accuracy of the solutions of Problem 2-1' with wind gradient are shown. In this chapter, Problem 2-1' with various conditions are calculated. Further, the performance of an example windmill ship is calculated. The numerical example is almost the same as in the previous chapter: R=1.0m, V_{AV}=10m/s, Ω=10πrad/s, B=2, ρ=1.225kg/m^3, L=5, M=36, N=10. The designated power, P_0 (W), and the wind gradient, w_G(m/s/m), are parameters. The influence coefficients are calculated without the effect of the vortex shear. The calculation condition of each case is shown in Table 9.1.

Table 9.1
Calculation conditions of each case.

Case No.	P_0(W)	w_G(m/s/m)
A-1	0	2.0
A-2	0	1.0
A-3	0	0.5
A-4	0	0.2
A-5	0	0.0

Case No.	P_0(W)	w_G(m/s/m)
B-1	100	2.0
B-2	100	1.0
B-3	100	0.5
B-4	100	0.2
B-5	100	0.0

Case No.	P_0(W)	w_G(m/s/m)
C-1	-100	2.0
C-2	-100	1.0
C-3	-100	0.5
C-4	-100	0.2
C-5	-100	0.0

9.2. Efficiency of Propeller in Various Conditions

Fig. 9.1 shows the average thrust, T_{AV}, in each case by circles. Fig. 9.1-a shows that the optimum propeller in the wind gradient can generate thrust without power supply, in theory. Especially, the optimum propeller in the wind gradient, 2m/s/m, generates 0.9N. It requires 9W to generate this 0.9N. Thus, this propeller absorbs the power that is as much as 9W from the wind gradient. Also, Fig. 9.1-b shows that the optimum propeller in the wind gradient generates more thrust than the optimum propeller in a uniform flow in theory. Thus, the advantage of the propeller in the wind gradient is obvious.

Both Fig. 9.1-a and 9.1-b show that T_{AV} increases progressively regardless of the value of P_0 as w_G increases. Figures also show that the curves of the polynomials exactly fit each result. In Fig. 9.1-a the polynomial is $0.228{w_G}^2$, and in Fig. 9.1-b the polynomial is $9.733+0.215{w_G}^2$. These polynomials indicate the following results: first, the increase of T_{AV} is proportional to the square of w_G. Thus, the great advantage of the propeller in the wind gradient can be expected when the absolute value of w_G is large. Second, the T_{AV} values of Case B-1 to B-5 are approximately given by superposing T_{AV} of Case A-1 to A-5 and T_{AV} of Case B-5 respectively. However, this superposition only yields an approximate T_{AV}, not an exact T_{AV}, since Problem 2-1' is expressed by the nonlinear functions. This nonlinearity can be seen in the polynomials. That is, the coefficient of ${w_G}^2$ of the polynomial for Fig. 9.1-a is 0.228 while that for Fig. 9.1-b is 0.215. Also, the thrust obtained by the expanded momentum theory in each case is shown in Fig. 9.1 by the broken lines. Although the value of the thrust obtained by the expanded momentum theory is almost twice as large as T_{AV}, the figure of the thrust given by the expanded momentum theory supports the results mentioned above.

9.3. Γ_{ij} Distribution in Various Conditions

Fig. 9.2 shows Γ_{ij} distributions of Case A-1 to A-4. The Γ_{ij} distribution of Case A-5 is not shown, since Γ_{ij} of Case A-5 is zero obviously. Figures shows that the Γ_{ij} distribution of each case is similar to each other and the value of Γ_{ij} is approximately proportional to w_G. However, the value of Γ_{ij} is not exactly proportional to w_G because Problem 2-1' is expressed by the nonlinear functions as mentioned above. This nonlinearity can be confirmed by calculating the error, (Γ_{ij} of Case A-1)-(Γ_{ij} of Case A-4)x10. If there is no nonlinearity in Problem 2-1', the error must be zero. Fig. 9.3 shows the distribution of the error and the nonlinearity of Problem 2-1'. However the nonlinearity is quite small. Thus, it is useful to obtain the approximate solution by multiplying the results of Case A-4.

Fig. 9.4 shows Γ_{ij} distributions of Case B-1 to B-5 and (Case B-5 + Case A-1). Figs. 9.4-a to 9.4-e show that Γ_{ij} distributions vary gradually, and Fig. 9.4-a agrees very well with Fig. 9.4-f. Thus it is seen that Γ_{ij} in an arbitrary condition is approximately given by the superposition of Case B-5 and Case A-1. The validity of this approximation can be evaluated by calculating the error, (Γ_{ij} of Case B-5) + (Γ_{ij} of Case A-1) - (Γ_{ij} of Case C-1). Fig. 9.5 shows the distribution of the error. The error of the approximation is about 1.5%, which is negligibly small.

9.4. Example of Windmill

The present method is also valid for designing an optimum windmill in the wind gradient. However, the optimum windmill obtained by the proposed method is not the conventional windmill that absorbs the energy of the wind as much as possible, but it is a special windmill that minimizes (drag) / (power). This special windmill is suitable for windmill ships, which generate thrust by rotating the screw by consuming energy transferred from the windmill, since the drag of the windmill decelerates the ship when ship moves against the wind.

An average drag of the windmill, D_{AV}, is identical to $-T_{AV}$ and the power generated by the windmill is given by $-P_0$. Thus the problem that gives the optimum windmill in the wind gradient is identical to the problem that gives the optimum propeller in the wind gradient. The calculation of the optimum windmill in a wind gradient is only a spe-

cial case of the optimum propeller in the wind gradient. The numerical example is shown in Table 9.1 as Case C.

Fig. 9.6 shows the average drag, D_{AV}, in each case by circles. Though the graph in Fig. 9.6-a is nearly the same as the graph shown in Fig. 9.1-a, the vertical axis indicates D_{AV} instead of T_{AV}. Fig. 9.6-b shows that the optimum windmill in the wind gradient generates less drag than the optimum windmill in uniform flow, in theory. Thus, the advantage of the windmill in the wind gradient is obvious.

The result of the calculation shown in Fig. 9.6-b can be fitted by a polynomial that is given by $10.291-0.243{w_G}^2$, and the thrust obtained by the expanded momentum theory in each case is shown by the broken line. Fig. 9.6-b supports the results obtained in Section 2. That is: first, the decrease of D_{AV} is proportional to the square of w_G. Second, D_{AV} of Case C-1 to C-5 are approximately given by superposing D_{AV} of Case A-1 to A-5 and D_{AV} of Case C-5 respectively.

Fig. 9.7 shows Γ_{ij} distributions of Case C-1 to C-5 and (Case C-5 + Case A-1). Figs. 9.7-a to 9.7-e shows that Γ_{ij} distributions vary gradually and Fig. 9.7-a agrees very well with Fig. 9.7-f. Thus, Γ_{ij} in an arbitrary condition is approximately given by the superposition of Case C-5 and Case A-1. The validity of this approximation can be evaluated by calculating the error, (Γ_{ij} of Case C-5) + (Γ_{ij} of Case A-1) - (Γ_{ij} of Case C-1). Fig. 9.8 shows the distribution of the error, which is about 1.9% and is negligibly small.

9.5. Example of Windmill Ship

From the result of the calculation, the performance of the windmill ship shown in Fig. 8.9 can be estimated. The hull is designed to be under the water surface in order to avoid the complicated calculation of wave drag. The numerical example is as follows: R=1.0m, $\Omega=10\pi$ rad/s, B=2, ρ = 1.225kg/m^3, V_{AV}=8.0m/s, w_G=2.0m/s/m, the velocity of the ship, V_S, is 2m/s, efficiency of the screw is 80%, the efficiency of the energy transmission is 80%, the fineness ratio of the hull, L/D is 8, the density of the water, ρ_W, is 1000kg/m^3, the drag coefficient of the hull, C_{DH}, is 0.03. From the result of the calculation of Case C-1, the windmill generates D_{AV}, 9.32N with power absorption 100W. The screw generates a thrust of T_S=32N, since the power supplied to the screw is 80W and efficiency of the screw is 80%. The effective thrust T_E is given by:

$$T_E = T_S - D_{AV} \tag{8.1}$$

From the above results, T_E is 22.7N. On the other hand, the drag of the hull in the water, D_H is given by:

$$D_H = \frac{1}{2}\rho_W {V_S}^2 C_{DH} Q^{2/3} \tag{8.2}$$

where Q is the volume of the hull and is approximately given by:

$$Q = \frac{4}{3}\pi\left(\frac{L}{2}\right)\left(\frac{L}{2L/D}\right)^2 \tag{8.3}$$

where L is the length of the hull. Further, the following equation holds:

$$D_H = T_E \tag{8.4}$$

Eqs. (8.1), (8.2) and (8.3) into Eq. (8.4) give:

$$L = 0.641\sqrt{T_S - D_{AV}} \tag{8.5}$$

From Eq. (8.5), the length of the hull is 3.05m^2.

If the wind gradient does not exist, D_{AV} is 10.29N from the result of the calculation of Case C-5. Therefore, the length of the hull is 2.99m^2. Further, the increase of the length of the hull by using the effect of the wind gradient is 2%, in this condition.

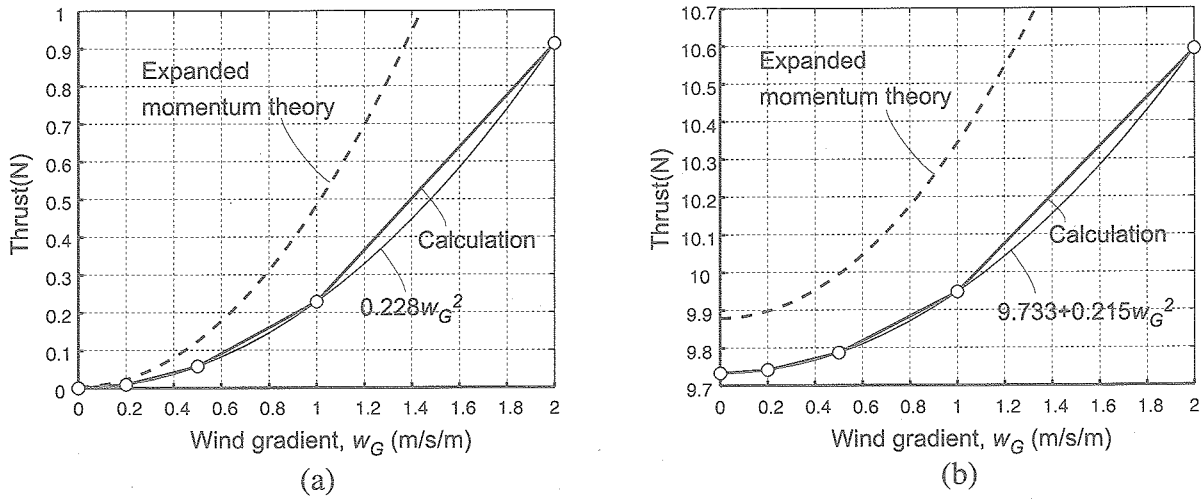

Fig. 9.1 Thrust *versus* wind gradient : (a) Case A; (b) Case B.

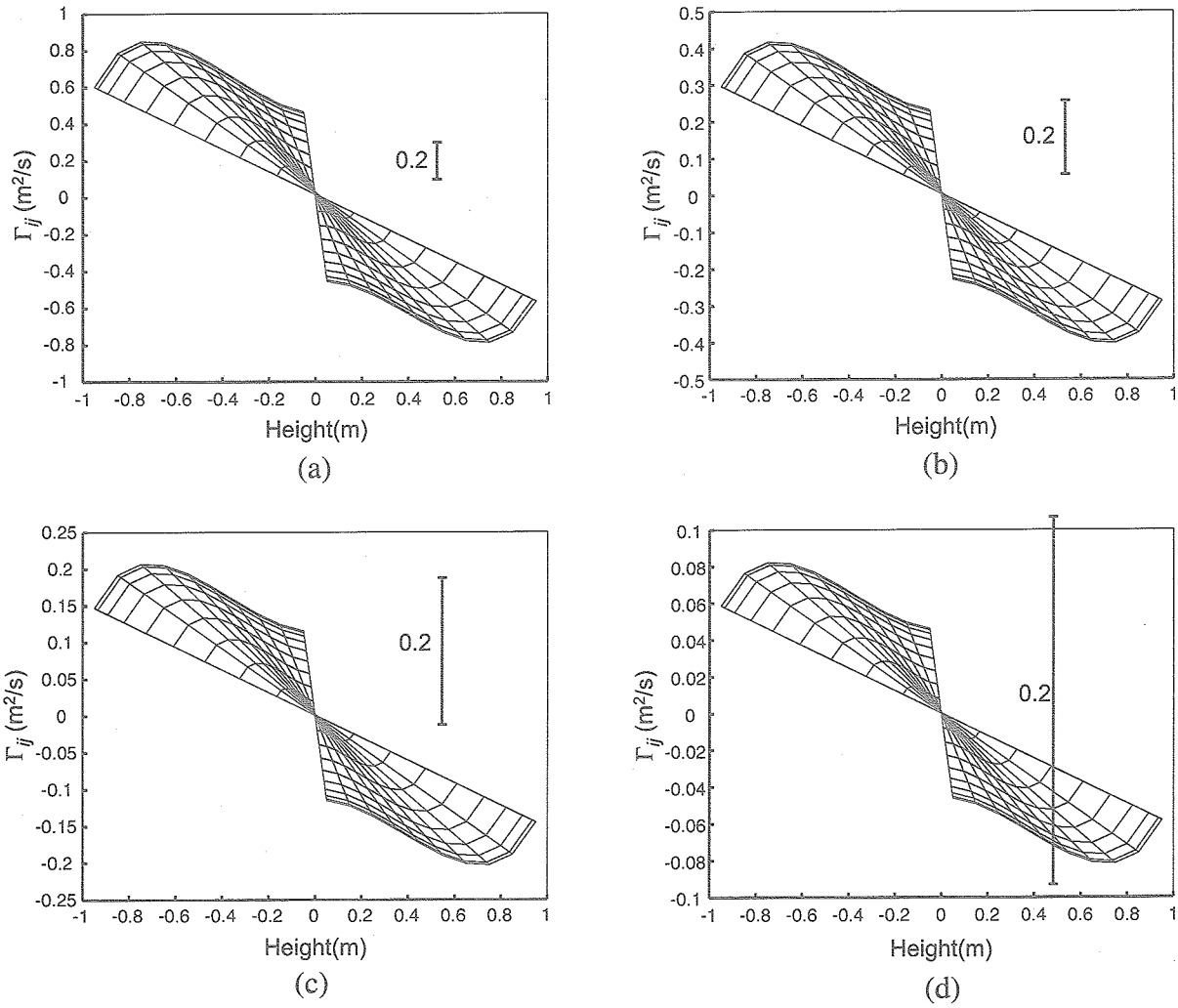

Fig. 9.2 Side view of the distribution of Γ_{ij}: (a) Case A-1; (b) Case A-2; (c) Case A-3; (d) Case A-4.

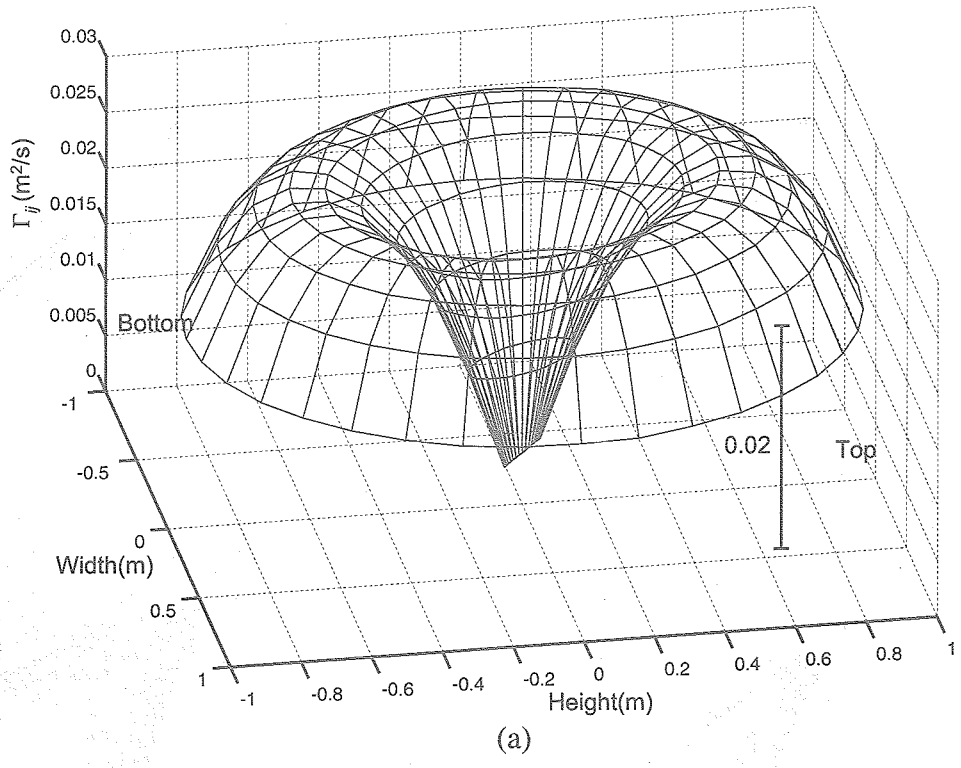

(a)

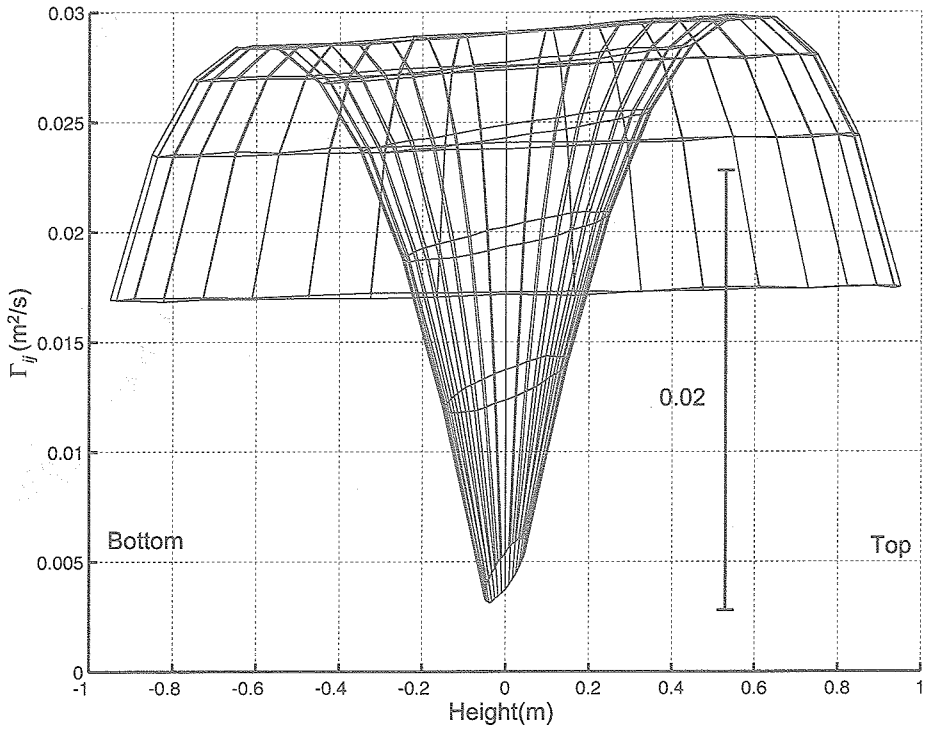

(b)

Fig. 9.3 (Γ_{ij} of Case A-1)-(Γ_{ij} of Case A-4)x10 : (a) bird's-eye view; (b) side view.

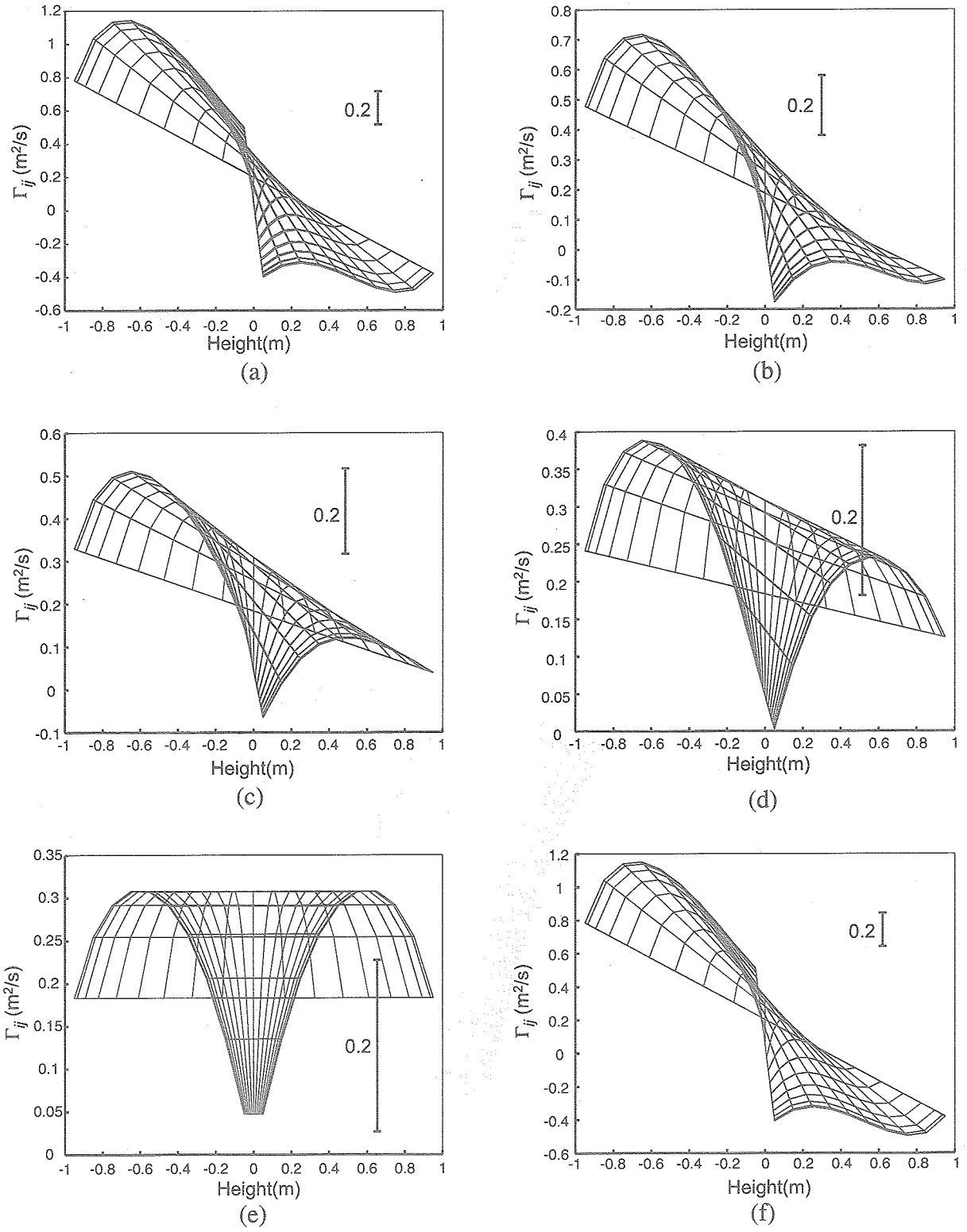

Fig. 9.4 Side view of the distribution of Γ_{ij}. (a) Case B-1; (b) Case B-2; (c) Case B-3; (d) Case B-4; (e) Case B-5; (f) Case B-5 + Case A-1.

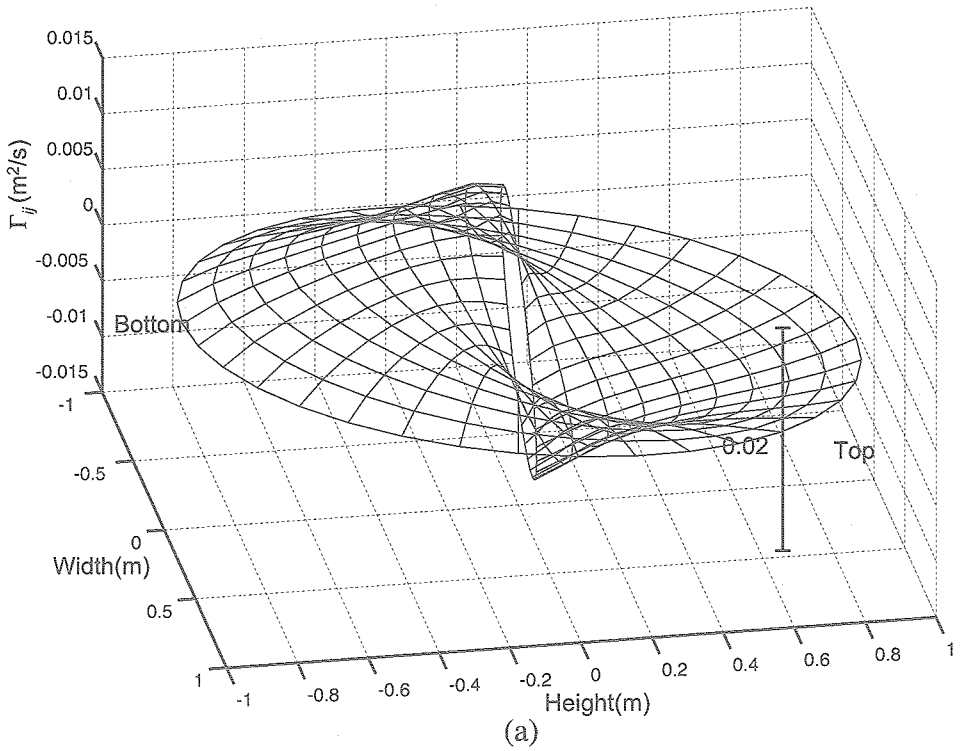

(a)

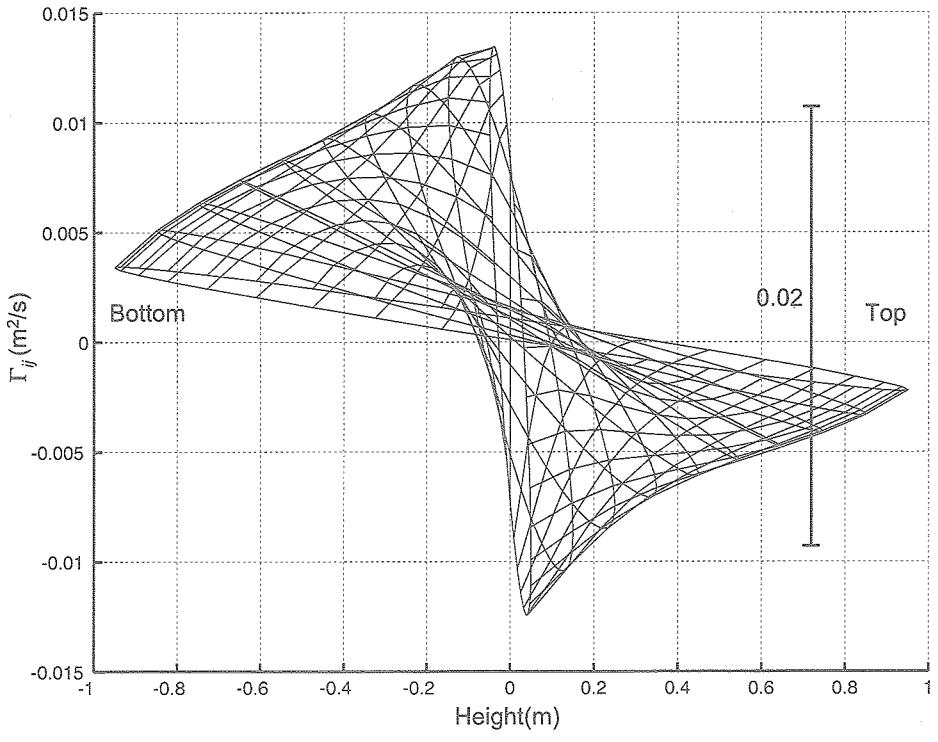

(b)

Fig. 9.5 (Γ_{ij} of Case B-5)+(Γ_{ij} of Case A-1)-(Γ_{ij} of Case B-1) : (a) bird's-eye view; (b) side view.

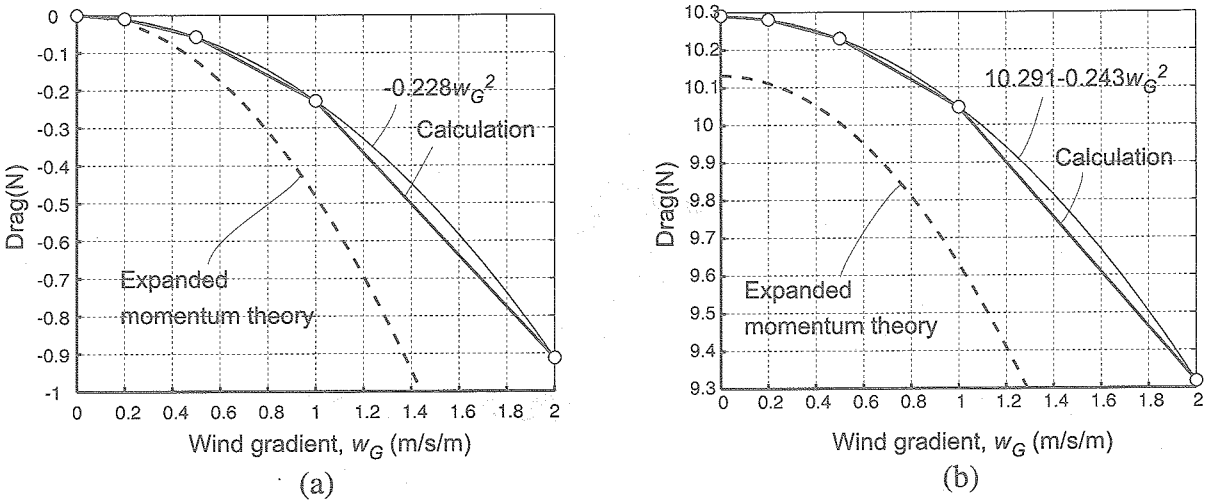

Fig. 9.6 Drag *versus* wind gradient : (a) CaseA; (b) Case C.

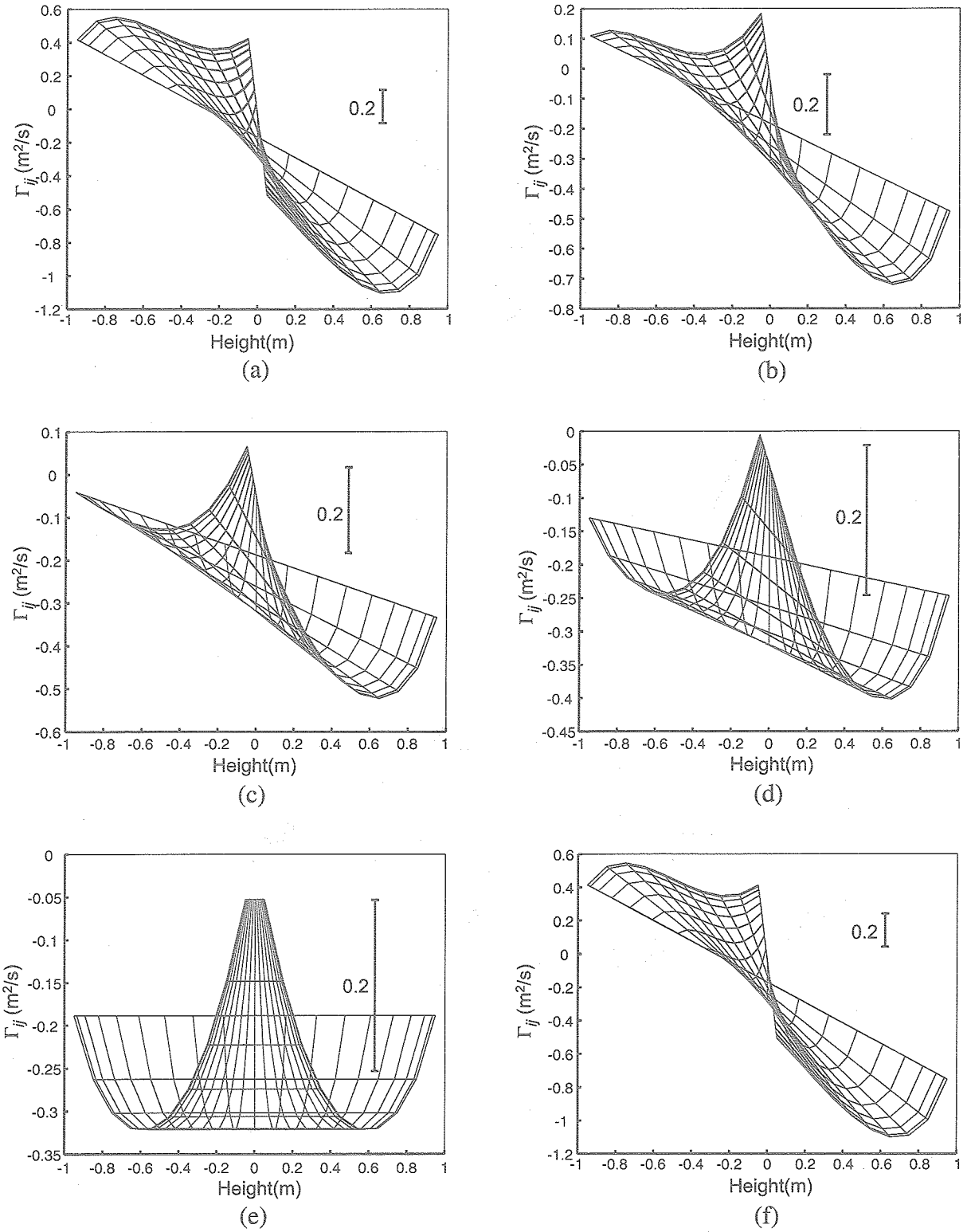

Fig. 9.7 Side view of the distribution of Γ_{ij}. (a) Case C-1; (b) Case C-2; (c) Case C-3; (d) Case C-4; (e) Case C-5; (f) Case C-5 + Case A-1.

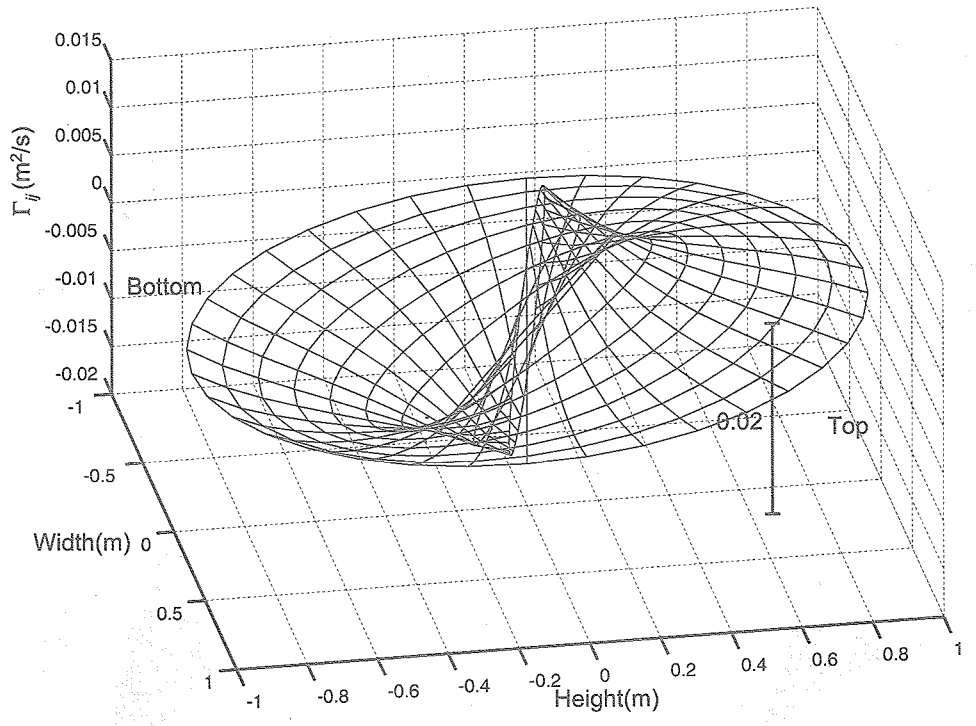

(a)

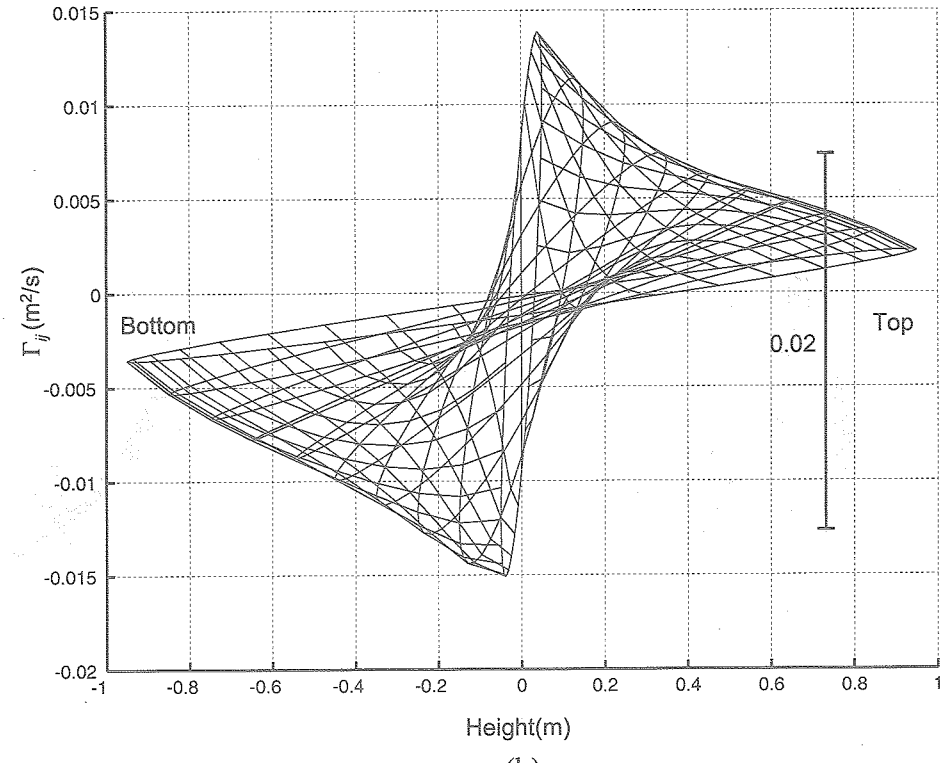

(b)

Fig. 9.8 (Γ_{ij} of Case C-5)+(Γ_{ij} of Case A-1)-(Γ_{ij} of Case C-1) : (a) bird's-eye view; (b) side view.

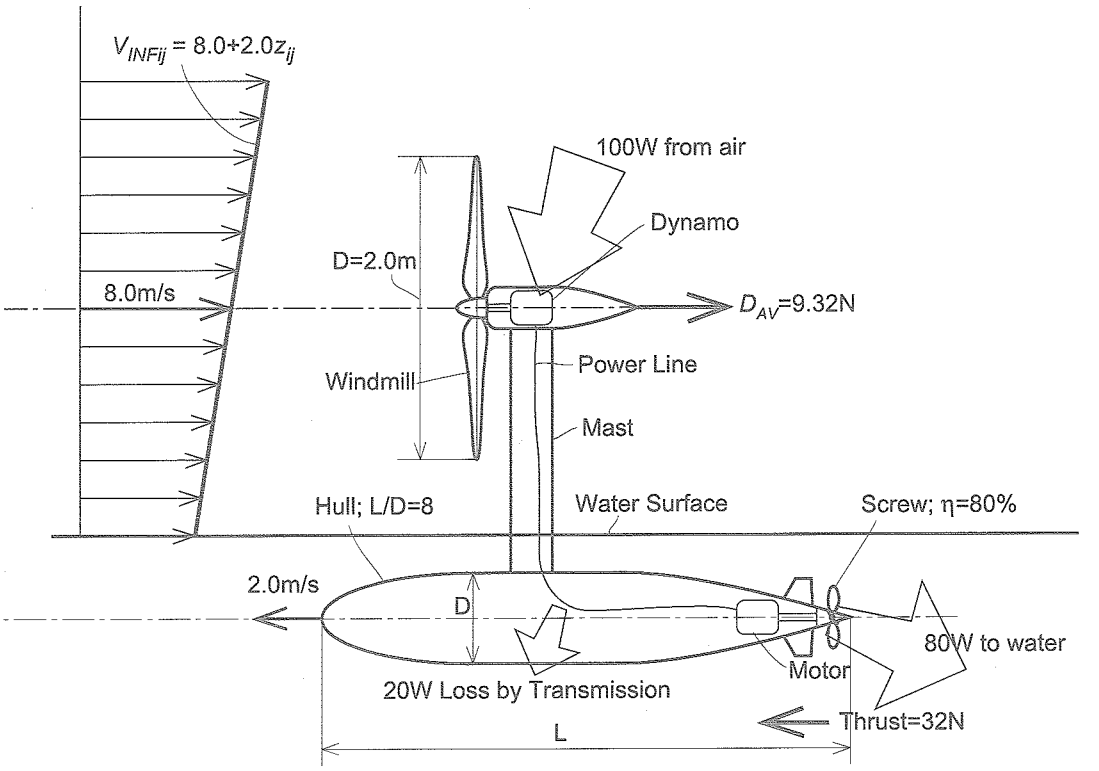

Fig. 9.9 Concept of the windmill ship. The velocity of the ship is 2.0m/s. V_{AV}=8.0m/s. w_G=2.0m/s. The windmill absorbs 100W from air. This power is transmitted via the dynamo, the power line and the moter. The efficiency of transmission is 80%. The efficiency of the screw is 80%.

10. Conclusions

Based on the lifting line theory, an optimum propeller or windmill design problem in a wind gradient has been transformed into a convex programming problem that consists of one quadratic objective function and one quadratic constraint function This transfer has important meaning, since the procedure for solving the resultant problem is quite simple. Furthermore, the reduction of the number of unknown variables based on the periodical characteristic of the solution tremendously reduced the number of the computational operation. As a result, by the present method consists of the above two procedures, an optimum propeller or windmill design problem in a wind gradient is easily solved.

Also, based on Prandtl's propeller theory, the validity and accuracy of the present method are carefully evaluated, and the result of the evaluation was very good. Further, it was shown that the shape of the vortex sheet of the optimum propeller in a wind gradient, which was expected to be sheared by the wind gradient, is kept approximately constant. Therefore, although it was expected that the influence coefficients with the effect of the vortex shear give more accurate solution than that without the effect of the vortex shear, influence coefficients should be calculated without effect of the vortex shear.

Many numerical examples are calculated and it was shown that the propulsive efficiency of an optimal propeller in a wind gradient is higher than that in a uniform wind. Further, the distribution of the induced velocity, local thrust and local power are calculated to investigate the mechanism of the propulsive efficiency increase. As a result, the mechanism is described as follows: first the propeller absorbs energy of the air whose velocity is higher

than the average velocity; second the propeller expels the energy to the air whose velocity is lower than the average velocity. Numerical examples for windmill are also calculated and the advantage of a windmill in a wind gradient has been shown. The performance of the windmill ship in a wind gradient has calculated and the advantage of the windmill ship with the effect of the wind gradient. Above all, the most important part of these results is that a propeller in a wind gradient can generate thrust even without power supply.

Though the circulation of the optimum propeller (windmill) has been shown, how to realize this circulation is not shown. One of the ideal methods for realizing this circulation given by the present theory is to arbitrarily control both the chord length and geometrical angle of the blade segments. However, it is very difficult to do that. Especially, the arbitrary control of the chord length is almost impossible, and only the arbitrary control of the geometrical angle of the blade segments can be possible, by use of smart materials. Thus, the chord length of the blade segments must be an adequately constant value, which means that the blade segments generate only drag when the required circulation is zero. Therefore, it is important to take the effect of the profile drag into consideration in designing the optimum propeller in the wind gradient. In addition, the optimum solution shown here is purely theoretical, since the effect of the profile drag is ignored. However, it is meaningful that the present method has shown that the optimum propeller without power input in wind gradient can generate thrust, in theory.

Acknowledgements

I would like to thank Prof. DeLaurier for supervising my study in UTIAS. I also wish to acknowledge valuable discussion with Prof. Martins and Mr. Fenton. Lastly, I would like to thank Mr. Nam for revising my English.

Appendix A

Limit of Prandtl's Propeller Theory

Both Prandtl's theory and Goldstein's theory must use the light disk-loading assumption, since the deformation of the vortex sheet can not be obtained analytically. There are three kinds of vortex sheet deformations: first, the contraction of vortex sheet as shown in Fig. A.1-a; second, the elongation of the pitch as shown in Fig. A.1-b; third, the roll up of the vortex sheet as shown in Fig. A.1-c.

The first phenomenon is caused by the acceleration of the induced velocity. The momentum theory shows the following relation between the axial induced velocity at propeller disk, v_X, and that far behind the propeller disk, w_X:

$$2v_X = w_X \tag{A.1}$$

Therefore, the axial velocity at the propeller disk, V_1, and that far behind the propeller disk, V_2, are given by:

$$V_1 = V_0 + v_X \tag{A.2}$$

$$V_2 = V_0 + 2v_X \tag{A.3}$$

where V_0 is the velocity of the air far ahead of the propeller disk. The conservation law requires that:

$$\rho S_1 V_1 = \rho S_2 V_2 \tag{A.4}$$

where ρ is density of air and S_1 S_2 are the area of the cross section of the stream tube. Eqs. (A.2) and (A.3) into Eq. (A.4) gives:

$$S_2 = \frac{V_0 + v_X}{V_0 + 2v_X} S_1 \tag{A.5}$$

Eq. (A.5) shows that the contraction of the vortex sheet exists. The second phenomenon is obviously caused by the acceleration of the induced velocity. The pitch of the vortex sheet is not constant, since V_1 is smaller than V_2, as mentioned above. If the effect of the rotating component of the induced velocity is negligible, the pitch of the vortex sheet at the propeller disk, d_1, and that far behind the propeller disk, d_2, is given by:

$$d_1 = 2\pi \frac{V_0 + v_X}{\Omega} \tag{A.6}$$

$$d_2 = 2\pi \frac{V_0 + 2v_X}{\Omega} \tag{A.7}$$

where Ω is the propeller angular velocity. Eq. (A.6) and Eq. (A.7) show that d_2 is longer than d_1. The third phenomenon is caused by the instability of the vortex sheet. It is generally known that the vortex sheet rolls up and makes vortex clouds.

The difficulty of the propeller design is caused by these phenomena, especially the second phenomenon. That is, Prandtl's theory and Goldstein's theory require the pitch of the vortex sheet to be constant, in spite of the fact that the pitch is not constant. Prandtl and Goldstein kept the rigorousness of their theory by using the light disk-loading assumption in which v_X is much smaller than V_0. Though this assumption make it difficult to apply their theories to practical propeller design, it is inevitable that one must use the constant-pitch vortex sheet in their theories. Thus the pitch used in Prandtl's theory and Goldstein's theory is the pitch, d_0, without the effect of the axial induced velocity given by:

$$d_0 = 2\pi \frac{V_0}{\Omega} \tag{A.8}$$

It is easily expected that the accuracy of Prandtl's theory and Goldstein's theory may increase by using d_1 or d_2 instead of d_0. However, the proper pitch for an accurate design, d, is longer than d_1 and shorter than d_2 obviously. There is, however, no analytical method to determine the value of d. Thus the attempt to increase the accuracy of Prandtl's theory or Goldstein's theory by the elongation of the vortex sheet into consideration is analytically fultile. Though it is impossible to analytically take the effect of the elongation of the vortex sheet into consideration, it is possible to do it by laborious iterative computations. However, it is generally known that the increase of the accuracy for the propeller design, achieved by such computation of the vortex shape, is small.

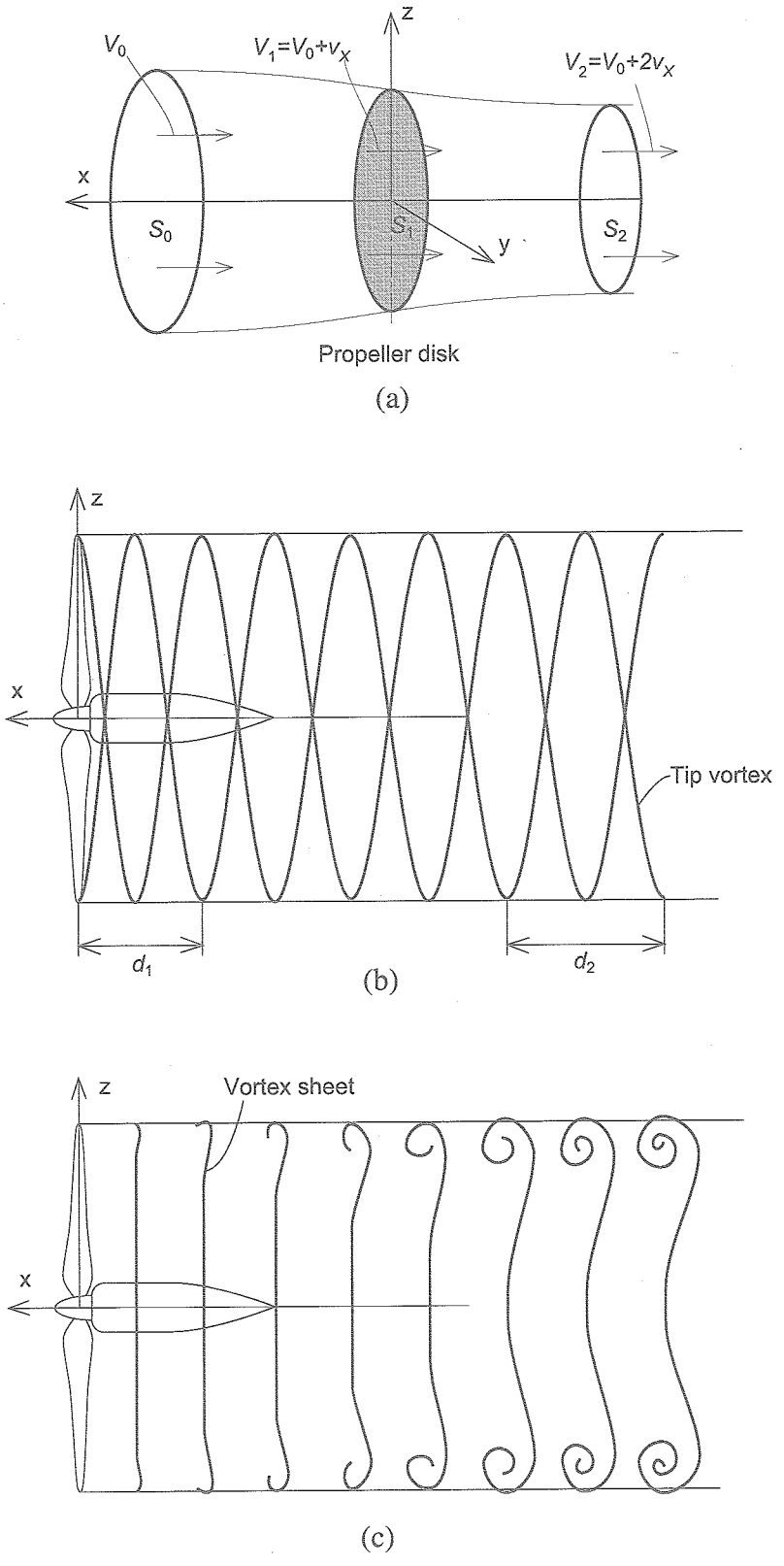

Fig. A.1 Deformation of the vortex sheet: (a) contraction of the flow tube; (b) elongation of the pitch of the vortex sheet; (c) roll up of the vortex sheet.

Appendix B

Procedure for Solving Problem 1-1' and 2-1'

The fundamental form of the problem treated in this paper is as follows:

Problem 1

$$\begin{aligned} &\text{minimize} && x^T Ax + x^T B \\ &\text{subject to} && x^T Cx + x^T D - P_0 \le 0 \end{aligned}$$

where A and C are m× m matrices, B, D and x are m vectors and P_0 is a scalar. A and C are not symmetric matrices in this paper. Thus the following operations are necessary.

$$\tilde{\mathrm{A}} = \frac{1}{2}\left(\mathrm{A}^T + \mathrm{A}\right) \tag{B.1}$$

$$\tilde{\mathrm{C}} = \frac{1}{2}\left(\mathrm{C}^T + \mathrm{C}\right) \tag{B.2}$$

From the result of the calculations in this paper, $\tilde{A}$ and $\tilde{C}$ are positive definite matrixes. Thus the following is a convex programming problem.

Problem 2

$$\begin{aligned} &\text{minimize} && x^T \tilde{A}x + x^T B \\ &\text{subject to} && x^T \tilde{C}x + x^T D - P_0 \le 0 \end{aligned}$$

Further, the following definitions are introduced for the later convenience:

$$f(\mathrm{x}) = \mathrm{x}^T \tilde{\mathrm{A}}\mathrm{x} + \mathrm{x}^T \mathrm{B} \tag{B.3}$$

$$g(\mathrm{x}) = \mathrm{x}^T \tilde{\mathrm{C}}\mathrm{x} + \mathrm{x}^T \mathrm{D} - P_0 \tag{B.4}$$

$$L(\mathrm{x},\lambda) = f(\mathrm{x}) + \lambda g(\mathrm{x}) \tag{B.5}$$

Problem 2 is solved by using the Kuhn-Tucker condition. It is, however, beyond the scope of this paper to discuss the condition. Thus the Kuhn-Tucker condition is not described here and only the procedure to solve Problem 2 is shown, which is as follows:

Step. 0 Solve the following equation.

$$\partial f / \partial \mathrm{x} = 0 \tag{B.6}$$

This may be rewritten as:

$$2\tilde{\mathrm{A}}\,\mathrm{x} + \mathrm{B} = 0 \tag{B.7}$$

Let the obtained solution be x^*. Evaluate the restrictive condition. If x^* satisfies the restrictive condition, x^* is the solution

Step 1 $\lambda^{(k)} = \lambda_0$, k=1. λ_0 must be positive. For example, λ_0=1.

Step 2 Solve the following equation:

$$\partial L / \partial \mathrm{x} = 0 \tag{B.8}$$

This may be rewritten as:

$$2\left(\tilde{\mathrm{A}} + \lambda^{(k)}\tilde{\mathrm{C}}\right)\mathrm{x} + \left(\mathrm{B} + \lambda^{(k)}\mathrm{D}\right) = 0 \tag{B.9}$$

Let the obtained solution be $x^{(k)}$.

Step 3 Evaluate the error defined by:

$$\varepsilon^{(k)} = \left\{g\left(x^{(k)}\right) - P_0\right\}^2$$

If $\varepsilon^{(k)} < \varepsilon_0$, $x^{(k)}$ is the solution, where ε_0 is a very small positive number.

Step 4 $\lambda^{(k)+} = \lambda^{(k)} + d\lambda$; where $d\lambda$ is a very small number.

Step 5 Solve the following equation:

$$2\left(\tilde{\mathrm{A}} + \lambda^{(k)+}\tilde{\mathrm{C}}\right)\mathrm{x} + \left(\mathrm{B} + \lambda^{(k)+}\mathrm{D}\right) = 0 \tag{B.10}$$

Let the obtained solution be $x^{(k)} + dx^{(k)}$.

Step 6 Calculate $\left(\partial g / \partial \lambda\right)^{(k)}$ given by:

$$\left(\partial g / \partial \lambda\right)^{(k)} = \left(2\mathrm{C}\mathrm{x}^{(k)} + \mathrm{D}\right)\frac{dx^{(k)}}{d\lambda} \tag{B.11}$$

Step 7 Calculate $\lambda^{(k+1)}$ given by:

$$\lambda^{(k+1)} = \frac{1}{\left(\partial g / \partial \lambda\right)^{(k)}}\left\{P_0 - g\left(x^{(k)}\right)\right\} + \lambda^{(k)} \tag{B.12}$$

k=k+1.

Repeat the procedure from Step 1.

Step 0 is the procedure for the special case where λ=0. The Kuhn-Tucker condition requires the solution to satisfy Eq. (B-8). In this procedure, the function $g(x)$ is a function of x transformed into the function $g(\lambda)$ that is the function of λ by using Eq. (B-8). Step 2 to Step 7 is the procedure to

search for a λ that satisfies $g(\lambda)=P_0$ by using the Newton-Raphson method. An example of function $g(\lambda)$ is shown in Fig. B.1. The calculating condition is the same as Case A-1 in Chapter 8.

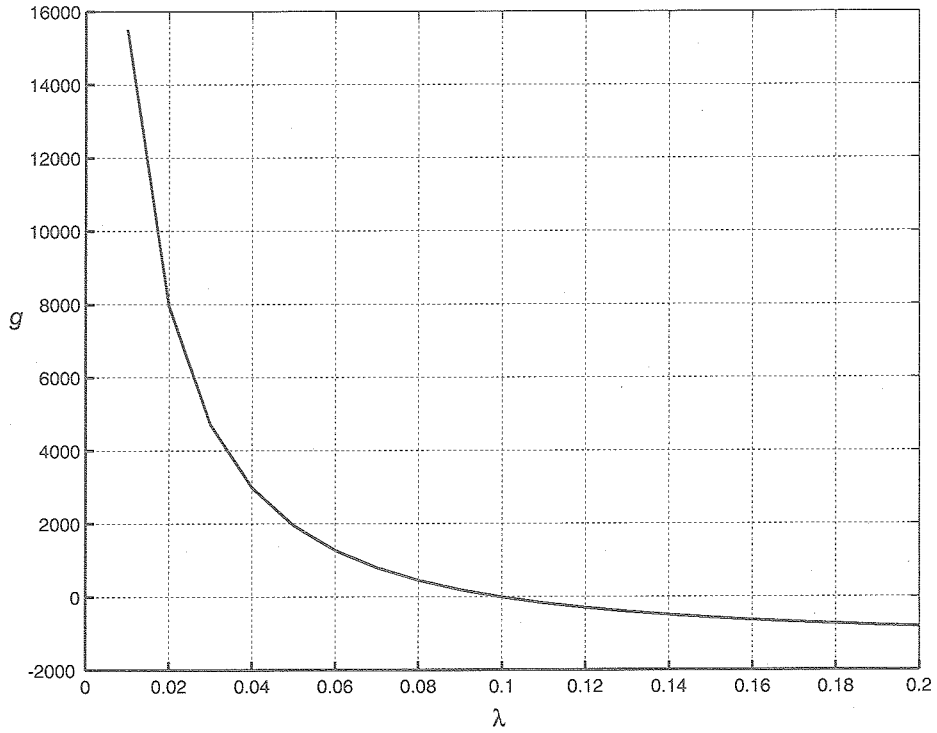

Fig. B.1 *g versus* λ.

Reference

1) Betz, A., Prandtl, L., "Schraubenpropellr mit geringstem Energieverlust (Screw Propellers with Minimum Induced Loss," Goettingen Reports 1919, pp.193-213
2) Goldstein, S., "On the Vortex Theory of Screw Propellers," Royal Society Proc. Series A, Vol.123, London, 1929, pp.440-465.
3) McLemore, H. C., "Wind-Tunnel Tests of a 1/20 Scale Airship Model with Stern Propellers," NASA Langley, TN D-1026, 1962
4) Petrone, F. J., Wessel, P. R., "High Altitude Superpressure Powered Aerostat (HASPA)," 1974
5) Stefan, K., "Design definition of a Lighter-Than-Air (LTA) High Altitude Powered Platform (HAPP). Volume 1," NASA-CR-168350-VOL-1 , 1982
6) Shlichting, H., "Boundary –Layer Theory," Seventh Edition, McGraw-Hill Inc., 1978, pp.635-647.
7) Glauert, H., "Airplane Propellers," Ed. by Durand, W., Aerodynamic Theory, Div. L Vol. 4, Peter Smith, Gloucester, MA, 1976, pp. 169-269.
8) Rockafellar, R. T., "Convex Analysis," Princeton University Press, 1970.
9) Larrabee, E. E., "Practical Design of Minimum Induced Loss Propellers," SAE, pre-print for the April 1979 Business Aircraft Meeting and Exposition, Wichita, KS.
10) Larrabee, E. E., "The Screw Propeller," Scientific American, Vol. 243, No. 1, July 1980, pp. 134-148.
11) Larrabee, E. E., French, S. E., "Minimum Induced Loss Windmills and Propellers,"

JAXA Research and Development Report
(JAXA-RR-03-016E)

Date of Issue : March 25, 2004

Edited and Published by :
Japan Aerospace Exploration Agency
7-44-1 Jindaiji-higashimachi, Chofu-shi,
Tokyo 182-8522 Japan

Printed by :
BCC Co., Ltd.
2-4-1 Hamamatsu-cho, Minato-ku, Tokyo 105-6114 Japan

Japan Aerospace Exploration Agency